DOVILĖ GIMŽAUSKAITĖ

RESEARCH OF THE CONVERSION OF LIQUID AND SOLID WASTES USING THERMAL PLASMA TECHNOLOGY

DOCTORAL DISSERTATION

Kaunas
2020

LITHUANIAN ENERGY INSTITUTE

DOVILĖ GIMŽAUSKAITĖ

RESEARCH OF THE CONVERSION OF LIQUID AND SOLID WASTES USING THERMAL PLASMA TECHNOLOGY

Doctoral Dissertation
Technological Sciences, Energetics and Power Engineering (T 006)

2020, Kaunas

Doctoral dissertation was prepared in 2015–2019 at Lithuanian Energy Institute Plasma Processing Laboratory
Part of the research presented in this dissertation was funded by the European Regional Development Fund (project No. 01.2.2-LMT-K-718-01-0005) under a grant agreement with the Research Council of Lithuania.
The studies were supported by the Research Council of Lithuania.

Scientific Supervisor:

Dr Vitas Valinčius (Lithuanian Energy Institute, Technological Sciences, Energetics and Power Engineering – T 006).

Doctoral dissertation has been published in:
http://ktu.edu

Editor:

Agnė Lukševičiūtė (“BELLA VERBA, UAB”)

LIETUVOS ENERGETIKOS INSTITUTAS

DOVILĖ GIMŽAUSKAITĖ

SKYSTŲ IR KIETŲ ATLIEKŲ KONVERSIJOS TAIKANT TERMINĖS PLAZMOS TECHNOLOGIJĄ TYRIMAS

Daktaro disertacija
Technologijos mokslai, energetika ir termoinžinerija (T 006)

2020, Kaunas

Disertacija rengta 2015–2019 metais Lietuvos energetikos institute, Plazminių technologijų laboratorijoje.
Dalis disertacijoje pateikiamų tyrimų buvo finansuojami iš Europos regioninės plėtros fondo, projekto (Nr. 01.2.2-LMT-K-718-01-0005) lėšų, pagal dotacijos sutartį su Lietuvos mokslo taryba (LMTLT).
Lietuvos mokslo taryba rėmė dalį disertacijoje pateikiamų mokslinių tyrimų.

Mokslinis vadovas:

Dr. Vitas VALINČIUS (Lietuvos energetikos institutas, technologijos mokslai, energetika ir termoinžinerija – T 006).

Interneto svetainės, kurioje skelbiama disertacija, adresas:
http://ktu.edu

Redagavo:

Agnė Lukševičiūtė (UAB “BELLA VERBA”)

CONTENT

ABBREVIATIONS

AC – alternating current

AD – anaerobic digestion

Ar – argon

Btu – quadrillion British thermal units

CCE – carbon conversion efficiency

DBD – dielectric barrier discharge

DC – direct current

DSC – differential scanning calorimetry

ECE – energy conversion efficiency

EDX – energy-dispersive X-ray spectroscopy

EIA – U.S. Energy Information Administration

ER – equivalence ratio

ICE – internal combustion engine

IEA CPS – International Energy Agency's Current Policies Scenario

IEA NPS – International Energy Agency's New Policies Scenario

IEA SDS – International Energy Agency's Sustainable Development Scenario

IEEJ – The Institute of Energy Economics, Japan

Ktoe – thousand tonnes of oil equivalent

LHV – lower heating value

LTE – local thermodynamic equilibrium

MW – microwave discharge

NAPL – non-aqueous phase liquid

OECD – Organisation for Economic Co-operation and Development

OECD-FAO – The Organisation for Economic Co-operation and Development (OECD) and the Food and Agriculture Organisation (FAO) of the United Nations

OPEC – Organisation of the Petroleum Exporting Countries

PAHs – polycyclic aromatic hydrocarbons

PCD – pulsed corona discharge

PM – particulate matter

RDF – refuse-derived fuel

RF – radio frequency induction

SEM – scanning electron microscopy

SER – specific energy requirement

TGA/DTG – thermogravimetric analysis

VCC – voltage-current characteristics

VOCs – volatile organic compounds

WtE – waste-to-energy

INTRODUCTION

The relevance of the work

The projections provided by the United Nations shows that the world population will grow to 10.9 billion in 2100 from the initial 7.7 billion in 2019 (United Nations, 2019a). Such tendency inevitably will lead to the increasing consumerism of energy and generation of various types of waste. Several models of the energy consumption predictions show that fossil fuel still will compose a considerable part of primary world energy in 2040, and liquid fuels (e.g. diesel, gasoline) will continue to play a vital role in industrial and transportation sectors (Newell et al., 2019). Additionally, contamination by solid and industrial waste is considered as one of the leading environmental issues in the global. Accordingly, the world bank group prognoses that solid waste generation will increase by 1.4 billion tonnes in 2050 from the initial 2.01 billion tonnes in 2016 (Kaza et al., 2018). Thus, waste management will require even more attention and effort in the future. Currently, waste management is based on the principle of the waste hierarchy, which is composed of five stages: prevention, reuse, recycle, recovery, and disposal. Despite many efforts to accomplish the first three stages, still, there is a part of the wastes that can only be handled by recovery (e.g. Waste-to-Energy conversion). Most of the presently used Waste-to-Energy technologies (e.g. anaerobic digestion, fermentation, torrefaction, liquefaction) are oriented mainly into the conversion of organic waste and are not very suitable for the conversion of various mixed or special wastes (e.g. industrial, hazardous wastes). Moreover, these technologies face other challenges, including a lengthy conversion process, neediness to use chemical reagents, generation of secondary pollutants, sensitivity to the changes in the environmental conditions. On the contrary, plasma technologies can be applied for the conversion of various types of waste, including special waste. Additionally, plasma technologies have no restrictions to process organic and inorganic wastes. Also, plasma offers several benefits to the waste conversion: the process is fast in time, the use of chemical reagents is not required. The high energy densities, high temperature, and reactive species ensure the decomposition of the organic compounds into synthesis gas (mainly H_2, CO) without the formation of the secondary pollutants. Meanwhile, the inorganics and minerals, that are not decomposed form environmental-friendly vitrified slag, which can be used in the construction sector. The generated synthesis gas can be used for the production of electricity, heat, or as a feedstock for the production of hydrogen, ammonia. Consequently, plasma technologies are considered as an advanced and viable solution for waste management in the future.

In this work, two types of waste (crude glycerol, and diesel fuel contaminated soil) are selected for the conversion process with the thermal plasma technology. Crude glycerol emerges in the industrial sector as a by-product of biodiesel production and composes for approximately 10 % of the total volume of biodiesel. Moreover, biodiesel production will likely continue to grow, since there is an intention to take ambitious climate change countermeasures which includes the decisions to reduce the

consumption of fossil fuel worldwide. As a result, the excess of crude glycerol will also increase and will continue to jeopardise biodiesel market stability. Therefore, ways of utilising waste glycerol are needed to be sought. Meantime, recollecting the predictions on energy consumption over the next few decades, fossil fuel still will remain a central energy source. Thus, increasing fuel demand and consumption increases the likelihood of fuel spillage into the environment, and this results in water or soil pollution. Soil contaminated with petroleum products (e.g. diesel fuel, gasoline, grease) becomes a sort of waste. Such soil has to be collected from the contamination site and remediated. Hence, effective and fast soil cleaning methods are being sought to avoid storing contaminated soil and incurring additional costs. Accordingly, the conversion of crude glycerol into synthesis gas and remediation of petroleum polluted soil using plasma technologies looks like a promising alternative to avoid negative economic and environmental consequences.

Although plasma-based technologies are considered as perspective methods for waste disposal, these technologies are not fully optimised, nor widely integrated into the industrial sector. In seeking to widen the use of such technologies, further experimental studies are needed. Consequently, the object of this work is the experimental application of thermal plasma technology for waste conversion.

Aim of the Doctoral Dissertation

To investigate the plasma conversion processes of liquid (crude glycerol) and solid (diesel-contaminated soil) wastes, determining the optimal performing conditions for the crude glycerol conversion process, and evaluating diesel fuel removal efficiency from the soil.

Tasks of the Doctoral Dissertation

In order to implement the aim of the doctoral dissertation, the following main tasks were carried out:

1. To investigate the influence of the type of plasma forming gas and the electric current on the electrical and thermal characteristics of the plasma torch and select the most suitable working conditions for the waste conversion process.
2. To perform crude glycerol conversion using air plasma and water vapor plasma, as well as to determine the influence of the gasifying agent type and flow rate to the crude glycerol conversion process by quantifying the conversion system in terms of the H_2/CO ratio, lower heating value, carbon conversion efficiency, energy conversion efficiency, and specific energy requirement.
3. To evaluate the efficiency of proposed plasma-based technology by calculating the mass and energy balance of the plasma system during the glycerol conversion process.
4. To experimentally investigate the diesel fuel contaminated soil remediation process, its dependence on pollutant concentration and the type of plasma forming gas, as well as to assess the contaminant removal efficiency.

Scientific novelty

1. The performed experimental researches broaden the understanding of plasma-based crude glycerol conversion features and allow better to define the parameters of the optimal conversion process.
2. The carried out researches allowed evaluating the application of the plasma-based conversion process for the remediation of contaminated soil.

Practical value

The proposed thermal plasma technology is suitable for gasification of various types of wastes, e.g. (industrial, solid waste). The usage of this technology not only can remove the excess of crude glycerol from the industrial sector but also may produce synthesis gas that can be used to generate additional energy, heat, or in the production of liquid fuels. Additionally, this technology removes petroleum products (e.g. diesel fuel) from the soil easily, quickly, and without the secondary pollution of the soil. Thus, the proposed technology has an ecological value. The obtained results can be successfully used in the development of new plasma technologies for waste disposal. Also, gained results can be used in the calculation, design of plasma-chemical reactors, and in predicting the course and consequences of waste conversion processes.

Statements carried out for defense

1. The carbon conversion efficiency and energy conversion efficiency increases, while specific energy requirement decreases with the increase of the gasifying agent amount in the total gasifying agent/crude glycerol ratio.
2. The conversion of crude glycerol with water vapour plasma is more efficient compared to the conversion of crude glycerol with air plasma.
3. Almost 1/3 and 1/2 of the electrical energy required for the formation of plasma could be recovered during the crude glycerol conversion with air plasma and water vapour plasma, respectively.
4. During the interaction between up to 160 g/kg diesel fuel contaminated soil and thermal plasma, the contaminant (diesel fuel) removal from the soil is achieved despite the pollutant concentration in the soil and the type of plasma forming gas (air or water vapour).

Scientific approbation of dissertation

The material of the doctoral dissertation has been published in four articles referred in the "Clarivate Analytics – Web of Science Core Collection" database. The material of the thesis has also been presented in seven international conferences, four of them took place abroad.

The structure and the content of the dissertation

The dissertation consists of an introduction, literature review, methodology, results, and discussion, conclusions, the list of references, and the list of scientific

publications, as well as acknowledgements. The dissertation is compiled of 109 pages, including 45 figures and 18 tables. The list of references has 197 sources.

1. LITERATURE REVIEW

1.1. The synergy between the growth of the human population, energy usage, and waste generation

The unfavourable impact of the synergy between the human population and the expanding world energy consumption on the state of the environment became indisputable these days. Thus, it seems appropriate to access the issues and suggestions addressed in this dissertation by first discussing the current and future situations of the human population and energy consumption as well as its possible effect on the environment through waste generation.

According to the medium-variant projection given by the United Nations, the global population will grow from 7.7 billion people worldwide in 2019 to around 9.2 billion in 2040, and 10.9 billion in 2100 (United Nations, 2019a). Beneath the global level, differences between different world regions exist. As a result of this, some regions (e.g. located in Europe) will continue to see decreasing population numbers. In contrast, the population in other areas will increase. More precisely, the middle scenario prognoses that until 2050 52 % (1.05 billion) of the global population increment will be concentrated in countries of sub-Saharan Africa and 25% of worldwide population in Central and Southern Asia (505 million) (United Nations, 2019).

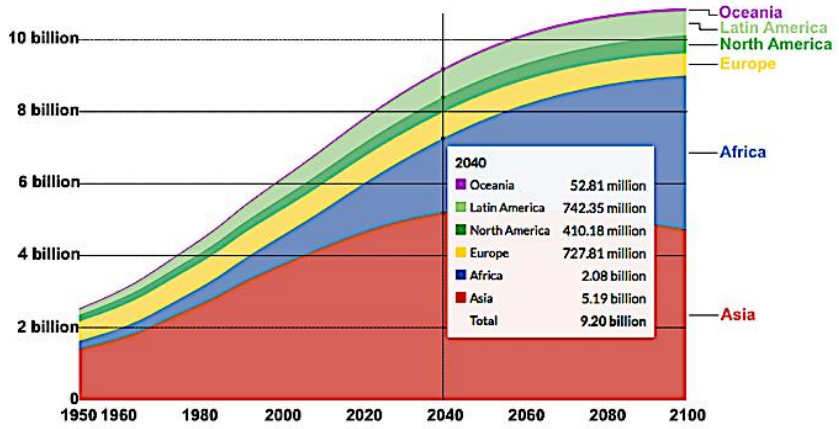

Fig. 1.1 World population by region projected to 2100 (Roser, 2019; United Nations, 2019a)

The growing population and economy will expand energy consumption. There are several models (Fig. 1.2) used to predict how energy consumption will change until 2040. All of these projections assume the same tendency – global energy consumption will grow 20–30 % or more through 2040 and beyond, led mainly by fossil fuels. Moreover, it is assumed that fossil fuel will compose 74–79 % of global primary energy in 2040 (Fig. 1.2). According to ambitious climate scenarios (e.g. IEA SDS), the share of fossil fuel in global primary energy will decrease to 60–62 % in 2040, from the initial 82 % in 2015 (Newell et al., 2019).

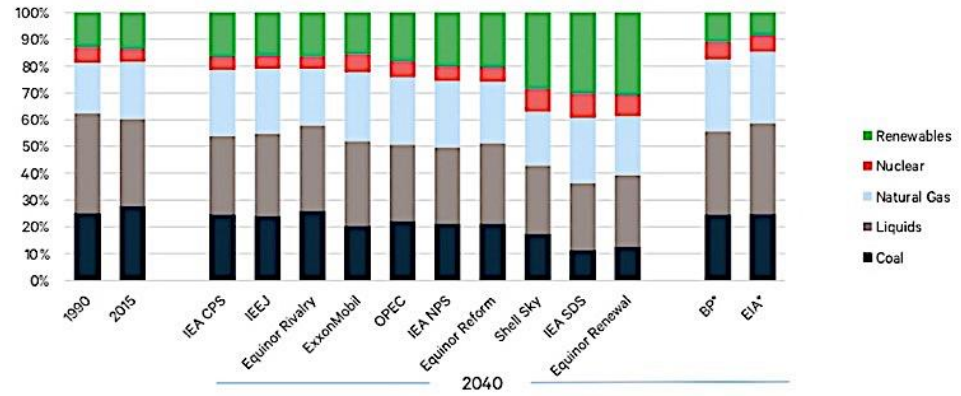

Fig. 1.2 Projection of shares of global primary energy consumption by fuel in 2040 (Newell et al., 2019). * BP and EIA scenarios exclude non-marketed biomass energy (e.g. wood, dung), while the rest of the outlooks include this in renewables

Furthermore, more than half of the projected growth in global energy consumption will take place in non-OECD regions, including Asia (mainly China, India), Africa, and the Middle East (EIA, 2019). These predictions coincide with the United Nations' projected distribution of population growth across the regions worldwide (Fig. 1.1).

Additionally, among the various sectors, the industrial sector not only constitutes more than 50% of the world's energy consumption part but also will maintain its position throughout the entire projection period achieving about 315 quadrillions Btu by 2050 (Fig. 1.3). Meanwhile, the transportation sector will remain second at the forefront as a user of the world's energy. Moreover, the majority of the increase in the industrial and transportation sector's energy use will occur in non-OECD countries (BP, 2019; EIA, 2019).

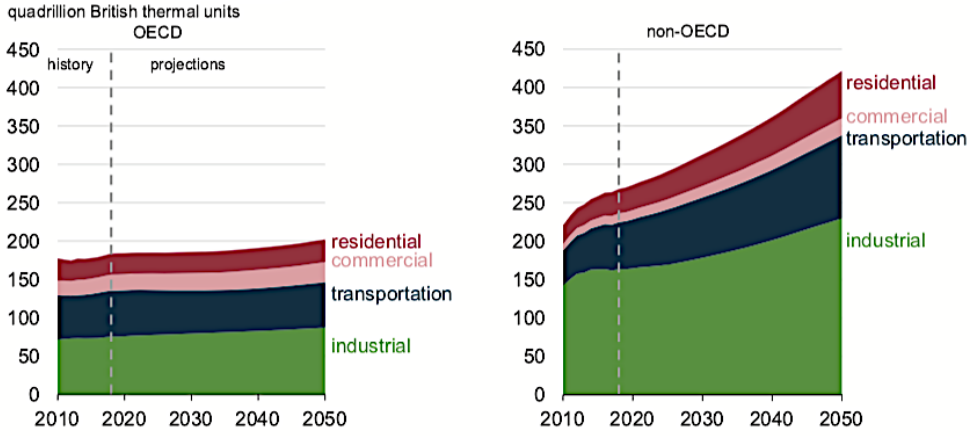

Fig. 1.3 Projection of energy consumption by sector until 2050 (EIA, 2019)

Despite the intention to take ambitious climate change countermeasures worldwide, liquid fuels (e.g. residual fuel oil, diesel, gasoline) will play a significant role in industrial and transportation sectors (Fig. 1.4). In the industry, liquid fuels will continue to be used as chemical feedstocks, provide process heat, and power equipment. This sector will account for about one-third of liquid fuels consumption by 2050. Also, liquid fuels will remain the predominant transportation fuels (59 % of total liquid fuels end-use), especially in non-OECD countries, where consumption will increase from 56 quadrillions Btu in 2018 to 85 quadrillion Btu in 2050 (about 50 % from 2018 to 2050). In general, the use of liquid fuels will increase by about 45 % in non-OECD countries, whereas, in OECD countries, will remain relatively stable (in OECD Europe will decline by 15 % to 24 quadrillions Btu in 2050) (EIA, 2019; ExxonMobil, 2019).

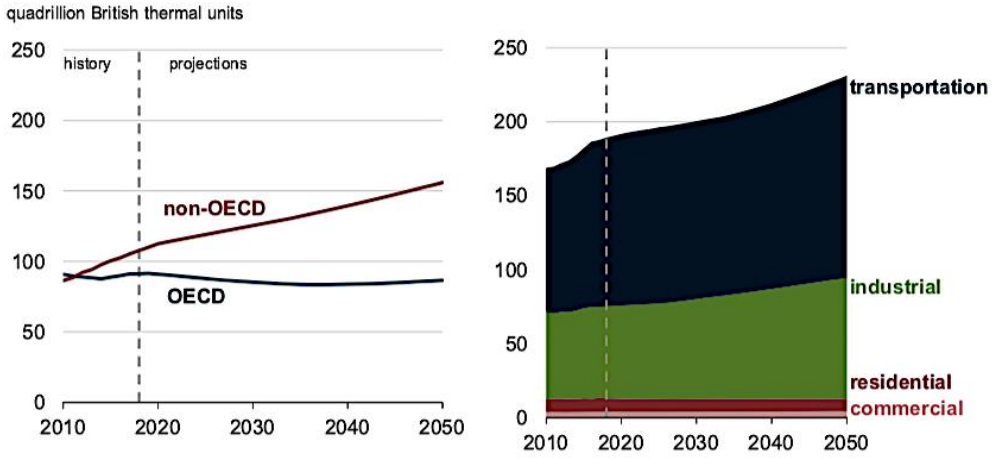

Fig. 1.4 Projection of petroleum and other liquids consumption until 2050 (EIA, 2019)

Every sector, including commercial, residential, transportation and industrial, inevitably generates waste and causes environmental pollution by using the sources of energy for the fulfilment of needs, or the creation of goods. Acid rain, global warming, odour emissions, and land-use are negative environmental impacts of fossil fuels usage and the disposal of the wastes (Zhang et al., 2020). Thus, increasing human population, urbanisation, industrialisation, and generally growing energy consumption will guarantee tremendous waste production and the adverse effects on the environment. Based on the latest statistics available, global solid waste generation reached 2.01 billion tonnes in 2016 (Fig. 1.5). The projections provided by World Bank states that 2.59 billion tons of solid waste will be generated annually worldwide by 2030. Meanwhile, solid waste generation across the world is expected to reach 3.40 billion tonnes by 2050 (Kaza et al., 2018).

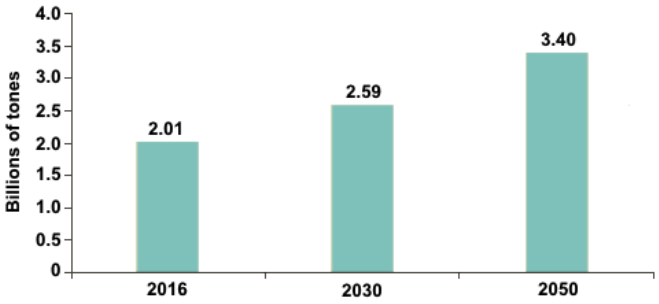

Fig. 1.5 Projected global solid waste generation (Kaza et al., 2018)

Also, it is expected that in the regions with growing low-income and lower-middle-income waste generation will increase. Hereby, it is projected that waste levels in Sub-Saharan Africa and South Asia regions will triple and double, respectively, in the next three decades with urbanisation and economic growth (Fig. 1.6). Whereas regions with higher-income including Europe and Central Asia as well as North America are anticipated to see waste levels increase more gradually by 2050 (Kaza et al., 2018).

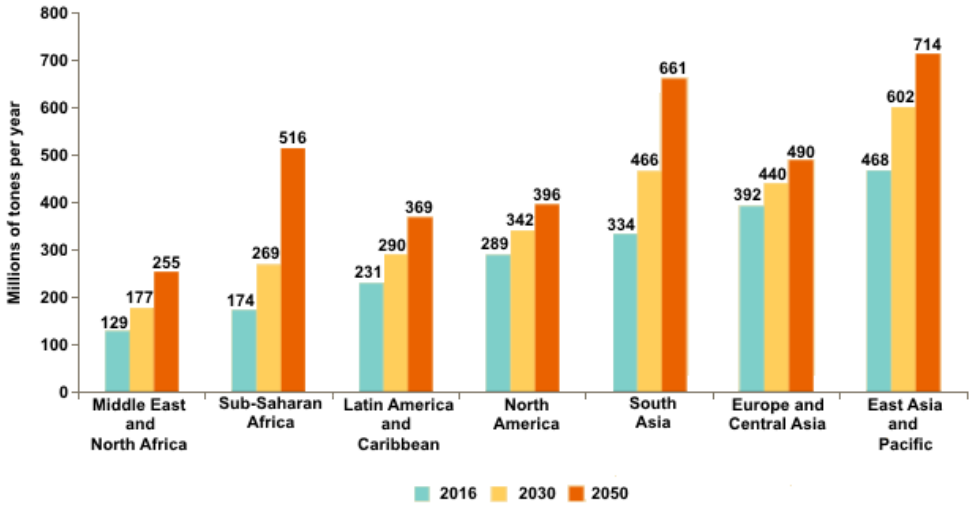

Fig. 1.6 Projected solid waste generation by region

In addition to solid waste, the World Bank also provides a few statistical information about special wastes. Several types of waste including industrial waste, agricultural waste, construction and demolition waste, hazardous waste, medical waste, electronic waste are classified as special wastes. According to Glushkov et al. (Glushkov et al., 2020), solid and industrial waste pollution is one of the main environmental issues worldwide. This statement can be well reasoned with statistical data (Fig. 1.7). The industrial waste is generated in much higher quantities than other special waste. Also, in the countries with available industrial waste generation data,

the trend shows that globally, industrial waste generation (12.73 kg/capita/day) is almost 18 times higher than municipal solid waste (Kaza et al., 2018).

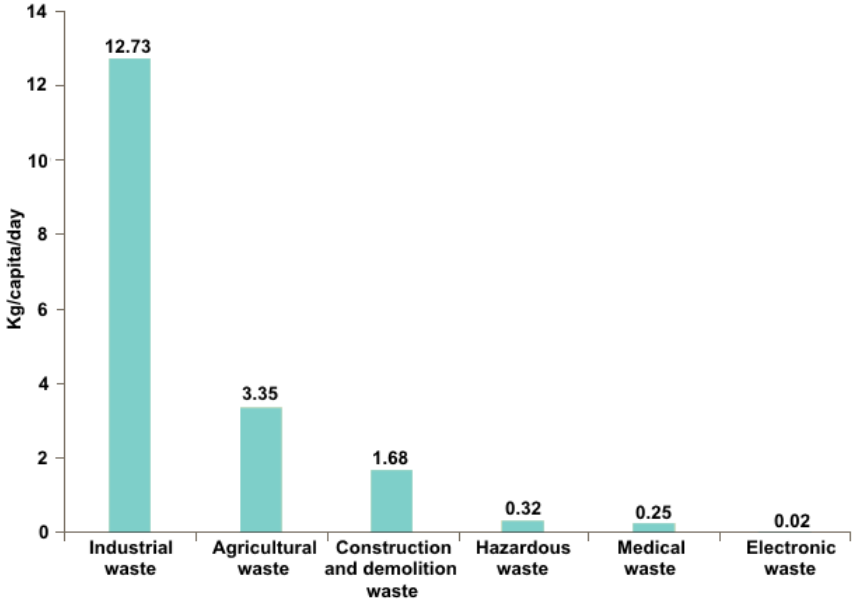

Fig. 1.7 Global average special waste generation (Kaza et al., 2018)

Moreover, the generation of industrial waste grows noticeably with an increase in income level (Table 1.1). Thus, economically developed counties produce the highest amount of industrial waste (42.62 kg/capita/day) (Kaza et al., 2018).

Table 1.1 Industrial waste generation rates (Kaza et al., 2018)

	Industrial waste generation, kg/capita/day
High income	42.62
Upper-middle income	5.72
Lower-middle income	0.36
Low income	No data

Based on the statistical projections presented above, waste management will require even more attention and effort in the future. Currently, trends in countries with high development levels and strong economies show that the sector of waste management is being aimed at attaining a circular economy. The circular economy is orienting on reducing landfilling and boosting reuse (Margallo et al., 2019). Consequently, the solid basis of the circular economy is built on the principle of the waste hierarchy and accordingly, sustainable waste management. Thus, developed countries are making efforts to be able to cope with the growing volume of industrial and solid waste in the most sustainable way. On the other hand, the situation of waste management in developing countries with growing economies is considerably

different. The most applied waste management choice in these countries is waste disposal in open dumpsites or sanitary landfills (Ferronato et al., 2019). Considering that the population and waste generation in these countries will continue to increase rapidly, environmental pollution will expand too. It remains to expect, that the waste management actions and ways performed by developed countries will become a strong example for developing countries that will allow reducing the negative impact on the environment in the future.

1.2. Sustainable waste management

The sector of the waste management evolved over many centuries from the careless disposal into open dumpsites to integrated management systems based on waste hierarchy. The principle of the waste hierarchy has been involved in national and international regulations. Waste hierarchy became an integral part of the EU Waste Framework Directive 2008/98/EC in 2008 (European Parliament and Council, 2008). In 2015, the Circular Economy Strategy from EU COM/2015/0614 (European Commission, 2015) defended the role of waste management based on the principle of the waste hierarchy as the way to lead to the best overall environmental outcome and to get valuable materials back into the economy. Also, the principle of the waste hierarchy was involved in the 12th sustainable development goal (also known as "responsible consumption and production") of the 2030 Agenda for Sustainable Development adopted by the 193 United Nations countries in 2016 (Pires et al., 2019; United Nations, 2016).

The principle of the waste management hierarchy is based on five steps (Fig. 1.8), including the prevention of waste generation, followed by reuse of materials repeatedly and then recycling. Whenever material reuse and recycle cannot be carried out, then recovery opens the possibility to generate energy from waste. And finally, waste disposal to landfills is a last resort (Cucchiella et al., 2017; Fernández-González et al., 2017).

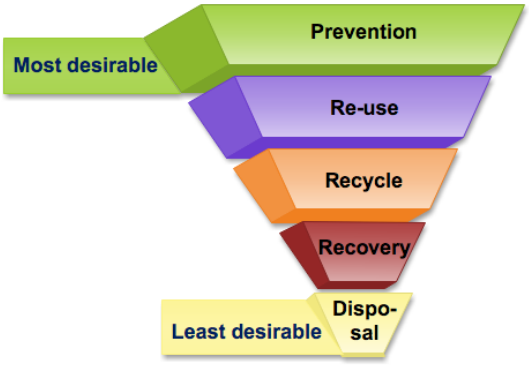

Fig. 1.8 The waste management hierarchy, adapted from Cucchiella et al. (Cucchiella et al., 2014)

Although much effort is made to implement the first three pyramid stages, still there is a part of the wastes that can only be managed by recovery. This recovery stage includes waste-to-energy conversion – the process of recovering energy from waste in the form of heat, electricity, or fuel. Waste-to-Energy conversion technologies can be classified into thermal, mechanical and thermal, thermo-chemical and biochemical technologies (Fig. 1.9). A brief description of these technologies followed by a table of advantages and disadvantages (Table 1.2) is provided below.

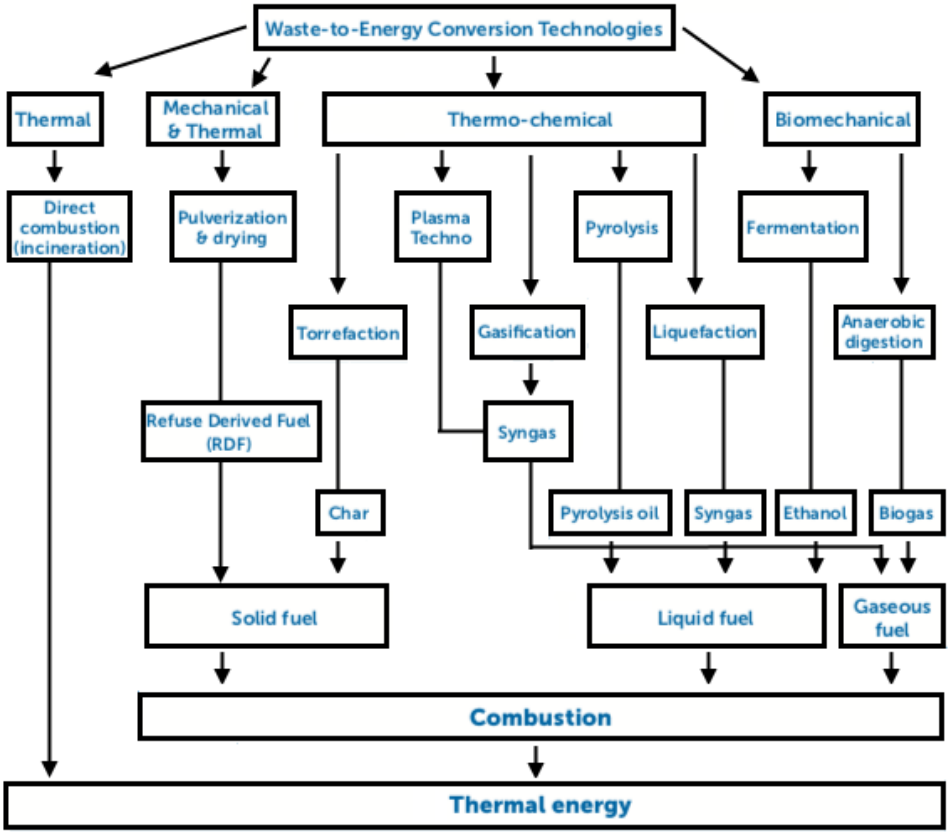

Fig. 1.9 Waste-to-energy conversion technologies (United Nations, 2019b)

Biochemical technologies can be divided into anaerobic digestion and fermentation. Since enzymes, bacteria, and other microorganisms are applied to break down biomass via the biochemical conversion process, these technologies are preferred for the wastes with a high percentage of biodegradable organic matter and high moisture content (Beyene et al., 2018; Kumar et al., 2017). The production of bio-ethanol occurs mainly through the fermentation of organic waste. Anaerobic digestion is defined as a process during which the biodegradation of organic waste and the generation of biogas (mainly CH_4 and CO_2) occurs in the absence of oxygen.

AD process has three main stages. The first stage is hydrolysis in which complex organic materials (i.e. proteins, carbohydrate, fats) are converted into soluble organic materials (i.e. amino and fatty acids, sugars). Fermentation is the second stage of the AD process in which organic molecules are break down into acetic acid, H_2, and CO_2. Methanogenesis is the last stage of the AD where CH_4 and CO_2 are produced from acetic acid and H_2 (AlQattan et al., 2018; Ouda et al., 2016).

One of the ways to recover energy from waste is the production of refuse-derived fuel (RDF). The RDF production process includes the treatment of municipal solid waste and non-hazardous industrial waste to gain fuel with a low concentration of organic matter and with high calorific value (16–18 MJ/kg). The production technology involves different stages, including mechanical separation (removal of unsuitable materials such as glass or metal), pulverisation, and drying. Thus, paper, textiles, wood, rubber, biomass are the wastes from which RDF is made (Sieradzka et al., 2020). Further, RDF is typically used in the combustion process.

Direct combustion (incineration) is described as the primary and most conventional thermal WtE conversion technology. The combustion process occurs in the oxygen environment with respect to the stoichiometric conditions at 850–1200 ºC. It is a well-established technology that could reduce the weight and volume of wastes by approximately 80 % and 70 %, respectively. The end product of combustion is hot combusted gases, mainly composed of carbon dioxide (CO_2), nitrogen (N_2), oxygen (O_2), and non-combustible materials. However, emission of pollutants, including sulfur oxides (SO_x), nitrogen oxides (NO_x), dioxins, and furans, particulate matters (PM) occurs during the incineration. Consequently, the pollutant/emissions control system is used in incinerators to reduce air pollutants (AlQattan et al., 2018; Ouda et al., 2016; Perna et al., 2018). Summarily, waste incineration allows energy retrieval in the form of heat or electricity. Accordingly, the hot combusted gases can be fed to the recovery boiler to generate steam, which can be used directly as a heat carrier or can be transferred to the steam turbine to produce electricity (Malinauskaite et al., 2017).

Torrefaction is another thermo-chemical conversion technology aimed to reduce the components of low molecular weight organic volatile, oxygen-containing functional groups and moisture content in the organic wastes. Generally, torrefaction is performed in an inert atmosphere (e.g. nitrogen) at a relatively lower temperature range from 200ºC to 300ºC. The torrefaction of organic wastes results in the generation of carbon-rich materials, which can be used as a replacement for conventional coal (Okolie et al., 2020; Tong et al., 2018). The torrefied solid material has about 30 % higher energy density than the initial biomass. Hence, this technology offers the way of converting organic matter into energy densified solid fuel with increased heating value, hydrophobicity, and homogeneity. The upgraded solid fuel can be used as a feedstock for the generation of heat, electricity (Iroba et al., 2017; Iwaszko et al., 2020; Niu et al., 2019).

Hydrothermal liquefaction is an alternative thermo-chemical conversion technology usually used for the conversion of wet organic feedstocks (e.g. food waste,

agricultural waste, sewage sludge, algae) into liquid fuel also known as bio-oil. In general, hydrothermal liquefaction is performed in a hot (200–400 ºC) and pressurised (4–25 MPa) water environment seeking to break down the solid structure into liquid products. During hydrothermal liquefaction, water is used as a reaction medium and acts as a reactant and catalyst. Consequently, the organic material can be directly processed without pre-drying process (Chen et al., 2019; Toor et al., 2011). Produced liquid fuel requires purification before its further usage as a fuel for boilers, burners, turbines. Also, bio-oils can be further upgraded into transportation fuels (gasoline, diesel), as their heating value (30–40 MJ/kg) is similar to that of crude petroleum oil. Moreover, hydrothermal liquefaction now is in the transition state from a laboratory pilot scale to a pilot industrial scale (Cao et al., 2017; Gollakota et al., 2018; Watson et al., 2020).

Pyrolysis is the technology for the thermo-chemical conversion of organic materials (carbonaceous substances) to liquid fuels (bio-oils), producer gas (mainly composed of CO, H_2, and CH_4) and biochar. Pyrolysis is performed in the absence of oxygen, (in an inert atmosphere such as nitrogen). Process temperature depends on the type of pyrolysis, but basically, it varies from 300 ºC to 800 ºC. At lower temperature (500–550 ºC), bio-oil, and biochar are the leading products, and at a higher temperature (>700 ºC), pyrolysis gases are the main product (Kumar et al., 2017; Kwon et al., 2019). Additionally, the heating value of pyrolysis gases from municipal solid waste is around 15 MJ/Nm^3. The heating value of bio-oils from carbonaceous waste is 38 MJ/kg. Comparatively, the heating value of biochar from a mixture of biodegradable and non-biodegradable waste is 33.6 MJ/kg. Consequently, the produced gases can be used in gas engines, gas turbines, fuel cells. Bio-oils can be used for the production of electricity, heat, syngas, or chemicals. Biochar can be combusted in pursuance to provide energy (AlQattan et al., 2018; Beyene et al., 2018; Czajczyńska et al., 2017).

Gasification is one of the most known thermo-chemical technology applied for the conversion of carbon-based feedstock (e.g. biomass, solid waste) into producer gas (mainly composed of H_2, CO, CO_2, and CH_4), char and tar. The gasification process appears in the presence of an oxidizing agent (air, oxygen, steam, CO_2, or mixtures of these) at the temperature range of 800–1600 ºC (depending on the type of gasifier). The gasification process includes four steps: feedstock heating and drying (around 100 ºC), devolatilisation also known as pyrolysis (around 125–700 ºC), oxidation (around 1000–1600 ºC) and reduction (around 800–1000 ºC). The major gasification product is synthesis gas which can be used for the production of electricity, heat, or used as feedstock for the production of chemicals and liquid fuels (Kumar et al., 2017; Ramos et al., 2018, 2019). Furthermore, the heating value of the produced gas depends on gasification agents. For example, during the gasification of municipal solid waste, the heating values were equal to 2.4 MJ/kg, 8.5 MJ/kg, and 15 MJ/kg, when the gasifying agents were air, oxygen and steam, respectively (Watson et al., 2018).

Plasma gasification is an emerging thermo-chemical technology suitable to decompose a wide range of organic and inorganic waste, including municipal solid waste, industrial waste, hazardous waste (Ibrahimoglu et al., 2020). During the plasma gasification process, the organic fractions of feedstock are converted into synthesis gas mainly composed of H_2 and CO. At the same time, the inorganics and minerals (e.g. glass, silicones, metals) that are not decomposed pass through a phase change from solid to liquid, and a vitrified slag is eventually produced (Janajreh et al., 2013; Li et al., 2016a). The vitrified slag can be used in the construction materials industry as a building material for brick, tiles, or cement. The synthesis gas can be used for the production of electricity, heat, as well as a chemical feedstock for the production of hydrogen, ammonia, methanol, or other liquid hydrocarbons (Agon et al., 2016). Additionally, plasma can be formed from air, O_2, steam, N_2, Ar, CO_2, or mixtures of these. In the plasma gasification process, a high-temperature (usually between 1500–5500 ºC, in some cases up to 14000 ºC), active plasma environment guarantees decomposition of toxic and unfavorable compounds (e.g. dioxins, furans, polycyclic aromatic hydrocarbons, volatiles) into its primary and harmless elements (in the gas phase). Also, the tar and char formation in the plasma gasification process is limited due to their conversion into synthesis gas or slag (Mazzoni et al., 2017). Thus, the process gives the ability to produce cleaner conversion products. Consequently, this is a substantial advantage plasma provides in comparison with the conventional gasification process (Sanlisoy et al., 2017).

Summarily, all of the above-described waste management methods have their advantages and, in the general sense, can be adapted to the Waste-to-Energy conversion process. However, the comparison of the disadvantages of the Waste-to-Energy methods (Table 1.2) reveals that a considerable part of the methods is more suitable for the decomposition of organic waste. Moreover, waste conversion using biomechanical WtE methods takes long processing time and is sensitive to changes in environmental conditions (e.g. temperature, overloads). The utilisation of incineration, pyrolysis, and gasification still causes secondary pollution and faces challenges converting wet and not homogeneous waste. On the one hand, liquefaction is suitable for the conversion of moisty organic materials. Still, on the other hand, this technology provides a relatively low temperature (200–400 ºC) which is not sufficient for the decomposition of special wastes including industrial, or hazardous waste. Plasma gasification technology has its benefits on the ability to handle various types of waste, including special wastes. Also, this technology has no restrictions to process organic and inorganic wastes. The high-temperature environment ensures a lower generation of pollutants that induces a greenhouse effect. Although this technology seems superior to others, it has its challenges such as high energy requirement, electrodes erosion, and the requirement for their change. Hence, equipment downtime causes additional costs. Furthermore, insufficient stakeholders' awareness of plasma technology leads to safety concerns and causes restricted technology commercialisation. Finally, Munir et al. (Munir et al., 2019) stated that one of the challenges related to plasma gasification usage for Waste-to-Energy processing is

limited understanding of the occurring processes via waste conversion. Also, the authors emphasised that further fundamental research is needed to gain additional information related to the conversion process, reaction kinetics, generated product analysis and thermodynamics that would help to deal with the current situation (partial awareness) by letting to understand the waste conversion process fully. Such research will contribute to the full realisation of plasma technology commercialisation in the future.

Table 1.2 Advantages and disadvantages of Waste-to-Energy technologies (AlQattan et al., 2018; Arena, 2012; Beyene et al., 2018; Cahyanti et al., 2020; Cao et al., 2017; Gollakota et al., 2018; Gray, 2014; Janajreh et al., 2013; Kapusta, 2018; Kumar et al., 2017; Materazzi et al., 2013; Mazzoni et al., 2017; Munir et al., 2019; Okolie et al., 2020; Ouda et al., 2016; Perna et al., 2018; Roser, 2019; Toor et al., 2011; United Nations, 2019b; Watson et al., 2020; Zhang et al., 2012)

Fermentation	
Benefits	**Limitation**
○ Does not contribute to the increase of CO_2 emission	○ Unsuitable for waste containing less organic matter ○ Limited on starch/cellulose/rich waste ○ Long processing time (6–48 h for ethanol)
Anaerobic digestion	
○ Preferred for biomass with high water content ○ Production of nutrient-rich digestate as an organic fertiliser ○ Produced biogas contains a higher amount of CH_4 and a lower amount of CO_2 compared to biogas produced in landfill ○ Cost-effective technology	○ Unsuitable for waste containing less organic matter ○ Sensitivity to temperature shocks and overloads ○ Space requirement ○ Less suitable to high in lignin (woody) material due to more prolonged degradation Long processing time (14–60 days)
Refuse Derived Fuel	
○ Waste stabilisation, sterilisation and size reduction ○ RDF pallets have a high calorific value	○ Land occupation for pallets storage ○ Air pollution from power plants where RDF is used ○ Ash formation and handling in power plant with RDF
Incineration	
○ Reduce waste volume and mass up to 80 % and 70 %, respectively ○ Can handle large amounts of waste ○ Quick treatment time Utilisation of bottom and fly ash of incineration plants in road construction, cement production and recovery of ferrous and nonferrous substances	○ Produces harmful pollutants (dioxins, furans, PM, SO_x, NO_x) ○ Fly ash from incineration poses existential health risks, including respiratory ones, through the carriage of toxic heavy metals such as mercury and lead. ○ Serious corrosion of the incineration system by alkali metals in solid residues and fly ash

	○ Required pollutant/emissions control system ○ High investment, operational and maintenance costs ○ Social opposition
Torrefaction	
○ Produced solid fuel can be used as a replacement to conventional coal ○ Produced solid fuel have hydrophobic nature and reduced biological degradation ○ Produced solid fuel has greater energy density and calorific value than the original biomass material Torrefied pellets generate significantly lower emissions compared with wood pellets at specific energy production	○ Inappropriate for waste containing less organic matter ○ Economic analysis shows that torrefied biomass is not yet competitive to wood pellets, due to the additional investment for torrefaction reactor ○ Required biomass pretreatment before processing it in energy applications
Liquefaction	
○ Appropriate for wet organic materials (pre-drying not required) ○ Water is used as a reaction medium, thus other chemicals are unnecessary ○ Process is versatile and environmentally friendly ○ Lower tar yield compared to pyrolysis	○ Management, purification of produced wastewater ○ Corrosion requires the use of expensive alloys, and the high operation pressures put tough requirements on process components such as feed pumps ○ The high investment cost
Pyrolysis	
○ Reduce waste volume up to 50–80 % ○ Recovers up to 80 % energy from waste ○ Residence time (10–100 min) ○ Produce high-quality fuel ○ Reduces flue gas treatment ○ Reduces land requirements Generated products have higher calorific values	○ Only appropriate for relatively homogeneous waste streams such as wood or plastic waste, agricultural residues, sewage sludge ○ Generation of pollutants (H_2S, HCl, NH_3, HCN, tar, PM) ○ Pyrolytic water production from organic materials ○ Coke production from liquid products ○ Cleaning of by-products ○ Corrosion of metal tubes used in pyrolysis ○ High operational and maintenance costs
Gasification	
○ Reduce waste volume up to 75–90 % ○ Residence time (30–60 min) ○ Limited formation of dioxins, NO_x, and SO_x compared to incineration, thus technology reduces greenhouse gas emissions ○ Bottom ash often produced as vitreous slag that can be used in road construction	○ Only suitable for relatively homogeneous waste streams such as wood waste, plastic waste, agricultural residues, sewage sludge ○ Waste size requirements (particle diameter up to 100 mm) ○ Waste with a high content of moisture cannot be used as a feedstock

	○ Produced syngas often contains a large amount of tar Generation of pollutants (H_2S, HCl, NH_3, HCN, PM, tar, heavy metals, alkaline compounds)
Plasma gasification	
○ Any kind of waste and different waste composition can be used ○ Reduce waste volume up to 90 % ○ Residence time: few seconds for the gas phase, minutes or hours for the liquids and solid (e.g. 30 min – 3 h) ○ No waste size requirements ○ Production of benign vitrified slag which can be used in the construction material ○ Steady-state conditions, fast start-up, and shutdown ○ Higher temperature causes lower production levels of NO_X, SO_X, tars, chars compared to conventional gasification or incineration, thus technology reduces greenhouse gas emissions	○ Requirement for appropriate waste sorting ○ High operating and maintenance cost due to high energy requirements ○ Highly reactive plasma causes electrodes erosion, thus the requirement for change of these components lead to equipment downtime and additional cost ○ Limited society awareness of plasma technology leading to safety concerns ○ Limited technology commercialisation ○ Insufficient understanding of processes

Consequently, the remaining part of this dissertation is intended to introduce the concept and current knowledge about plasma as well as to broaden fundamental research data about waste conversion using plasma technology. In this work, thermal plasma technology is used for the conversion of two types of waste, crude glycerol, which emerges in the industrial sector as a by-product of biodiesel production, and diesel fuel contaminated soil. Since there is an intention based on political decisions to reduce the consumption of fossil fuel worldwide, biodiesel production will likely continue to grow. As a result, the excess of crude glycerol will also increase and will continue to jeopardise biodiesel market stability. Meanwhile, recollecting the projections on energy consumption over the next few decades, fossil fuel still will remain a leader. Hence, the contamination of soil and water with petroleum products will likely continue as well. Therefore, the conversion of crude glycerol into synthesis gas, as well as remediation of petroleum contaminated soil utilising plasma technology seems like a promising alternative in seeking to avoid negative economic and environmental consequences.

1.3. The concept and classification of plasma

Plasma is the fourth state of matter that is often described as either partially or fully ionised gas. In the plasma state, the gas consists of electrons, ions, and neutral species. At least part of the species in plasma is in electronically excited states, as a result of this generating a highly reactive environment for chemical reactions (Zheng et al., 2010).

Traditionally, there are two main types of plasmas: high temperature and low temperature. In this dissertation, the attention is given to the low temperature atmospheric pressure plasmas. Within this type of plasmas, there are two distinct divisions: thermal plasma or "quasi-equilibrium" and non-thermal plasma or "non-equilibrium". The thermal plasma is characterised by a high energy density and equality between the temperature of heavy particles and electrons ($T_h \approx T_e$). In such plasma, a local thermodynamic equilibrium (LTE) exists, and the temperature of the thermal plasma can vary from (2–20)×10^3 K. The atmospheric non-thermal plasma is characterised by a high temperature of electrons and a low temperature of heavy particles ($T_e \gg T_h$) (Gomez et al., 2009; Rahman et al., 2015; Samal, 2017). The higher the difference between the T_e and T_h, the higher the deviation from the LTE conditions exist (Tendero et al., 2006). Whereas, the temperature of the non-thermal plasma may range from 300 K to 2000 K depending on the type of electrical discharges (Nehra et al., 2008).

Additionally, the thermal plasma has higher enthalpy, and temperature, as well as the high material conversion rates, is reached without using catalysts, compared with the non-thermal plasma. Also, thermal plasma has high chemical reactivity, fast process kinetics, and high energy conversion efficiency (Hrabovsky et al., 2018; Rahman et al., 2015). These features are particularly useful in completely breaking down contaminants or waste. Therefore, thermal plasma was chosen for waste conversion research presented in this dissertation.

1.4. The generation of thermal plasma: types of plasma torches

The generation of thermal plasma can be achieved by using a direct current (DC), an alternating current (AC), a radio frequency induction (RF), or a microwave discharge (MW) (Sauchyn et al., 2012).

RF plasma torch usually consists of an electromagnetic coil and a cylindrical ceramic tube (Fig. 1.10 a).

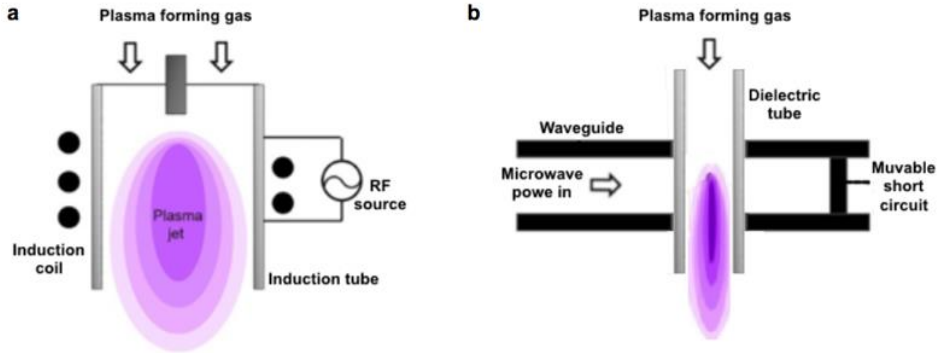

Fig. 1.10 Thermal plasma torches: a – radio--frequency inductive-coupled plasma, b – microwave plasma (Kim et al., 2019; Murphy et al., 2018)

The induction heating mechanism provides the energy needed to generate plasma. Hence, an oscillating current in the coil produces an alternating magnetic field inside the tube where an electrically conducting medium (i.e., plasma) is present. Under the alternating magnetic field, eddy currents, which disperse heat via the Joule heating process, are produced in the medium. The generated energy is sufficient for the continuous ionisation of the injected gas, thus providing plasma sustainment. Temperatures in RF inductive-coupled plasmas range from 3000 K to 10000 K and are relatively low compared to DC thermal plasma arcs (8000–16000 K). RF plasma torches can be used in the material processing field (e.g. nanoparticle production). However, due to the usage of oscillator electronics, RF plasma systems exhibit low efficiency (40–70 %) (Kim et al., 2019; Murphy et al., 2018; Ruj et al., 2014).

The most common design of microwave plasma torch is a tube (ceramic or quartz) passing through a waveguide (Fig. 1.10 b). The waveguide is tuned, so the electric field is maximum at the location of the tube. The plasma forming gas flows through the tube, which is transparent to microwave radiation, intersecting with a rectangular waveguide to initiate the discharge. The injection of the gases guarantees the stabilisation of electromagnetic surface waves launched from a microwave source. This type of plasma can be applied to material processing (e.g. the fabrication of nanomaterials) (Bogaerts et al., 2018; Kim et al., 2019; Murphy et al., 2018). However, MW plasma is not widely used as DC and RF plasmas.

In DC plasma torch, applied high-voltage between cathode and anode guarantees the initial generation of the electric arc in DC plasma torch and gases flow around the arc column for heating via conductive, convective, and radiative heat exchanges (Kim et al., 2019). Furthermore, the DC plasma torches can be divided into transferred and non-transferred arc torches (Fig. 1.11).

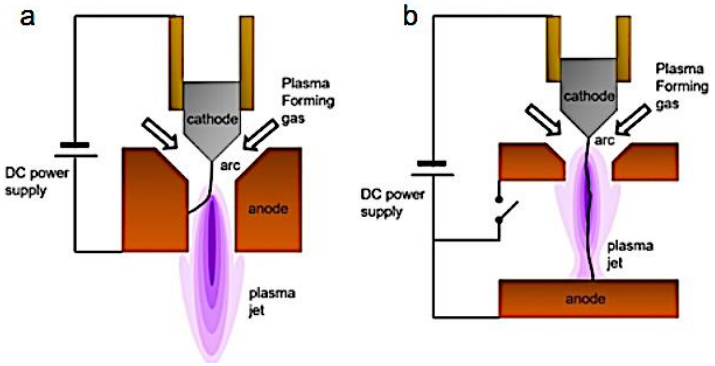

Fig. 1.11 Thermal plasma torches: a – non-transferred arc, b – transferred arc (Kim et al., 2019)

In terms of the transferred arc plasmas, one of the electrodes (anode) can be the treated material and is placed in an electrically grounded metallic vessel (Fig. 1.11 b). Hence, an electrically conductive material should be chosen as a reacting material, most often graphite (Huang et al., 2007; Safa et al., 2014). This type of torches can produce extremely high thermal fluxes since the plasma arc is formed outside the

water-cooled body of the torch. Thus, temperatures in DC transferred arc plasmas ranges from 12000 K to 20000 K. Moreover, transferred arc plasma can be used in arc welding, plasma cutting, melting processes, and waste treatment (Murphy et al., 2018; Ruj et al., 2014; Tatarova et al., 2014).

The DC non-transferred arc torches are those where a high-temperature arc is contained inside the discharge chamber of the plasma torch and it interacts with a flowing gas to produce a hot jet into which the material to be processed can be injected for in-flight melting and vaporisation (Fig. 1.11 a) (Gomez et al., 2009; Tatarova et al., 2014). Temperatures in DC non-transferred arc plasmas ranges from 8000 K to 16000 K. Li et al. (Li etal., 2012) pointed out that this type of the torches is one of the most widely used thermal plasma devices which operate under atmospheric pressure. Typically, this type of plasma can be used for plasma spraying, gasification, waste treatment (Murphy et al., 2018).

Summarily, in materials processing, the DC arc plasmas dominate because they are relatively insensitive to the changes in process conditions, have a more stable operation (the arc is more stable), and better process control. Moreover, DC plasma systems exhibit efficiency (above 70 %) higher than RF plasma systems (40–70 %) (Kim et al., 2019; Tang et al., 2013; Tatarova et al., 2014). However, a more significant drawback of DC arc plasmas is electrode erosion, and the neediness to replace them from time to time. After the evaluation of plasma torches benefits and limitations, the DC non-transferred thermal plasma was chosen to apply for the waste (crude glycerol and diesel fuel contaminated soil) conversion research presented in this dissertation.

1.5. The generation of thermal plasma: types of plasma forming gas

Plasma technologies are based on the generation of charged particles (electrons, ions) and reactive radicals (Fig. 1.12).

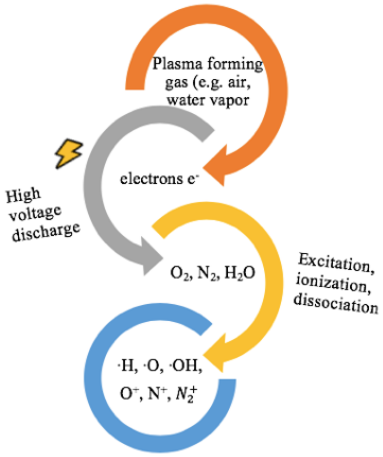

Fig. 1.12 Simplified scheme of plasma formation, adapted from Wang et al. (Wang et al., 2014a)

These plasma species initiate and accelerate plasma-chemical reactions. The type of radicals depends on the type of gas used for the plasma formation. Generally, the use of Ar, N_2, H_2, O_2, and air as a plasma forming gas has become a traditional choice (Chau et al., 2011; Tang et al., 2013). Especially air has become preferable due to its easy accessibility and utilisation. However, the air has a high amount of nitrogen, and the formation of unfavourable NO_x can be obtained. Also, atomic N, N^+, N_2^+ have lower oxidative potentials compared to ·O radicals (Wang et al., 2010). The argon plasma has low enthalpy and low thermal conductivity, hence the lower degradation potential of organic pollutants compared to air or oxygen plasmas. Currently, much attention attracts plasma torches operating on water vapour/steam. Water vapour consists of hydrogen and oxygen; besides, atomic hydrogen has higher thermal conductivity than atomic nitrogen or oxygen (Rutberg et al., 2013a). Also, water vapour plasma has a high enthalpy and a high oxidation-reduction capacity (Hrabovsky et al., 2017; Ni et al., 2012). This plasma contains ·H, ·O, and ·OH radicals, and the latter one is considered the second most reactive species next to fluorine atom (Cheng et al., 2016). Also, ·H radicals are significantly more reactive than ·O radicals (which are the leading radicals in the O_2 or air plasmas). Thus, this infers that the plasma environment consisting of ·H, ·O, and ·OH radicals can induce more intensive decomposition of the organic pollutants such as diesel fuel, or crude glycerol. Furthermore, during the operation of the DC water vapour plasma torches instead of pure water a mixture of gas and water vapour is usually used, thus ensuring the reduction of the cathode erosion as well as enabling to extend the lifetime of the system.

1.6. Parametric characteristics of the plasma torches

Before the practical usage of the plasma technology for waste or another material conversion, it is crucial to establish the parametric characteristics of the plasma torch. It is the only way to ensure a stable operating mode because every plasma torch has its inherent voltage-current characteristics (VCC) according to its geometry, flow rate, and type of the working gas used (Pan et al., 2011). Hence, voltage-current characteristics are the most important characteristics of the plasma arc, helping to determine optimal parameters of the plasma torch. Typical examples of voltage-current characteristics of arc, which is burning in channels with different diameters, are given in Fig. 1.12. In the case, when channel walls influence the properties of the arc and part of the plasma arc energy is transferred to the channel walls, or when channel walls restrict the growth of the arc diameter via the increase of the arc current, the curve of the voltage-current characteristic become rising (Fig. 1.12 a). Such type of curve shows a stable work of the plasma torch. In the case, when arc burns in the large-diameter channel, the influence of the channel walls on the arc properties is small, and the current increase causes a decrease of the arc voltage. Thus, the curve of the voltage-current characteristic becomes falling (Fig. 1.12 b). Such type of curve shows the unstable work of the plasma torch (Boulos et al., 1994; Howatson, 1976).

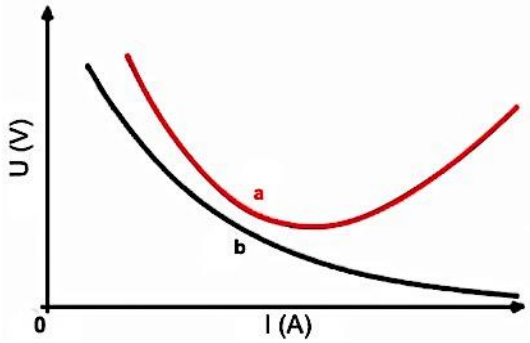

Fig. 1.12 Voltage-current characteristics of the plasma arc in the channel with: a – smaller diameter limited by walls, b – larger-diameter (Howatson, 1976)

A number of voltage-current characteristics evaluations have been performed for developing plasma technologies. Several examples are provided below.

Mohsenian et al. has evaluated the VCC of twin DC thermal plasma torch applied to polymer waste treatment (Mohsenian et al., 2015). Researchers stated that voltage-current characteristics depend on working gas flow rates of the plasma torch and found that arc voltage increases with the increase of argon gas flow rate (from 21 slpm to 41 slpm). Lee et al. investigated the voltage-current characteristics of the DC arc plasma torch with a distributed anode spot (Lee et al., 2007). They have noticed the same tendency as Mohsenian et al.; the greater the argon flow rate, the higher the arc voltage is (Fig. 1.13). Also, researchers noted that all of the voltage-current characteristics have decreasing curves that slightly increases at the highest arc currents.

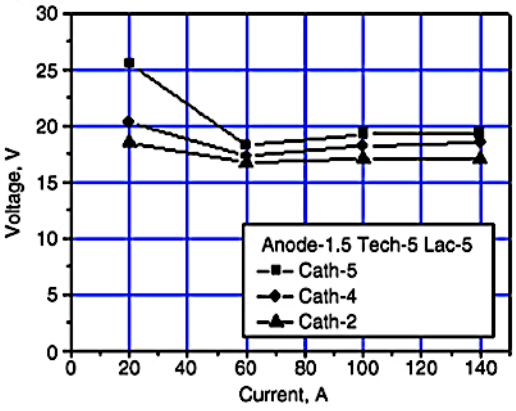

Fig. 1.13 Voltage-current characteristics dependence on the Ar flow rate in the cathode channel (W cathode ø 3.2 mm; d_A =1.5 mm; L_{AC} =2 mm; Q_{ArT} =5 nl/min; Q_{ArC} =2–5 nl/ min) (Lee et al., 2007)

Rutberg et al. (Rutberg et al., 2013b) have established the voltage-current characteristics of a three-phase steam-air plasma torch designed for gasification of

high-caloric waste. Researches compared VCC for different ratios of steam/air flow rates (Fig. 1.14) and noticed that growth in the proportion of air causes a decrease in voltage. Also, they stated that VCC is dropping in all cases due to the discharge temperature increase with the growth of the current.

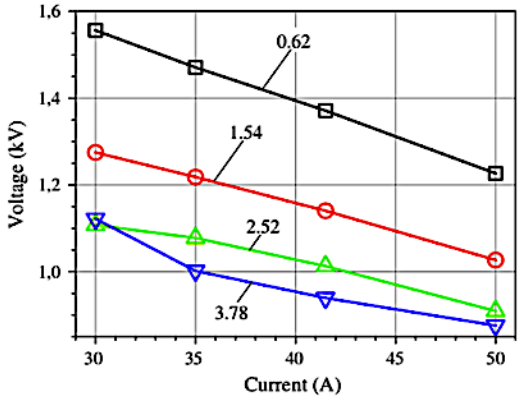

Fig. 1.14 Voltage-current characteristics of steam-air plasma torch; steam flow rate is equal to 3.7 g/s, and air flow rate is shown for different regimes in g/s (Rutberg et al., 2013b)

Liu et al. (Liu et al., 2018) investigated voltage-current characteristics of DC steam plasma torch. The effect of the arc current, the diameter of the stepped anode and the flow rate of the working gas on the arc voltage are shown in Fig. 1.15.

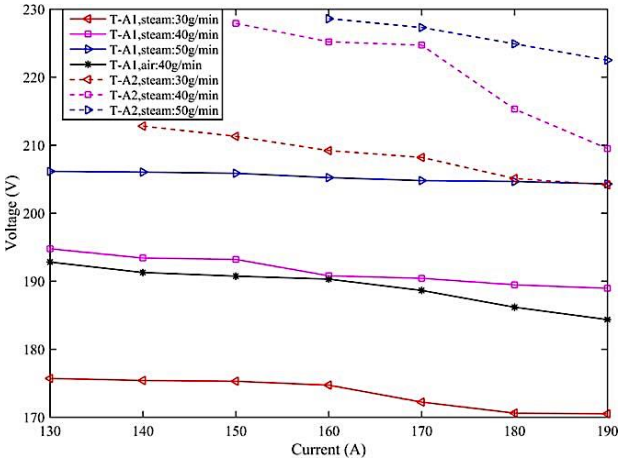

Fig. 1.15 Voltage-current characteristics of steam plasma torch using different anodes T-A1 (d_1, d_2 equal to 10 and 18 ($x10^{-3}$ m)) and T-A2 (d_1, d_2 equal to 20 and 30 ($x10^{-3}$ m)). N_2 as shielding gas flow is 25 g/min (Liu et al., 2018)

Researchers noticed that the arc voltage slightly decreases with the increase of the arc current when the steam flow rate is constant. Also, they noted that the arc voltages are higher when the anode diameter is larger (T-A2). Moreover, they found out that the arc voltages increases noticeably with the increase of the steam flow rate

when the arc current is constant. Finally, scientists stated that the arc voltage depends on the type of plasma forming gas and emphasised that the arc voltage is lower when air is used as a working gas compared to steam at the same gas flow rate (40 g/min) (Liu et al., 2018).

The determination of plasma torch parametric characteristics applying the experimental method gives the experimental data allowing to gain a complete description of the plasma torch characteristics. However, the experimental method is expensive and requires an extended period for the study as well as a heavy workload. Thus, the second, mathematical method based on the theory of similarity is often applied. This method allows obtaining a generalisation for calculation of the discharge characteristics in the plasma torch without a large number of experiments. Hence, only some experiments are required to apply the theoretical formulas (Bublievsky et al., 2015; Li et al., 2005). Consequently, the latter method is also used in this dissertation. More detailed information on the application of similarity theory to determine plasma torch parametric characteristics is given in the methodology section.

1.7. Crude glycerol – a by-product of biodiesel production

Fluctuating crude oil prices, domestic policies (e.g. mandates and production subsidies), aspiration to increase the share of renewable fuels in overall energy balance and willingness to reduce the net climate impact of energy use, encouraged production and consumption of biodiesel worldwide (Deepayan et al., 2018; Naylor et al., 2017, 2018). Correspondingly, global biodiesel production (Fig. 1.16) considerably increased from 2.1 billion liters in 2004 to 37.3 billion liters in 2017 (REN21, 2017, 2018).

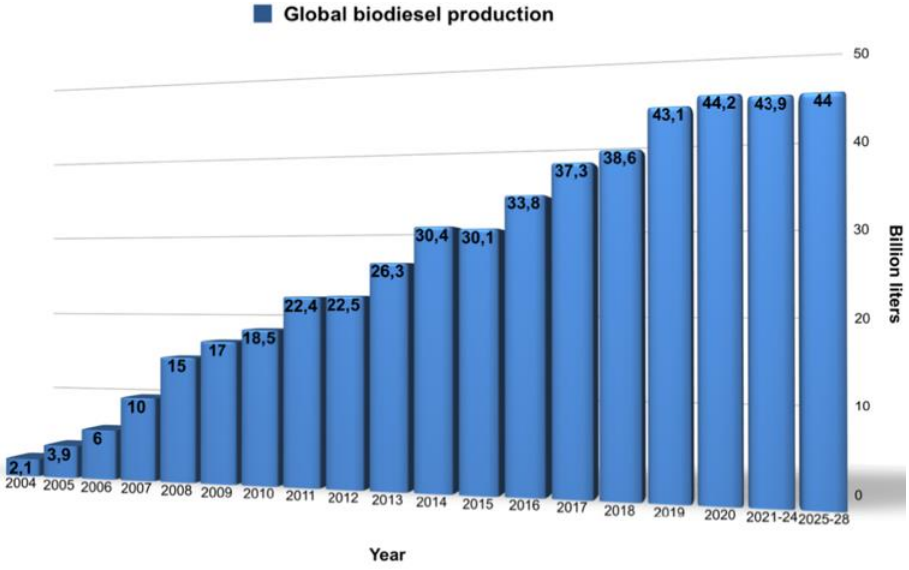

Fig. 1.16 Global biodiesel production from 2004 to 2017 and projection of its production from 2018 to 2028 (OECD-FAO, 2017, 2019; REN21, 2017; REN21, 2018)

Also, it is expected that the world biodiesel production will grow from 37.3 billion liters in 2017 to 44 billion liters by 2028 (OECD-FAO, 2017, 2019). Furthermore, significant changes in biodiesel utilisation in the European Union (EU) transport sector were observed between 2010 and 2018 (Fig. 1.17). Consumption of biodiesel raised from 8018 ktoe to 13906 ktoe (EurObserv'ER, 2010, 2019).

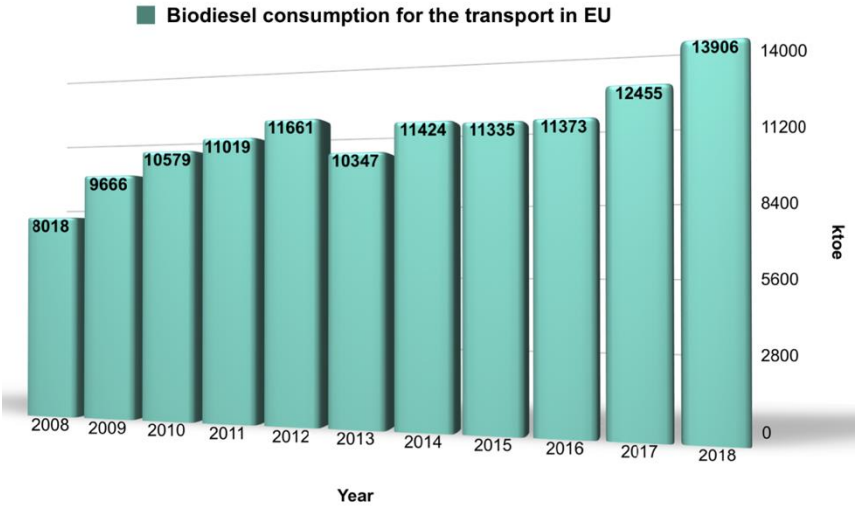

Fig. 1.17 Biodiesel consumption for the transport sector in European Union from 2008 to 2018 (EurObserv'ER, 2010, 2011, 2012, 2013, 2014, 2015, 2016, 2017, 2018, 2019)

The EU began to use biodiesel as a substitute for conventional diesel, which traditionally prevailed in the EU transport before. This tendency allowed the EU to become one of the leading biodiesel producers in the world, comprising 37 % of global output (Naylor et al., 2017; Torry et al., 2011; UFOP, 2018). Moreover, the EU's general demand for diesel fuel continues to rise. The latter trend as well as domestic policies further induces the expansion of biodiesel production in the EU (Deepayan et al. 2018; Naylor et al., 2017). It is expected that the European Union, the United States, Brazil, Argentina, Indonesia, considered as the main biodiesel producers, will further continue their leadership in the development of the biodiesel market.

However, even if biodiesel is acknowledged as a sustainable substitute to fossil fuels (Anitha et al., 2016; Nanda et al., 2016), the production of biodiesel via transesterification process has a by-product – crude glycerol. Crude glycerol usually accounts for 10 % of the total volume of biodiesel production (Algoufi et al., 2017; Bagheri et al., 2015; Kong et al., 2016; Sanchez et al., 2012; Yus et al., 2018). As a result, increasing biodiesel production rises surplus generation of glycerol. Thus, it negatively affects the biodiesel market and causes an environmental problem because it cannot be safely disposed to the environment (Da Silva et al., 2009; Rahman et al., 2017). Since crude glycerol is not hazardous to the environment, it still contains impurities such as alcohol (typically methanol), free fatty acids, fatty acids methyl

esters, organic and inorganic salts, monoglycerides, diglycerides, vegetable colours, oil, alkali metals, soaps, diols, and water (Hájek et al., 2010; Liu et al., 2012; Varrone et al., 2013; Yang et al., 2012). These impurities prevent the use of crude glycerol in lieu of pure glycerol in the pharmaceutical, food, cosmetics, cleaning industries. Furthermore, the removal of impurities from crude glycerol is economically unprofitable (He et al., 2017; Menezes et al., 2018).

Nevertheless, conversion of excess crude glycerol into higher value-added products, including alcohol, bio-oil, biomethane, synthesis gas (H_2+CO), and hydrogen looks like a viable and promising option (He et al., 2017). Essentially, the generation of synthesis gas and hydrogen is a potentially-economic and environmentally-benign solution. Thus, synthesis gas can be used to produce electricity, chemicals and/or liquid fuels (e.g. dimethyl ether, methanol, hydrogen, methane, ammonia) (Jia et al., 2017; Sanlisoy et al., 2017). Hydrogen, as an environmentally friendly energy carrier, can be used in fuel cells and the transport sector. Also, it can be used in the pharmaceutical and chemical industries (Bepari et al., 2017; Schwengber et al., 2016a). Consequently, diverse methods such as fermentation, liquefaction, digestion, steam reforming, pyrolysis, gasification are to be used for the conversion of crude glycerol (Fig. 1.18) (He et al., 2017).

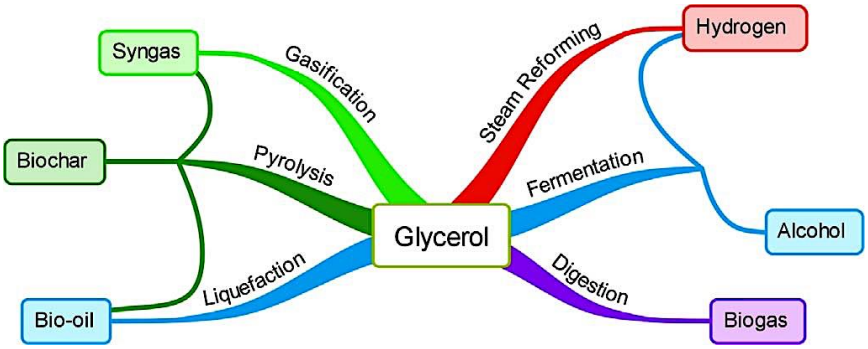

Fig. 1.18 Glycerol conversion methods and products that can be received from glycerol (He et al., 2017)

Moreover, the utilisation of thermal plasma for crude glycerol gasification provokes a great interest. Firstly, the conversion process is fast in time and any additional materials or special catalysts are not required. Secondly, the generation of higher value-added products, as well as the complete decomposition of organic compounds, is obtained. Thus, crude glycerol gasification into syngas can possibly promote economic development by increasing the market value of glycerol and biodiesel. This was obtained in a number of studies. Zhang et al. (Zhang et al., 2017b) performed the gasification of glycerol into synthesis gas by a rotating DC arc plasma. It was determined that carbon conversion increased from ~35 % to ~100 % with the increase in input power from 7 kW to ~17 kW. However, carbon conversion decreased with the increase of the feeding rate of crude glycerol from 30 g/min to 50g/min. Moreover, the energy conversion efficiency of 66 % and a gaseous mixture of CO (38

%) and H_2 (56 %) were observed. Yoon et al. (Yoon et al., 2013) used microwave plasma to gasify crude glycerol. It was observed that increasing O_2/fuel ratio from 0 to 1.2, caused the decrease of the cold gas efficiency from ~98 % to ~5 % and decrease of the synthesis gas heating value from ~3000 kcal/Nm^3 to ~100 kcal/Nm^3. Moreover, increasing O_2/fuel ratio induced the increase of the carbon conversion from ~80 % to ~93 %. Furthermore, it was also found that increasing microwave power from 1 to 1.8 kW, raised the H_2 and CO content in the synthesis gas. It also led to the increased synthesis gas heating value, carbon conversion, and cold gas efficiency. Also, Yoon et al. (Yoon et al., 2010) used a bench-scale entrained flow gasifier for the utilisation of the crude glycerine with air as a gasification agent. It was stated that the values of carbon conversion and cold gas efficiency increased by more than 75 % and 60 %, respectively, as the air ratio increased from 0.17 to 0.32. Besides, the H_2 and CO content in the producer gas slightly increased as the air ratio increased. Watanabe et al. (Watanabe et al., 2013) performed the decomposition of glycerine by DC water plasma torch at atmospheric pressure. It was found that at glycerine concentration of 5 mol % and the power of the plasma torch being equal to 0.55–1.05 kW, glycerine was decomposed mainly into H_2 (68.9–71.1 %), CO_2 (18.9–23.0 %), and CO (0.2–0.6 %). The content of produced synthesis gas (H_2 and CO) was equal to 69–72 %. Nevertheless, traces of formic acid (HCOOH) and formaldehyde (HCHO) were detected in the liquid effluent. Based on experimental research it was concluded that the waste treatment process using DC water plasma torch is suitable for being an alternative green technology for organic waste decomposition. Tamošiūnas (Tamošiūnas, 2014) in his dissertation, presented the research of glycerol conversion by using DC thermal plasma torch at atmospheric pressure. Water vapour was used as a plasma forming gas. The researcher evaluated the effect of the water vapour flow rate (2.63–4.48 g/s), glycerol flow rate (2–4 g/s), and plasma torch power (48–56 kW) on the glycerol conversion process. Also, the quantification of the plasma system in terms of energy efficiency and specific energy requirement was carried out. Obtained results showed that the generation of producer gas increased from 54 % to 59 %, when the $H_2O/C_3H_8O_3$ ratio increased from 1.3 to 2.2 at the constant glycerol flow rate (2 g/s), and at varying water vapour flow rate from 2.63 g/s to 4.48 g/s. Also, it was noted that with the increase of glycerol content from 2 g/s to 4 g/s at the plasma torch power of 53 kW and water vapour flow rate of 3.71 g/s, the generation of producer gas increased from 59 % to 65 %, whereas at the plasma torch power of 56 kW and water vapour flow rate of 4.48 g/s, the generation of producer gas increased from 57 % to 62 %, respectively. Moreover, it was noticed that with an increase of the plasma torch power from 48 kW to 56 kW, producer gas generation from glycerol conversion increased from 59 % to 89 %, while the glycerol conversion to char decreased from 40 % to 11 %. Furthermore, it was stated that at the constant glycerol flow rate (2 g/s), the energy conversion efficiency increased from 40 % to 51 %, whereas the specific energy requirement decreased from 72 kJ/mol to 59 kJ/mol, when the water vapour flow rate and plasma torch power varied from 2.63 g/s to 4.48 g/s and 48 kW to 56 kW, respectively. In the case, when the glycerol flow rate was equal to 4 g/s, the

energy conversion efficiency increased from 51 % to 52 %, whereas the specific energy requirement decreased from 46 kJ/mol to 44 kJ/mol, when water vapour flow rate and plasma torch power ranged from 3.71 g/s to 4.48 g/s and 53 kW to 56 kW, respectively. The researcher concluded that the better glycerol conversion using thermal water vapour plasma could be achieved at the higher water vapour flow rate and plasma torch power. Also, the author inferred that future work should focus on the establishment of the optimal glycerol conversion process (Tamošiūnas et al., 2016).

Although the above-presented research shows that plasma can be used for the conversion of crude glycerol, there is still insufficient data to achieve optimal process performance. The information about the mass and energy balance of the plasma technologies is weak. Thus it is difficult to evaluate the efficiency of the presented plasma systems. Consequently, one of the aims of this dissertation was to continue the research of crude glycerol conversion into synthesis gas using a direct current (DC) thermal arc plasma, which was started by Tamošiūnas and presented in his dissertation. The latter one was prepared in Lithuanian Energy Institute, Plasma Processing Laboratory, as well as this present dissertation. Secondly, the purpose was to evaluate the crude glycerol gasification system in terms of the H_2/CO ratio, the lower heating value, the carbon conversion efficiency, the cold gas efficiency, the energy conversion efficiency, and the specific energy requirement. And finally, to evaluate the mass and energy balance of the proposed technological system allowing to determine the effectiveness of the thermal plasma gasification system. In such a way, seeking to contribute and supplement existing crude glycerol conversion experimental studies results and general information of this research area.

1.8. Soil contamination with petroleum products

Soil pollution refers to the presence in the soil of a chemical or substance out of place and/or present at a higher than the normal concentration that has adverse effects on any non-targeted organism. Soil pollution generally is inconspicuous, meaning that frequently it cannot be visually seen and directly assessed. Consequently, soil pollution is identified as the third threat to soil functions in Europe, obscured only by soil erosion (first threat) and organic matter decline (second threat). The major sources of soil pollution are of anthropogenic origin. The main anthropogenic sources of soil pollution are the chemicals used in or produced as by-products of industrial activities, municipal and domestic wastes, including wastewater, agrochemicals, and petrol-derived products. These chemicals are released in the environment in two ways: accidentally (e.g. oil spills, leaching from landfills) and intentionally (e.g. use of fertilisers, pesticides) (Cachada et al., 2018; FAO and ITPS, 2015; JRC, 2018; Rodríguez-Eugenio et al., 2018).

The breakdown of the main sources causing soil contamination in Europe as a percentage of sources over the total number of sources identified are shown in Fig. 1.19. European shares have been calculated as average over 22 European Economic Area countries. More than two-thirds of the local soil contamination is caused by

waste disposal and treatment (38.1 %), as well as industrial and commercial activities (34 %). The remaining soil contamination comes from storage (10.7 %), others (8.1 %), transport spills on land (7.9 %), and military (3.4 %). Nuclear operations induce negligible soil pollution (0.1 %). The explanation of what compose "storage" and "others" is given in Table 1.3 (EEA, 2014).

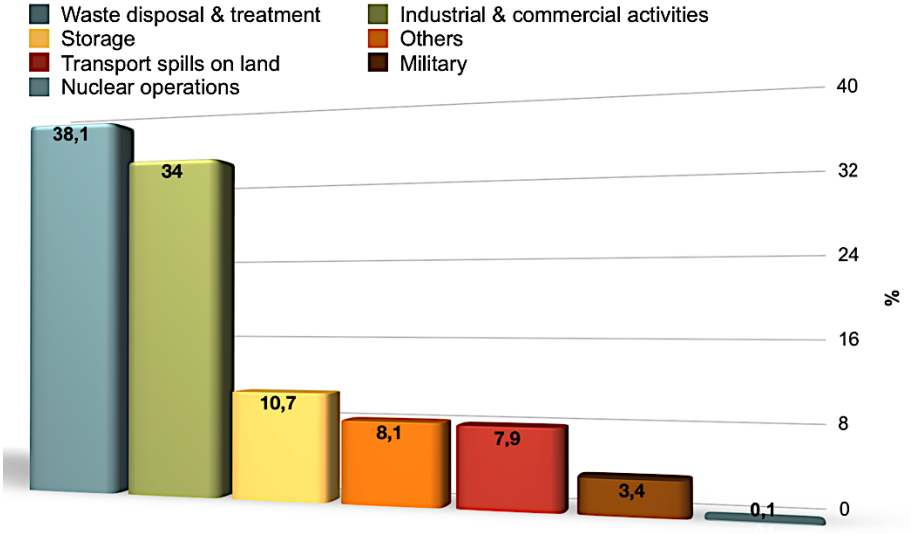

Fig. 1.19 Key sources of soil contamination in Europe, adapted from the European Economic Area (EEA, 2014)

Table 1.3 Distribution of soil contamination sources, adapted from the European Economic Area (EEA, 2014)

Industrial and commercial activities	○ industrial and commercial services ○ mining ○ oil extraction and production ○ power plants
Storage	○ oil storage ○ oil extraction and storage sites ○ obsolete chemical storage ○ storage of manure ○ other storage
Transport spills on land	○ oil spills ○ other hazardous substance spills
Military	○ military operations ○ war-affected areas
Others	○ other sources (e.g. shooting ranges) ○ agricultural sites (pesticide and mineral fertilisers storages, farms) ○ wastewater treatment facilities

The main contaminant categories affecting soil in Europe are heavy metals (35 %), mineral oils (24 %) followed by polycyclic aromatic hydrocarbons (11 %), aromatic hydrocarbons (10 %), and chlorinated hydrocarbons (8 %) (Fig. 1.20). The rest contamination belongs to phenols (2 %), cyanides (1 %), and other contaminants (9 %) (EEA, 2014).

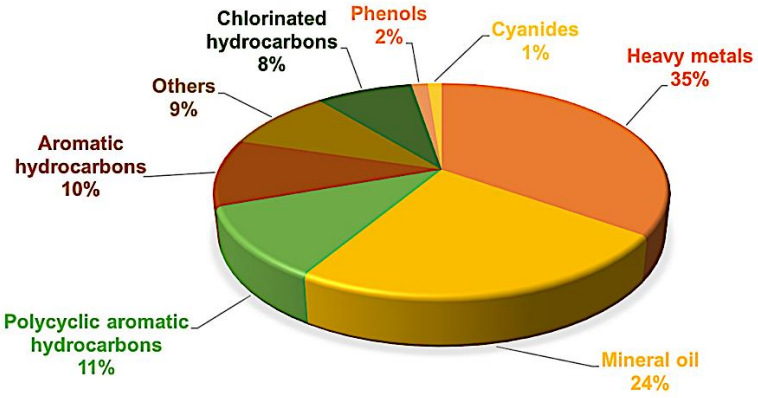

Fig. 1.20 Contaminants affecting soil in Europe, adapted from the European Economic Area (EEA, 2014)

Additionally, according to the European Environmental Agency, the production sector causes 60 % of contribution to local soil contamination in Europe, while the service sector induces 32 %. Moreover, gasoline stations are the main sources of soil contamination (15 %) for the service sector (EEA, 2014).

Thus, soil contamination by petroleum hydrocarbons is a frequent problem worldwide, especially since global economic activities are strongly related to petroleum-based energy sources (Lominchar et al., 2018; Scafutto et al., 2017). Among various products, which constitutes the term petroleum hydrocarbons, diesel fuel is recognised as one of the most common soil pollutants due to its broad usage in transport (cars, trucks, trains, ships), mining equipment, excavation machinery (Khudur et al., 2015; Lominchar et al., 2018; Reşitoğlu et al., 2015). Also, due to its penetration into the soil in various ways such as leakage from underground storage tanks, accidental spills, improper waste disposal practices, and leaching landfills (Lahel et al., 2016; Roy et al., 2014). Generally, diesel fuel consists of saturated hydrocarbons (alkanes, cycloalkanes, such as naphthenes) and unsaturated hydrocarbons (olefins, aromatics), which contains C_9-C_{27} carbon atoms. Also, a slight content of sulphur, nitrogen, oxygen, and metal compounds constitutes diesel fuel (Chen et al., 2017; Demirbas et al., 2017; Vempatapu et al., 2017). The difference in the chemical composition of crude oil, as well as dependence on different refining processes and standards, causes a variation of hydrocarbons mixture from which diesel fuel is produced (Aleme et al., 2010; Szymkowicz et al., 2018). Because of wide and careless usage of crude oil in the form of various fuels, it is hard to avoid any leakage or accidents, which causes negative impact on terrestrial ecosystems via

soil contamination. Diesel fuel, gasoline, greases, kerosene and other petroleum hydrocarbons strongly adsorbs and remains in the soil, which is difficult to eliminate such pollutants from this medium (Bocos et al., 2015; Sandu et al., 2017). Thus, the remediation of these contaminants is essential.

Various soil remediation technologies such as biological (e.g. phytoremediation), chemical (e.g. chemical oxidation), physical (e.g. soil flushing), thermal (e.g. thermal desorption), physicochemical (e.g. solvent extraction), and integrated (e.g. physical-biological, chemical-biological) are used for this purpose (Lim et al., 2016). However, some of these technologies have drawbacks including long treatment time, required specific conditions for the growth of the microbial community, consumption of chemical reagents and generation of secondary pollutants (Boulakradeche et al., 2015; Wang et al., 2015; Zhang et al., 2017a).

In the meantime, Ma et al. (Ma et al., 2018) indicated that remediation technology, which can work in a short timeframe and is highly efficient, has a possibility to emerge as a priority for redeveloping contaminated soil sites. Recently, plasma technologies have attracted attention due to advantages of high efficiency, no special requirements for the pre-treatment of the raw soil, no needs of supplementary materials (all energy required for chemical processes comes from plasma), rapid remediation process, broad applicability for diverse contaminants and different concentrations, and avoidance of secondary pollution of soils (Tamošiūnas et al., 2012; Zhang et al., 2017a).

One of the first research of kerosene contaminated soil treatment with non-thermal dielectric barrier discharge plasma was performed by Redolfi et al. (Redolfi et al., 2009, 2010). Researches pointed out that the total degradation efficiency of kerosene reached nearly 90 %. Wang et al. (Wang et al., 2014b, 2014a) used a multi-channel pulsed discharge plasma system to treat soil contaminated with organic pollutant (p-Nitrophenol). In both cases, it was determined that approximately 45.7–90.7 % of p-Nitrophenol was degraded depending on the voltage used. Aggelopoulos (Aggelopoulos, 2016) investigated remediation of soil contaminated by 2,6-dichloropridine and n-dodecane using a non-thermal DBD reactor. Both contaminants were completely degraded after the plasma treatment process regardless of soil type and initial contaminant concentration. Lu et al. (Lu et al., 2017) investigated the remediation of soil contaminated by polycyclic aromatic hydrocarbons using pulsed corona discharge plasma. Researches indicated that after 40 minutes of the remediation process, PAHs degradation efficiency varied from 50.5 % to 74 % depending on the initial pollutant concentration (200 mg/kg–50 mg/kg, respectively). Moreover, Li et al. (Li et al., 2016b) carried out remediation of phenanthrene contaminated soil using pulsed DBD plasma and referred that removal efficiency reached up to 89.8 % depending on the voltage used. Zhan et al. (Zhan et al., 2019) used pulsed corona discharge plasma to treat soil contaminated with gasoline. Researchers performed a broad study by evaluating various factors (e.g. gas flow rate, type of the plasma forming gas, initial gasoline concentration, soil pH, etc.) influents to contaminated soil treatment success. In the case of gas flow rate, it was determined

that degradation efficiency of gasoline increased from 70 ± 3.2 % to 83 ± 3.9 % with the increase of gas flow rate from 0 L/min to 0.6 L/min, respectively, and decreased to 60 ± 3.3 % when flow rate was 6 L/min. Also, it was noted that the gasoline degradation efficiencies were 86 ± 4.3 %, 84 ± 5.3 %, 39 ± 2.6 %, and 23 ± 3.6 % under air, oxygen, argon, and nitrogen atmospheres, at the same soil moisture content (1.8%), thus demonstrating that the efficiency of gasoline degradation depended on the type of plasma forming gas. Moreover, researchers stated that 88 ± 3.2 % of gasoline was degraded after the 60 min treatment process of polluted soil when initial gasoline concentration was 2 g/kg. Obtained degradation efficiency was approximately 15 % higher than at the initial gasoline concentration of 3 g/kg and 33 % higher than at the initial gasoline concentration of 4 g/kg. Furthermore, researchers indicated that alkaline (pH=8.9) and neutral (pH=7.2) soil conditions were more beneficial to gasoline degradation than acidic conditions (pH=3.1 and 5.9). Accordingly, at a pH of 8.9, 75 ± 4.3 % of gasoline was degraded within 60 min. Obtained degradation efficiency was approximately 2 %, 14 %, and 57 % higher than at a pH of 7.2, 5.9 and 3.1, respectively.

Although there is some research on non-thermal plasma application for the remediation of soil contaminated by petroleum-based pollutants, these technologies are still new and insufficiently explored. Also, non-thermal plasma technologies cannot yet provide 100 % contaminant removal from the soil. Furthermore, the data about the usage of thermal plasma technologies for the remediation of polluted soil was not found. In this regard, the research of thermal plasma applicability for the remediation of soil contaminated by petroleum-based pollutants is needed. Consequently, one of the purposes of this dissertation was to perform such research and evaluate the ability of thermal plasma to clean the polluted soil completely, as well as supplement the existing knowledge of soil remediation with plasma technologies.

1.9. Chemical reactions taking place in a plasma-chemical gasification system

The ability to initiate the gasification process in the plasma-chemical reactor starts with the formation of the plasma environment. Plasma consists of the generated electrons, ions, reactive radicals, as well as excited atoms and molecules. Depending on the type of the plasma forming gas, the energetic electrons emitted from cathode interacts with gases and forms reactive radicals. In the case when the water vapour is used as a plasma forming gas, the plasma reactive species (O·, H· and OH·) are formed during the chemical reactions which are provided below (Davazdah Emami et al., 2016; Maghbouli et al., 2014):

$$H_2O + e^- \rightarrow H\cdot + OH\cdot + e^- \quad (1.1)$$

$$H_2O + O\cdot \rightarrow 2OH\cdot \quad (1.2)$$

$$H_2 + O\cdot \rightarrow OH\cdot + H\cdot \quad (1.3)$$

$$H_2 + OH\cdot \rightarrow H_2O + H\cdot \quad (1.4)$$

In the case of air as a plasma forming gas, the generated plasma reactive species (O·, N·) also can form the nitrogen oxides via the gas-phase reactions (Cubas et al., 2019; Du et al., 2008; Sarangapani et al., 2016; Shen et al., 2019):

$$O_2 + e^- \rightarrow 2O\cdot + e^- \quad (1.5)$$

$$N_2 + e^- \rightarrow 2N\cdot + e^- \quad (1.6)$$

$$N\cdot + O\cdot \rightarrow NO \quad (1.7)$$

$$NO + O\cdot \rightarrow NO_2 \quad (1.8)$$

Hence, plasma technology is based on the generation of charged particles and reactive radicals. These highly energetic species, as well as high plasma temperature, creates the environment needed to initiate waste (e.g. crude glycerol, diesel fuel) conversion reactions and accelerate the kinetics of waste decomposition into gaseous compounds (mainly H_2, CO, and CO_2).

The main chemical reactions of glycerol conversion are given below (Freitas et al., 2014; Gallo et al., 2012; Schwengber et al., 2016b; Wang, 2010):

Glycerol decomposition (cracking):

$$C_3H_8O_3 \leftrightarrow 4H_2 + 3CO \quad (1.9)$$

Glycerol partial oxidation reactions:

$$C_3H_8O_3 + 0.5O_2 \leftrightarrow 2CO + CO_2 + 4H_2 \quad (1.10)$$

$$C_3H_8O_3 + 1.5O_2 \leftrightarrow 3CO_2 + 4H_2 \quad (1.11)$$

Glycerol complete oxidation reaction:

$$C_3H_8O_3 + 3.5O_2 \leftrightarrow 3CO_2 + 4H_2O \quad (1.12)$$

Methanation/hydrogenation:

$$CO + 3H_2 \leftrightarrow CH_4 + H_2O \quad (1.13)$$

Methanation:

$$\mathrm{CO_2 + 4H_2 \leftrightarrow CH_4 + 2H_2O} \quad (1.14)$$

Steam reforming:

$$C_3H_8O_3 + 3H_2O \leftrightarrow 3CO_2 + 7H_2 \quad (1.15)$$

Water-gas shift:

$$CO + H_2O \leftrightarrow CO_2 + H_2 \quad (1.16)$$

Hydrogenolysis:

$$2C_3H_8O_3 + H_2 \leftrightarrow 3CH_4 + 3CO_2 + 3H_2O \quad (1.17)$$

Water splitting (dissociation):

$$2H_2O \rightarrow 2H_2 + O_2 \quad (1.18)$$

The general chemical reactions of diesel fuel conversion are submitted below (Lee et al., 2010; Lutz et al., 2004; Martin et al., 2015; Maximini et al., 2012):

Partial oxidation:

$$C_nH_m + \frac{n}{2}O_2 \rightarrow nCO + \frac{m}{2}H_2 \quad (1.19)$$

$$C_nH_m + \frac{n}{2}(O_2 + 3.76N_2) \rightarrow nCO + \frac{m}{2}H_2 + 3.76(\frac{n}{2})N_2 \quad (1.20)$$

$$C_nH_m + n(O_2 + 3.76N_2) \rightarrow nCO_2 + \frac{m}{2}H_2 + 3.76nN_2 \quad (1.21)$$

Complete oxidation:

$$C_nH_m + \left(n + \frac{m}{4}\right)O_2 \rightarrow nCO_2 + \frac{m}{2}H_2O \quad (1.22)$$

Steam reforming:

$$C_nH_m + nH_2O \rightarrow nCO + (n + m/2)\,H_2 \quad (1.23)$$

Water-gas shift reaction:

$$CO + H_2O \leftrightarrow H_2 + CO_2 \quad (1.24)$$

Apart from general reactions (1.19–1.24), the side reactions (formation of coke) can occur:

Boudouard reaction:

$$2\,CO \leftrightarrow C + CO_2 \quad (1.25)$$

Reverse gasification:

$$CO + H_2 \leftrightarrow C + H_2O \quad (1.26)$$

Decomposition:

$$C_nH_m \leftrightarrow nC + m/2H_2 \quad (1.27)$$

The presented reactions will help to explain and understand the experimental results obtained during the waste conversion, which are provided in the results and discussion section.

1.10. Substantiation of the thesis topic and the author's contribution to the work

The literature review provided projections of changes in the human population and energy consumption worldwide, as well as statistics on the present waste generation in the world. Also, the forecasts of future global waste production were presented. Further, the focus was on familiarising with the technologies currently in

use for the waste-to-energy conversion process and analysing their advantages and disadvantages, in such a way highlighting the general situation in this area. The presented information showed that most technologies are not well suited for the conversion of various mixed or special wastes (e.g. industrial, hazardous wastes), but more suitable for the conversion of organic wastes. Also, these technologies face other issues such as long periods of the conversion process, sensibility to the changes in the environmental conditions, generation of secondary pollutants, usage of chemical reagents. Meanwhile, plasma technologies can be applied for the conversion of various types of waste, including special wastes. Also, plasma technologies have no limitations to process organic and inorganic wastes and are considered as a viable solution for waste management in the future. Thus, after this, the emphasis was placed on plasma technologies and its application for the conversion of liquid (crude glycerol) and solid (petroleum hydrocarbons contaminated soil) waste. However, the use of plasma technologies for the conversion of these wastes is not sufficiently studied. The presented research data shows that plasma technologies can be applied for the conversion of crude glycerol, but there is still negligible information to achieve optimal process performance. Also, the data about the mass and energy balance of the plasma technologies is insufficient, and it is hard to evaluate the efficiency of the represented plasma systems. In terms of solid waste conversion, the application of plasma technologies for the remediation of petroleum hydrocarbons contaminated soil can also be attributed to the field consisting of insufficient research. Only non-thermal plasma applications for the remediation of soil contaminated by petroleum hydrocarbons have been found in the scientific literature. Meanwhile, no studies presenting the use of thermal plasma for soil remediation have been found.

After the revision of the scientific literature, it was decided to perform three types of experimental research:

- Determination of electrical and thermal characteristics of the plasma torch. These experiments will allow selecting plasma forming gases that will provide the most stable performance of the plasma torch and the most suitable environment for waste conversion. Different plasma torches have different parametric characteristics, therefore, conducting these types of experiments is essential.
- Conversion of crude glycerol into synthesis gas using a direct current (DC) thermal arc plasma. The main emphasis is placed on finding suitable operation conditions for the optimal crude glycerol conversion and determination of system efficiency through the calculation of energy and mass balances. Also, the accent is placed on carrying out system quantification in terms of the H_2/CO ratio, the lower heating value, the carbon conversion efficiency, the energy conversion efficiency, and the specific energy requirement. These experimental studies are a continuation of previous research conducted at the Lithuanian Energy Institute, Plasma Processing Laboratory.

- Remediation of diesel fuel contaminated soil using a direct current (DC) thermal arc plasma. These experimental studies will allow evaluating the suitability of thermal plasma to treat petroleum-hydrocarbons polluted soil. The main emphasis is placed on the determination of soil remediation process dependence on plasma forming gas and contaminant concentration. These experimental researches will complement the understanding of the plasma-based soil remediation process.

Summarily, the amount of waste generation is continuously increasing, and the ways are being sought to deal with it most sustainably and efficiently. Thus, experimental research and evaluation of the obtained results will reveal the potential of thermal plasma technology to convert liquid and solid waste and will complement a vital area of waste management.

2. METHODOLOGY

2.1. Material used

The thermal plasma technology was applied for gasification of the crude glycerol and remediation of soil contaminated by diesel fuel. The crude glycerol was obtained from "Rapsoila, UAB" producing biodiesel mainly from rapes. The composition of the crude glycerol is listed in Table 2.1. The feedstock contains 85 wt % of $C_3H_8O_3$, and the remaining 15 wt % consists of Na_3PO_4, CH_3RCOOH, CH_3OH, and H_2O, respectively.

Table 2.1 The composition of the crude glycerol

Chemical compound	Concentration, wt %
$C_3H_8O_3$	85.00
H_2O	9.00
Na_3PO_4	4.00
CH_3RCOOH	1.50
CH_3OH	0.50

The clean loamy-sandy soil was collected from the Kaunas region, Lithuania (Fig. 2.1). The soil was dried in an oven at 70±1 °C for 24 hours to ensure smooth and stable supply through a screw feeder to the reactor. After drying, the soil was sieved through a 2-mm mesh to remove stones and other debris. Dried and sifted soil was artificially polluted in the Lithuanian Energy Institute, Plasma Processing Laboratory, by commercial diesel fuel at different concentrations of 80±3 g/kg, 120±3 g/kg, and 160±3 g/kg, respectively. After contamination, the soil samples were left at room temperature (22±1 °C) for 2 days.

Fig. 2.1 The clean loamy-sandy soil

Before experiments of the solid waste (diesel fuel contaminated soil) conversion with thermal plasma, the ultimate analysis (CHNS) and proximate analysis of the clean and contaminated soil were performed and are shown in Table 2.2. Measurements revealed that as the concentration of diesel fuel increased from 80±3 g/kg to 160±3 g/kg, the concentration of carbon in the contaminated soil raised to

5.4±1.32 %, 7.06±1.26 %, and 8.51±1.33 %, respectively, from the initial concentration of 2.16±1.39 % of the clean soil. The same tendency was observed with hydrogen concentration, which increased to 0.68±0.42 %, 0.92±0.43 %, and 1.15±0.44 %, respectively, from the initial 0.26±0.43 % concentration of the clean soil. While nitrogen and sulphur content in the soil remained unchanged or below the limits of detection. Moreover, increased diesel fuel concentration in the soil increased moisture content in the soil (1.71±0.02–1.78±0.02 %), from the initial 0.45±0.02 % concentration of the clean soil. Also, the content of ash in soil decreased with the increase of diesel fuel concentration in the soil.

Table 2.2 Ultimate and proximate analysis of clean and contaminated loamy-sandy soil

Ultimate analysis	Clean soil, wt %	Diesel contaminated soil, wt %		
		80 g/kg[a]	120 g/kg	160 g/kg
Carbon (C)	2.16±1.39	5.40±1.32	7.06±1.26	8.51±1.33
Hydrogen (H)	0.26±0.43	0.68±0.42	0.92±0.43	1.15±0.44
Nitrogen (N)	< 0.01	< 0.01	< 0.01	< 0.01
Sulphur (S)	< 0.01	< 0.01	< 0.01	< 0.01
Oxygen (O)[b]	2.49	5.28	6.39	7.49
Proximate analysis				
Moisture	0.45±0.02	1.75±0.02	1.76±0.02	1.78±0.02
Ash	94.62±3.78	86.87±3.47	83.85±3.35	81.05±3.24

[a] Diesel concentration in the soil, g/kg

[b] By difference

2.2. Experimental setup

The thermal plasma used for gasification and remediation processes were generated using the DC plasma torch. The plasma torch consists of a copper cathode junction containing a tungsten button-type emitter (used in the presence of noble gas (Ar)) or with hafnium emitter (used in the presence of oxygen-containing gas) and a step-formed copper anode. A stair-shaped cylindrical anode is positioned along the axis in one line with the cathode, and it is used to fix the mean arc length (Zhukov et al., 1999). The electrodes of the plasma torch are separated by the neutral section and the insulation rings. The rings have inlet holes for the tangential supply of a shielding and plasma forming gas. The experimental setup also contains the sub-systems which slightly differ depending on the type of the plasma forming gas as well as the nature

of the use of the plasma technology (Fig. 2.2–2.3). In all cases, the plasma system is operating under atmospheric pressure. And the plasma-chemical reactor used in experimental researches is 1 m long and 0.40 m in diameter.

The crude glycerol gasification system is shown in Fig. 2.2. It is comprised of an atmospheric pressure DC arc plasma torch (1), a power supply system (2), a gas supply system (3), a plasma-chemical reactor (4), a crude glycerol supply system (5), a condenser (6), and a gas chromatograph (7). A similar experimental system was used in earlier research (Tamošiūnas et al., 2016).

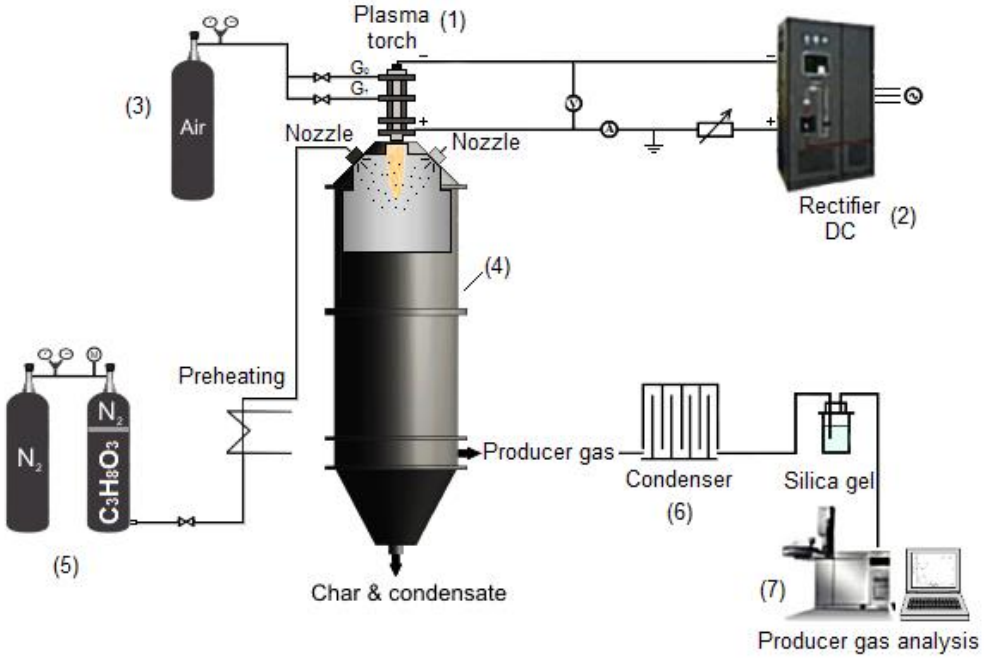

Fig. 2.2 Plasma-chemical crude glycerol gasification system

The plasma torch and the nozzles for crude glycerol supply are installed in the upper part of the reactor so that the glycerol flow is directed at an angle of 45±0.10 degrees to the plasma stream. In the middle of the reactor, an exhaust chamber for the producer gas is installed. At the bottom of the reactor, there is a section for the removal of condensate and char.

The crude glycerol was fed through the spray nozzles to the plasma-chemical reactor at the rate of 5.64 ±0.20 g/s. The pressure in the spraying line was controlled by N_2 gas from a cylinder and retained at 10±0.1 bars (optimal operation pressure). In order to increase the fluidity, spraying stability, and atomisation of the crude glycerol, it was preheated to 70±0.5 °C before the injection into the plasma-chemical reactor.

The atmospheric pressure DC arc plasma torch was used to produce active radicals and species from the air as well as to generate high-temperature plasma stream. Usually, the power of the plasma torch depends on the current intensity, voltage, and the flow rate of the plasma forming gas. Thus, during the experiments, the power of the plasma torch ranged from 45.6 kW to 56 kW (current 160 A, voltage 285–350 V, airflow rate 2.70–4.90 g/s). The mean temperature of the plasma stream entering the reactor was 4400 ±130 K.

When the water vapour was used as a plasma forming gas, the gasification system was supplemented with a steam generator and a superheater. Moreover, during the experiments, the power of the plasma torch ranged from 56.00 kW to 62.40 kW (current 160 A, voltage 350–390 V, water vapour flow rate 2.90–5.15 g/s). The mean temperature of the plasma stream entering the reactor was 2800±150 K.

Hence, the effects of the gasifying agent (air plasma and water vapour plasma) and the plasma torch power on the conversion of crude glycerol to synthesis gas were investigated. The experimental parameters of the crude glycerol conversion process are summarised in Table. 2.3:

Table 2.3 The experimental parameters of the crude glycerol conversion to synthesis gas

	Crude glycerol conversion using:	
Parameter	Air plasma	Water vapor plasma
Arc current, A	160	160
Arc voltage, V	300–350	350–390
Power, kW	45.6–56	56–62.4
Glycerol flow rate, g/s	5.64 ±0.20	5.64 ±0.20
Gasifying agent flow rate, g/s	2.70–4.90	2.90–5.15
Plasma torch thermal efficiency (η), %	60–74	69–76
Mean T_{plasma}, K	4400±130	2800±150
Crude glycerol lower heating value, wt %	14.36±0.03	14.36±0.03

A scheme of the plasma-chemical soil remediation system is shown in Fig. 2.3. It consists of an atmospheric pressure DC arc plasma torch (1), a plasma-chemical reactor (2), a steam generator (3), a superheater (4), an air supply system (5), a power supply system (6), a condenser (7), and a gas analyser (8).

The soil remediation system is slightly modified, compared with the crude glycerol gasification system. The screw feeder of the soil is fitted in the upper part of the reactor so that the soil could flow the reactor straight to the bottom of it. The plasma torch also is installed at the top of the reactor, but this time it is directed at an angle of 45±0.10 degrees to the soil flow. Such construction ensures conditions for the interaction of active species with the contaminants in the soil.

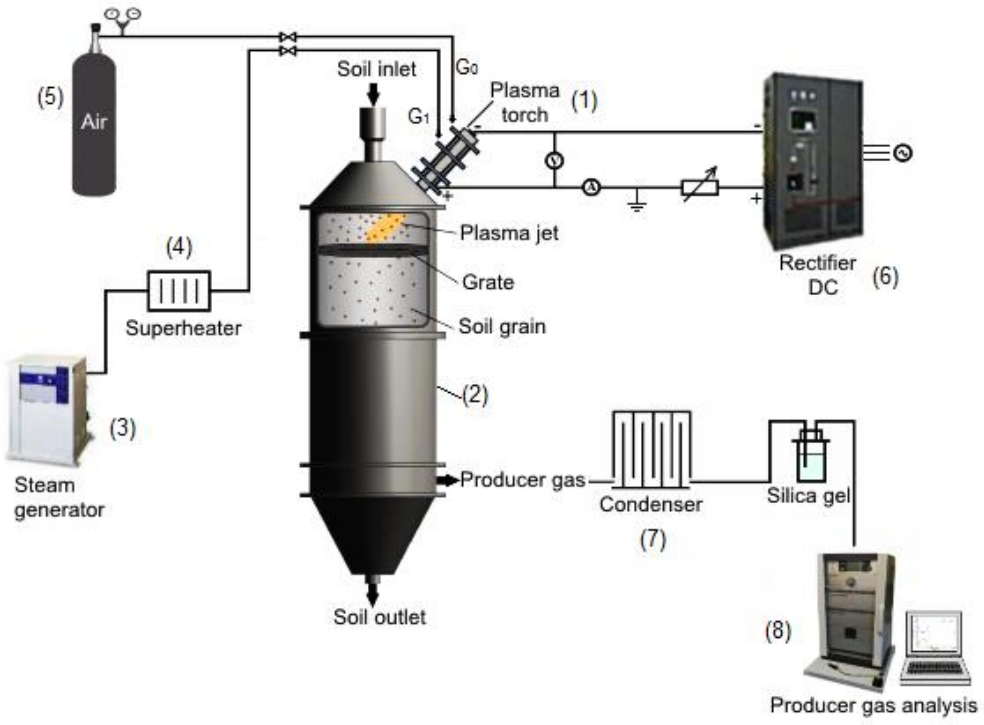

Fig. 2.3 Plasma-chemical soil remediation system

The treatment of the polluted soil with water vapour or air plasma was performed under atmospheric pressure for 24±1.60 minutes. The soil was supplied to the plasma-chemical reactor through the solid materials feeder at a feed rate of 1.50±0.01 g/s. The power of the plasma torch was 56 kW, at the water vapour flow rate of 3.80 g/s, current of 160 A and voltage of 350 V. The mean temperature of the plasma stream entering the reactor was 2880±60 K. When the air was used as a plasma forming gas, the power of the plasma torch and air flow rate were equal to 52.80 kW and 4.90 g/s, respectively at a current of 160 A and voltage of 340 V. The operating temperature of the air plasma system was 4100± 113 K.

Accordingly, the experimental parameters of the diesel fuel conversion from the soil are summarised in Table. 2.4:

Table 2.4 The experimental parameters of the diesel fuel contaminated soil remediation with thermal plasma

	Remediation of diesel fuel polluted soil with:	
Parameter	Air plasma	Water vapor plasma
Arc current, A	160	160
Arc voltage, V	330	350
Power, kW	52.8	56
Soil feed rate, g/s	1.50±0.01	1.50±0.01
Diesel fuel content in the soil, g/kg	80±3, 120±3, 160 ±3	80±3, 120±3, 160 ±3
Gasifying agent flow rate, g/s	4.90	3.80
Plasma torch thermal efficiency (η), %	71–75	74–77
Mean T_{plasma}, K	4100±113	2880±60

2.3. Determination of electrical and thermal characteristics of the plasma torch

The voltage-current characteristics (VCC) are one of the fundamental characteristics of the plasma torch, which allows to determine whether the operation of the system is stable (the curve of VCC rises or remains constant), or unstable (the curve of VCC drops). The use of a ballast rheostat in the electrical circuit helps to prevent the dropping VCC curves. However, it reduces the overall electrical efficiency of the plasma system but minimises the pulsations of the arc voltage determined by a large-scale shunting. Therefore, these disadvantages can be eliminated by using a cylindrical anode with a sudden expansion (a stair-shaped) of the channel. This type of anode leads to the prevention and minimisation of a large-scale shunting of the electric arc (Zhukov et al., 2007).

Analysis of electrical and thermal plasma characteristics using homogeneous physical equations is complicated. Therefore, in order to generalise the plasma torch characteristics, a theory of similarity is often applied. This theory provides a reasonable way to construct the relationship between the experimental data and mathematical formula. Consequently, the experimental workload could be reduced and the corresponding plasma characteristics can be predicted (Ma et al., 2015). The fundamental principles of the generalisation of the electrical and thermal characteristics of the plasma torch, which is a base of this work, were described in detail by Zhukov et al. (Zhukov et al., 2007). As they present, the theory of similarity is based on similarity criteria derived from homogeneous physical equations after making the latter dimensionless. However, when plasma torch works in the same medium (e.g. air, steam/water vapour), the analysis of plasma characteristics becomes more efficient by replacing the dimensionless similarity criteria into the dimensional complexes. Thereby, the criterion coefficients which reflect the physical properties are considered to be constant and are transferred from the dimensionless similarity criteria. Therefore, the dimensional complexes consist of the regime (G – the total gas flow rate (g/s), I – the arc current (A), p – the pressure in the arc chamber (Pa)) and

construction (d – the anode diameter (m), l – the length of the anode (m)) parameters (Zhukov et al., 2007).

Hereinafter-provided criteria (Eq. 2.1–2.4) were used to derive dimensional complex (Eq. 2.5) devoted to generalising the electrical characteristics of the plasma torch.

$$K_1 = \frac{I_0^2}{\sigma_0 h_0 G_0 d}; \tag{2.1}$$

$$K_2 = \frac{p_0 d}{a}; \tag{2.2}$$

$$K_3 = \frac{G_0}{\rho_0 \upsilon_0 d}; \tag{2.3}$$

$$K_4 = \frac{\sigma_0 U_0 d}{I_0}; \tag{2.4}$$

$$\frac{Ud}{I} = A\left(\frac{I^2}{Gd}\right)^m \left(\frac{G}{d}\right)^n (pd)^k \left(\frac{l}{d}\right)^r; \tag{2.5}$$

where, σ – the electric conductivity (S/m), h – the enthalpy (kJ/kg), a – $8kT/\pi d^2$, ρ – density (kg/m^3), υ – kinematic viscosity of the fluid (m^2/s), U – the arc voltage (V), A – the coefficient, and m, n, k, r – the exponents are constant values depending on the plasma torch construction and operating regime (Grigaitienė et al., 2011).

Additionally, in order to establish the coefficients and exponents of similarity complexes, the logarithmic equations should be used. The below-provided logarithmic equation (Eq. 2.6) illustrates the determination of the coefficient of the energy criterion. Moreover, the exponent m is determined by the graphical method (Zhukov et al., 2007).

$$\lg\frac{Ud}{I} = A\left(\frac{I^2}{Gd}\right)^m \tag{2.6}$$

In fact, the generalisation of the thermal characteristics of the plasma torch is similar to the generalisation of the electrical characteristics (Grigaitienė et al., 2011):

$$\tilde{\eta} = B\left(\frac{I^2}{Gd}\right)^m \left(\frac{G}{d}\right)^n (pd)^k \left(\frac{l}{d}\right)^r \tag{2.7}$$

where $\tilde{\eta}$ – the integral coefficient of heat transfer, B – the coefficient established from the dependence of efficiency from the arc current.

In this dissertation, four experimental conditions were investigated using gases or the mixtures of the gases, including water vapour, air, air/water vapour and

Ar/water vapour for the plasma formation and cathode protection. The working potential of each type of plasma was established at variable ranges of the current and voltage used. The main operational characteristics of the plasma torch are given in Table 2.5:

Table 2.5 The experimental parameters of the plasma torch

	Water vapour	Air	Air/water vapour	Ar/water vapour
Arc current (A)	180–200	160–220	160–220	160–220
Arc voltage (V)	250–325	294–410	243–343	220–268
Arc power (kW)	45–64	47–90	46–71	40–58
Total gas flow rate, G_1+G_2 (g/s)	3.30–4.65	4.00–12.00	3.40–5.65	4.30–5.65
Plasma torch efficiency, η (%)	68–71	76–85	60–75	59–70

2.4. Determination of the plasma torch thermal mode

In addition to the determination of the thermal and electrical characteristics of the plasma torch, it is also essential to determine the thermal mode of the plasma torch. The colorimetric method is a primary experimental method used to determine thermal losses in the plasma torch. Importantly, the radiation, convection, and conduction can be ignored by applying this method. Hence, it is sufficient to measure the current and voltage of the plasma torch, the gas flow rate, the cooling water flow rate, and its temperature changes.

Accordingly, the power of the plasma torch is calculated by Eq. (2.8):

$$P = I \cdot U \tag{2.8}$$

where P is the power of the plasma torch (W).

Part of the generated power is lost with the cooling water of the plasma torch walls, Eq. (2.9):

$$Q_w = G_w \Delta t_w c_p \tag{2.9}$$

where Q_w is a heat flow to the cooling water (kW), G_w is a flow rate of the cooling water (kg/s), Δt_w is a change in the cooling water temperature (°C), c_p is the specific heat of the cooling water (kJ/(kg·K)).

Consequently, the power supplied to the heated gas stream is calculated by Eq. (2.10):

$$Q_f = P - Q_w \tag{2.10}$$

where Q_f is a power of the thermal plasma flow (kW), Q_w is a heat flow to the cooling water (kW).

Thus, the thermal efficiency of the plasma torch (η) determines the efficiency of the equipment, Eq.(2.11):

$$\eta = \frac{Q_f}{P} \tag{2.11}$$

The integral coefficient of the heat transfer (η̃) determines the ratio of the heat losses in the plasma torch to the heat content of the plasma jet (Zhukov et al., 2007) Eq.(2.12):

$$\tilde{\eta} = \frac{1-\eta}{\eta} \tag{2.12}$$

where η is the thermal efficiency of the plasma torch.

The calculation of the mean plasma temperature was performed according to the heat balance equation (Eq. 2.13), corresponding to plasma enthalpy $H_f = f(T_f)$

$$H_f = \frac{P_{PT}}{G} + H_f^0 \tag{2.13}$$

where H_f is plasma enthalpy (kJ/kg), Q_{PT} is an energy content in the plasma torch (kW) G is a plasma forming gas flow rate (kg/s), H_f^0 is enthalpy under standard conditions (kJ/kg)

2.5. Evaluation of the crude glycerol gasification system

In pursuance of assessing of the crude glycerol gasification system, it was quantified in terms of the H_2/CO ratio, the lower heating value, the carbon conversion efficiency, the cold gas efficiency, the energy conversion efficiency, and the specific energy requirement (Petitpas et al., 2007; Tamošiūnas et al., 2014).
The synthesis gas yield:

$$Y_{synthesis\ gas} = \frac{m_{synthesis\ gas}}{m_{feedstock}} \times 100\% \tag{2.14}$$

where $Y_{synthesis\ gas}$ is a yield of the synthesis gas (%), $m_{synthesis\ gas}$ is a mass flow rate of generated synthesis gas (kg/s), $m_{feedstock}$ is a mass flow rate of the crude glycerol (kg/s).
Lower heating value:

$$LHV = 10.78\ H_2(\%) + 12.63\ CO\ (\%) + 35.88\ CH_4(\%) + 56.5\ C_2H_2(\%) + 64.5\ C_2H_6(\%) + 93.21\ C_3H_8\ (\%) \tag{2.15}$$

where LHV is a lower heating value (kJ/Nm^3), H_2, CO, CH_4, C_2H_2, C_2H_6, C_3H_8 are the content of the gaseous products in the producer gas (vol. %).

Carbon conversion efficiency:

$$CCE\ (\%) = \frac{[X_{CO} + X_{CO_2} + X_{CH_4} + X_{C_2H_2}]_{OUT}}{X_{M,IN}} \times 100\% \quad (2.16)$$

where CCE (%) is carbon conversion degree (%), $X_{CO,CO_2,CH_4,C_2H_2,OUT}$ is a mass flow rate of the carbon in the gas produced (kg/s), $X_{M,IN}$ is a mass flow rate of injected feedstock (crude glycerol) (kg/s).

Energy conversion efficiency:

$$ECE = \frac{(H_2 + CO)_{synthesis\ gas} \times LHV_{synthesis\ gas}}{P_{plasma} + X_{M,IN} \times LHV_{M,IN}} \times 100\% \quad (2.17)$$

where ECE is the energy conversion efficiency (%), $(\mathrm{H_2 + CO})_{\mathrm{synthesis\ gas}}$ is a mass flow rate of synthesis gas (kg/s), $LHV_{synthesis\ gas}$ is a lower heating value of synthesis gas (MJ/nm^3), $\mathrm{P_{plasma}}$ is a plasma torch power (W), $X_{M,IN}$ is a mass flow rate of injected feedstock (kg/s), $LHV_{M,IN}$ is a lower heating value of injected feedstock (MJ/kg).

Specific energy requirement:

$$\mathrm{SER} = \frac{\mathrm{P_{plasma}}}{(\mathrm{H_2 + CO})_{\mathrm{synthesis\ gas}}} \quad (2.18)$$

where SER is a specific energy requirement (kJ/mol), $\mathrm{P_{plasma}}$ is a plasma torch power (kJ), $(\mathrm{H_2 + CO})_{\mathrm{synthesis\ gas}}$ is a molar flow rate of synthesis gas (mol/s).

2.6. Evaluation of thermal arc plasma energy and mass balances

The determination of the energy efficiency of the thermal plasma gasification system was performed by evaluating mass and energy balance in separate nodes of the technological system (plasma torch, plasma-chemical reactor and estimation of possible ways to use producer gas). All mass and energy balance calculations were performed under these constant conditions: the ambient temperature of 20 °C and the pressure of 101.325 kPa.

1. Plasma torch:

The energy and mass balance in the plasma torch (Fig. 2.4) was evaluated according to the equations (2.19–2.24).

$$\mathrm{Q}_{PT} = \left(\mathrm{Q}_{wv} + \mathrm{Q}_{Air} + \mathrm{Q}_{glyc} + P_{PT}\right) - (\mathrm{Q}_{cw} + \mathrm{Q}_{aw}) \quad (2.19)$$

where Q_{PT}, Q_{wv}, $\mathrm{Q}_{Air,}$ Q_{glyc}, Q_{cw} and Q_{aw} is an energy content in the plasma torch, water vapour, glycerol, cooling water of the cathode and cooling water of the anode, respectively (kWh), P_{PT} is a power of the plasma torch (kWh).

$$Q_{wv} = \left(\frac{G_{wv} \times C_{p\,wv} \times (T_{wv} - T_0)}{3600}\right) + \left(\frac{G_{wv} \times h_{wv}}{3600}\right) \quad (2.20)$$

where Q_{wv} is an energy content in the water vapour (kWh), G_{wv} is a water vapour flow (kg/h), $C_{p\,wv}$ is the specific heat of water vapour (kJ/(kg·K)), T_{wv} is a temperature of water vapour (ºC), T_0 is an ambient temperature (ºC), h_{wv} is an enthalpy of water vapour (kJ/kg).

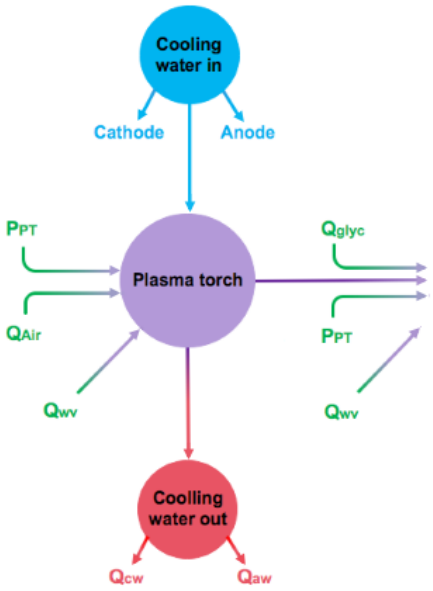

Fig. 2.4 The energy and mass balance in the plasma torch

$$Q_{Air} = \left(\frac{G_{Air} \times C_{p\,Air} \times (T_{Air} - T_0)}{3600}\right) + \left(\frac{G_{Air} \times h_{Air}}{3600}\right) \quad (2.21)$$

where Q_{Air} is an energy content in the air (kWh), G_{Air} is an airflow (kg/h), $C_{p\,Air}$ is the specific heat of the air (kJ/(kg·K)), T_{Air} is a temperature of air (ºC), T_0 is an ambient temperature (ºC), h_{Air} is an enthalpy of air (kJ/kg).

$$Q_{glyc} = \left(\frac{G_{glyc} \times C_{p\,glyc} \times (T_{glyc} - T_0)}{3600}\right) + \left(\frac{G_{glyc} \times h_{glyc}}{3600}\right) \quad (2.22)$$

where Q_{glyc} is an energy content in the glycerol (kWh), G_{glyc} is a glycerol flow (kg/h), $C_{p\,glyc}$ is the specific heat of glycerol (kJ/(kg·K)), T_{glyc} is a temperature of glycerol (ºC), T_0 is an ambient temperature (ºC), h_{glyc} is an enthalpy of glycerol (kJ/kg).

$$Q_{cw} = \left(\frac{G_{cw} \times C_{p\,w} \times (T_{cw} - T_0)}{3600}\right) \quad (2.23)$$

where Q_{cw} is an energy content in the cooling water of the cathode (kWh), G_{cw} is a cooling water flow of the cathode (kg/h), $C_{p\,w}$ is the specific heat of water (kJ/(kg·K)), T_{cw} is a temperature of cooling water in the outlet of a cathode (ºC), T_0 is an ambient temperature (ºC).

$$Q_{aw} = \left(\frac{G_{aw} \times C_{p\,w} \times (T_{aw} - T_0)}{3600}\right) \quad (2.24)$$

where Q_{aw} is an energy content in the cooling water of the anode (kWh), G_{aw} is a cooling water flow of the anode (kg/h), $C_{p\,w}$ is the specific heat of water (kJ/(kg·K)), T_{aw} is a temperature of cooling water in the outlet of an anode (ºC), T_0 is an ambient temperature (ºC).

2. Plasma-chemical reactor:

The equations (2.25–2.28) led to estimate the energy and mass balance in the plasma-chemical reactor (Fig. 2.5).

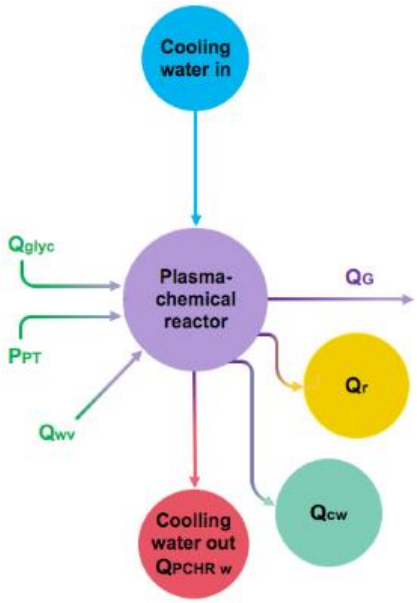

Fig. 2.5 The energy and mass balance in the plasma-chemical reactor

$$Q_G = Q_{PT} - Q_{PCHR\,w} - Q_{cw} - Q_r \quad (2.25)$$

where Q_G is an energy content in the producer gas (kWh), Q_{PT} is an energy content in the plasma torch (kWh), $Q_{PCHR\,w}$ is an energy content in the cooling water

of the plasma-chemical reactor (kWh), Q_{cw} is an energy content in a condensate of water vapour (kWh), Q_r is an energy content lost in the plasma-chemical reactor due to radiation (kWh).

$$Q_G = \left(\frac{G_G}{3600} \times T_G\right) + \left(\frac{G_G}{3600\,\rho_G}\right) \times LHV_G \times 1000 \quad (2.26)$$

where Q_G is an energy content in the producer gas (kWh), G_G is a producer gas flow (kg/h), T_G is a temperature of producer gas (ºC), ρ_G is a density of producer gas calculated by the dry composition of the producer gas (kg/m^3), LHV_G is a lower heating value of the producer gas (kJ/Nm^3).

$$Q_{PCHR\,w} = \left(\frac{G_{PCHRw} \times C_{p\,w} \times (T_{PCHRw} - T_0)}{3600}\right) \quad (2.27)$$

where Q_{PCHRw} is an energy content in the cooling water of the plasma-chemical reactor (kWh), G_{PCHRw} is the cooling water flow in the plasma-chemical reactor (kg/h), $C_{p\,w}$ is the specific heat of water (kJ/(kg·K)), T_{PCHRw} is the temperature of cooling water in the outlet of the plasma-chemical reactor (ºC), T_0 is the ambient temperature (ºC).

$$Q_{cw} = \left(\frac{G_{cw} \times C_{p\,w} \times T_0}{3600}\right) \quad (2.28)$$

where Q_{cw} is an energy content in a condensate of water vapour (kWh), G_{cw} is a flow of water vapour condensate (kg/h).

3. Estimation of possible ways to use producer gas:

Before the evaluation of scopes to use producer gas, it should be noted that producer gas passing through the heat exchanger (gas cooler) loses some of its energy (Fig. 2.6).

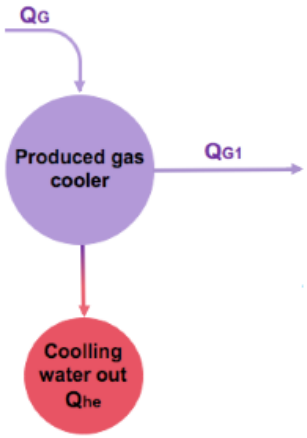

Fig. 2.6 The energy losses in the heat exchanger

The energy losses in the heat exchanger are calculated by equations (2.29–2.30):

$$Q_{G1} = Q_G - Q_{he} \tag{2.29}$$

where Q_{G1} is an energy content in the producer gas after passing through the heat exchanger (kWh), Q_{he} is an energy content in the cooling water of the heat exchanger (kWh).

$$Q_{he} = \left(\frac{G_{he} \times C_{p\,he} \times (T_{he} - T_0)}{3600}\right) \tag{2.30}$$

where Q_{he} is an energy content in the cooling water of the heat exchanger (kWh), G_{he} is the cooling water flow in the heat exchanger (kg/h), T_{he} is the temperature of cooling water in the heat exchanger (ºC).

Ultimately, generated producer gas can be utilised for the generation of thermal energy in the boiler, or electrical and thermal energy in the internal combustion engine or microturbine (Fig. 2.7).

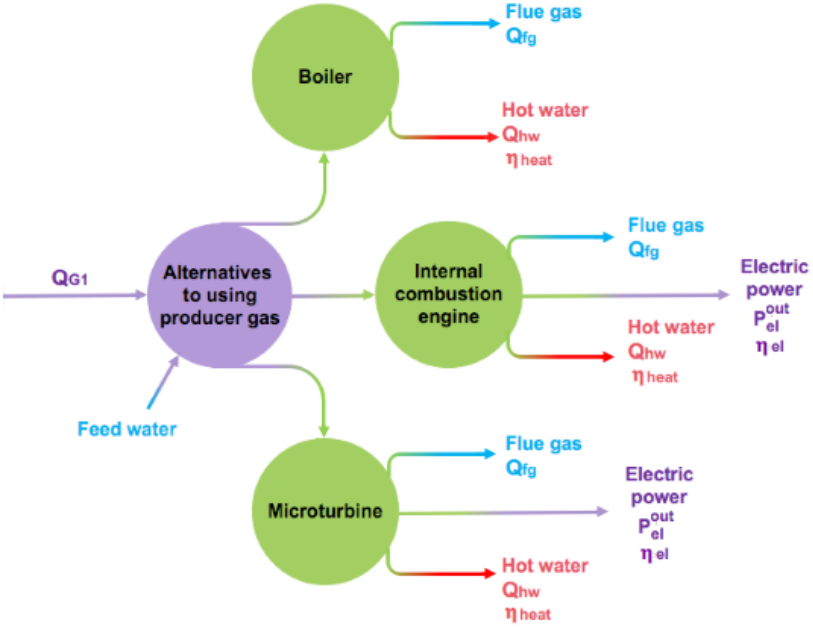

Fig. 2.7 The alternative ways to use generated producer gas

The efficiency of these usage ways is evaluated by equations (2.31-2.33):

$$Q_{fg} = \left(\frac{G_{fg} \times (T_{fg} - T_0)}{3600}\right) \tag{2.31}$$

where Q_{fg} is an energy content in the flue gas (kWh), G_{fg} is a fuel gas flow (kg/h), T_{fg} is a temperature of flue gas (ºC), T_0 is an ambient temperature (ºC).

$$\eta_{heat} = \left(\frac{\mathrm{Q}_{hw}}{\mathrm{Q}_{glyc} + \mathrm{Q}_{wv} + P_{PT}} \times 100\% \right) \quad (2.32)$$

where η_{heat} is a thermal efficiency of the producer gas usage process (%), Q_{hw} is an energy content accumulated in the hot water (kWh), Q_{glyc} is an energy content in the glycerol (kWh), Q_{wv} is an energy content in the water vapour (kWh), P_{PT} is a power of the plasma torch (kWh).

$$\eta_{el} = \left(\frac{P_{el}^{out}}{\mathrm{Q}_{glyc} + \mathrm{Q}_{wv} + P_{PT}} \times 100\% \right) \quad (2.33)$$

where η_{el} is an electrical efficiency of the producer gas usage process (%), P_{el}^{out} is an electrical energy content in the internal combustion engine or microturbine gained from producer gas (kWh), Q_{glyc} is an energy content in the glycerol (kWh), Q_{wv} is an energy content in the water vapour (kWh).

Additionally, the electrical efficiency of the plasma gasification system was evaluated by equation (2.34):

$$\eta_{el} = \left(\frac{P_{el}^{out}}{P_{el}^{in}} \times 100\% \right) \quad (2.34)$$

where η_{el} is an electrical efficiency of the plasma gasification system (%), P_{el}^{in} is a total power input (kWh).

2.7. Estimation of uncertainties in measurements and calculations

Measurement is a process whereby the value of a quantity is estimated. All experimental measurements are accompanied by errors. Measurement process errors are the basic elements of uncertainty analysis. Measurement errors are categorised as systematic or random. Systematic error is defined as the portion of the total measurement error that remains constant in repeat measurements of a quantity. Random error is defined as the portion of the total measurement error that varies in the short-term when the measurement is repeated (NASA, 2010).

Systematic uncertainties can be evaluated by the calculation of reduced relative error (Lith. redukuotoji santykinė paklaida) σ_i. The maximum measurable value (x_{max}) that can be measured by a device is determined by the scale of the device or the measuring range of the device. Measurement accuracy is defined by the relative error σ_i, which is also known as the instrument accuracy scale. σ_i is defined as a ratio between the absolute error of the measured value (Δx_i) and the x_{max}, expressed in a percentage (Tamošiūnas, 2014):

$$\sigma_i = \frac{\Delta x_i}{x_{max}} \times 100\%. \quad (2.32)$$

The best method for reducing the effects of random errors on measurement is to repeat the measurement and calculate the mean and the standard deviation from this data. Suppose the measurements of N physical quantities, $x_1,x_2,...,x_N$. The fluctuations responsible for the spread of readings are random, consequently, they are equally likely to be higher as lower than the accepted value. The arithmetic mean is a way of dividing any random errors among all the readings. Therefore, the adoption of the mean $\overline{x}$ is the best estimate of the quantity x (Hughes et al., 2010):

$$\overline{x} = \frac{1}{N}(x_1 + x_2 + \cdots + x_N) = \frac{1}{N}\sum_{i=1}^{N} x_i\,; \tag{2.33}$$

where $\overline{x}$ is an arithmetic mean of all measurement values, N is a number of measurements, x_i is a result of the i^{th} measurement

In this case, the absolute error of the individual measurements is expressed as (Tamošiūnas, 2014):

$$\Delta x_i = \overline{x} - x_i\,; \tag{2.34}$$

Δx_i equally likely to be positive as negative.

Relative error σ_i (Lith. santykinė paklaida) is defined as a ratio between the absolute error of the measured value (Δx_i) and the measurement result ($\overline{x}$):

$$\sigma_i = \frac{\Delta x_i}{\overline{x}} \times 100\%. \tag{2.35}$$

The standard deviation indicates the random uncertainty of any one of the measurements used to calculate S_x and is defined as (Pengra et al., 2009):

$$S_x = \sqrt{\sum_{i=1}^{N} \frac{(x_i - \overline{x})^2}{N-1}}; \tag{2.36}$$

The mean value of the measurements has less random uncertainty than any one of the individual measurements. Thus, the standard deviation of the mean value of the set measurements $S_{\overline{x}}$ is expressed as:

$$S_{\overline{x}} = \sqrt{\sum_{i=1}^{N} \frac{(x_i - \overline{x})^2}{N(N-1)}} = \frac{S_x}{\sqrt{N}}. \tag{2.37}$$

The relative standard deviation is defined as:

$$\sigma_{(X)} = \frac{S_{\overline{x}}}{\overline{x}} \times 100\%. \tag{2.38}$$

Additionally, the uncertainty ($u_{(X_{ran})}$) due to random error generally must be computed by multiplying the standard deviation of a sample of measured values by the Student's t-statistic with a 95% confidence level (p = 95 %) (NASA, 2010):

$$u_{(X_{ran})} = t_{95,N-1} S_x \quad or \quad u_{(X_{ran})} = t_{95,N-1} S_{\overline{x}} \tag{2.39}$$

Also, if the relative error is below, or equal to 5 %, the obtained results are considered as sufficiently accurate and reliable. If relative error varies between 5–10 % results are of satisfactory accuracy. If relative error is greater than 10 %, the obtained results are unreliable (Tamošiūnas, 2014). Consequently, the errors of the performed experiments are given in Table 2.6.

Table 2.6 Measured values and measurement errors

No.	Setting value	Limits for measurement	Device, absolute error, or calculation equation	Relative error ± %
1.	Current of the plasma torch	160–220 A	Milivoltmeter ±0.2 mV	0.08–0.16
2.	Voltage of the plasma torch	220–410 A	Voltmeter ±0.2 V	0.05–0.08
3.	Power of the plasma torch	43.2–62.4 kW	Eq. 2.8	0.5–1
4.	Supplied gas flow rate	2.7–5.7 g/s	Diaphragm $\pm 0.1 \cdot 10^{-3}$ m; critical flow nozzle	1
5.	The temperature of water vapour supplied to the plasma torch	510 K	Thermocouple Pt 100	0.3
6.	The temperature of crude glycerol	343–344 K	Thermometer ±1°C	0.2
7.	Ambient air temperature	291–295 K	Thermometer ±1°C	0.7
8.	Lengths and diameters of the elements of the plasma torch and plasma-chemical reactor	$2–250 \cdot 10^{-3}$m	Slider $\pm 0.02 \cdot 10^{-3}$	0.015–0.04
9.	Amount of the cooling water in the system	0.07–016 kg/s	Diaphragm $\pm 0.1 \cdot 10^{-3}$ m; Diaphragm sensor $\pm 0.1 \cdot 10^{-3}$ m;	0.1
10.	Heat flow	11.7–23.3 kW	Eq. 2.9	1–4
11.	The mean temperature of the plasma stream	2800–4400K	Eq. 2.13	Up to 6
12.	Elemental composition of the soil	Up to 100 %	EDS	1–2
13.	Thermal analysis of the soil		TGA/DTG	4
14.	Analysis of produced gas concentrations	Up to 100 %	Gas chromatograph, gas analyser	2

2.8. Equipment used for the analysis of treated materials and producer gas

Soil analysis was done before and after interaction with thermal plasmas. The surface morphology of clean soil, diesel fuel contaminated soil and plasma remediated soil was analysed by the scanning electron microscopy (SEM, Hitachi S-3400N). The elemental composition of clean, contaminated, and plasma remediated soil was investigated by the energy-dispersive X-ray spectroscopy (EDX, Bruker Quad 5040). The elemental composition of the samples for each experimental case was measured three or four times. Evaluation of the carbon, hydrogen, nitrogen, and sulphur (CHNS) content in the soil was performed by a FLASH 2000 elemental analyser. The measurements of carbon, hydrogen and nitrogen content in the clean and contaminated soil were performed according to LST EN ISO 16948:2015 standard requirements. Sulphur was measured according to BM-8B/3-BO0:2012 methodical. The oxygen content was determined by the difference. Thermal properties of the clean and diesel fuel contaminated soil were investigated by thermogravimetric analysis (thermogravimetric (TGA/DTG) and differential scanning calorimetry (DSC)) using NETZSCH STA 449 F3 Jupiter analyser with a SiC furnace. The measurement of producer gas concentrations, which were generated during the interaction between the contaminated soil and thermal plasma stream was performed by the multi-component gas analyser (MRU SWG 300^{-1}). Also, during the interaction between crude glycerol and thermal plasma stream, produced gas was analysed by the multi-component gas analyser and the gas chromatograph (Agilent 7890A) equipped with dual-channel thermal conductivity detectors (TDCs) and a valve system. The concentrations of producer gas for each experimental case were measured three times.

3. RESULTS AND DISCUSSION

In order to ensure smoother material conversion and remediation process, it is necessary to choose the optimal working conditions of the plasma torch. The electrical and thermal characteristics of the plasma torch define and enable to evaluate optimal working conditions of the plasma device. Thus, the determination of these characteristics is crucial. Electrical and thermal characteristics, as well as the performance of the plasma torch, depends on the working parameters used, including current, voltage, plasma forming gas. Therefore, the influence of these parameters should be firstly investigated.

3.1. Electrical characteristics of the plasma torch

Seeking to guarantee a stable work of the plasma torch, the curve of the voltage-current characteristics (VCC) must rise or remain constant. In the present study, the voltage-current characteristics observed as slightly decreasing, steady or rising depending on the used arc current and the plasma forming gas.

Figure 3.1 illustrates the voltage-current characteristics of the four different types of plasma (water vapour, air, air/water vapour and Ar/water vapour) determined when the total gas flow rate was equal to 4.2±0.1 g/s.

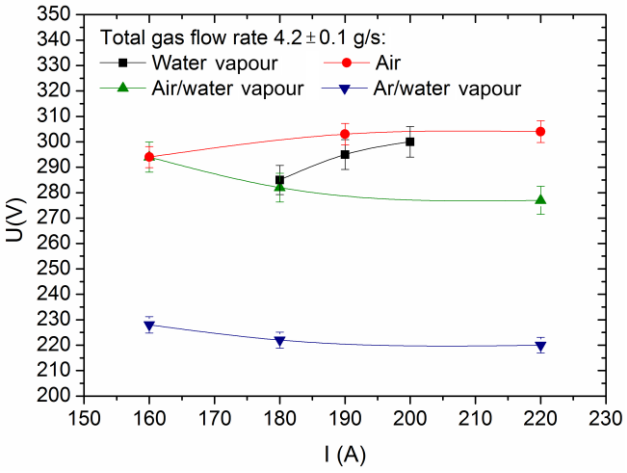

Fig. 3.1 The voltage-current characteristics (VCC) of the water vapour, air, air/water vapour and Ar/water vapour plasma torches when total gas flow rate equal to 4.2±0.1 g/s

In the cases of Ar/water vapour and air/water vapour, the voltage-current characteristics are slightly dropping in the range of current intensity of the electric arc between 160 and 190 A. The main reason of the VCC decrease could be the shunting (small and large scale) of the electric arc. At the same current intensity, the VCC of air and water vapour are increasing, thus indicating a more stable work of the plasma torch. In the range of 195–220 A, the VCC becomes constant in the cases of Ar/water vapour, air/water vapour and air. In this respect, it can be stated that at higher current

levels the electric arc becomes more stable. However, the VCC of the water vapour plasma torch remains increasing even between 190–200 A of current intensity. Moreover, the water vapour plasma torch did not work at the higher current intensity (>200 A) as well as at the lower current intensity (<160 A) because of the geometrical parameters of the plasma torch.

Furthermore, a noticeable difference in the measured voltage was observed between the used gases and the mixtures of gases. The lowest voltage was recorded using a mixture of Ar and water vapour, whereas the highest voltage was determined using the air. This trend can be explained by the physical properties of the gas. Since argon is a monoatomic noble gas, the voltage required to breakdown the gas and induce the electric discharge is lower compared to air, or triatomic H_2O vapour. As the result, the presence of argon serving as a shielding gas to protect the cathode exhibited the reduction of the electric field in the mixture of Ar/water vapour and thus, the arc voltage decreased. Zhukov et al. (Zhukov et al., 2007) stated that if a relative argon content in the mixture of gas exceeds 25 %, the arc voltage can be reduced by 1/3. In this experiment, a relative argon content ranged from 10 to 17 % depending on the changing water vapour flow rate. Besides, using the water vapour and the mixture of air/water vapour, a higher voltage was measured in the first substance. This tendency can be explained by the fact that the voltage required to breakdown the gas and induce the electric discharge is higher in the water vapour than in the mixture of the air/water vapour. Thus, water vapour has a higher strength of the electrical field compared to the mixture of the air/water vapour.

After the analysis of the primary experimental results, the VCC of the plasma torch operating on different types of gases were generalised and are shown in Fig. 3.2.

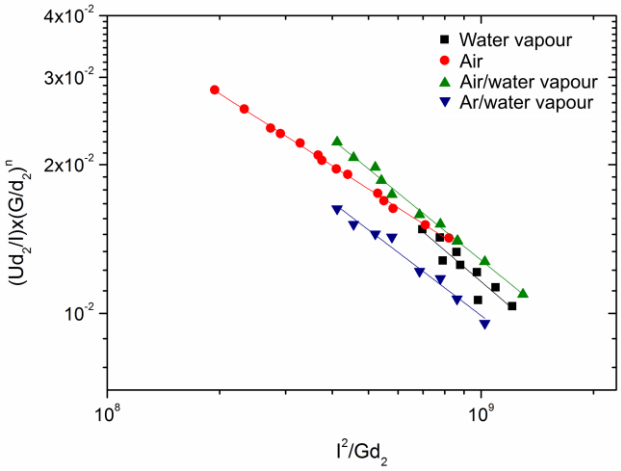

Fig. 3.2 The generalised water vapour, air, air/water vapour and Ar/water vapour plasma torch VCC

Figure 3.2 shows that the distribution of the VCC measuring points is quite equivalent in the cases of Ar/water vapour, air/water vapour, as well as air and this,

identifies a stable work of the plasma torch. However, the measuring points are fractionally scattered in the case of water vapour. The water vapour condensates on plasma torch inner walls, and compared with a mixture of the water vapour and gas, causes higher erosion of the electrodes. Thus, fractionally scattered points distribution could be explained by the influence of electrodes erosion, which initiates lightly jerking, pulsating arc burning (the oscillations of the plasma jet) and slightly unstable work of the plasma torch.

In order to ensure the maximum system efficiency, it is essential to obtain the most stable work of the plasma torch. In this respect, air and the mixtures of air/water vapour and Ar/water vapour showed the most stable operation of the torch. Furthermore, it is evident that the values of the electrical characteristics of Ar/water vapour are lower compared with the air, the water vapour and the mixture of air/water vapour. This once again can be explained by the influence of the strength of the electric field in the arc column, which depends on the type of gas and its physical properties. More precisely, the strength of the electric field for argon, air and water vapour are 5–8 V/cm, 10–15 V/cm and 20–27 V/cm, respectively (Zhukov et al., 2007). It is obvious that the strength of the electric field required to cause the voltage breakdown in the mixture of Ar/water vapour is lower compared with the rest mixtures of gases used. Since argon affected the reduction of the voltage in the mixture of Ar/water vapour, the operation of the plasma torch was the most stable. Air and mixture of air/water vapour also ensured the stable work of the plasma torch. The slightly unstable operation of the plasma torch was observed in the case of water vapour due to the lightly higher erosion of the electrodes.

The general equations of the electrical characteristics were determined by the theory of similarity (applying Eq. 2.5) and the obtained coefficient A, as well as the exponents m, n, is provided in Table 3.1

Table 3.1 Coefficient and exponents of the general equations of the plasma torch electrical characteristics

Plasma forming gas	A	m	n
Water vapour	3.5×10^2	-0.49	-0.24
Air	2.15×10^2	-0.46	-0.21
Air/water vapour	2.8×10^3	-0.59	-0.09
Ar/water vapour	0.65×10^3	-0.53	-0.15

3.2. Thermal characteristics of the plasma torch

The generalised thermal characteristics of the plasma torch operating on Ar/water vapour, air/water vapour, air and water vapour, respectively are shown in Figure 3.3. It is evident that the distribution of the measuring points is equivalent, and there are no significant outliers in all cases except air.

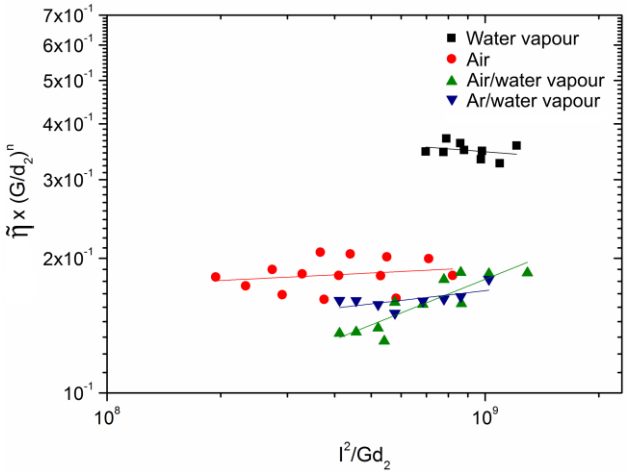

Fig. 3.3 The generalised thermal characteristics of the water vapour, air, air/water vapour and Ar/water vapour plasma torch

The general equations of the thermal efficiency of the plasma torch were determined on the basis of the theory of similarity (applying Eq. 2.7) and the obtained coefficient A, as well as the exponents m, n is given in Table 3.2.

Table 3.2 Coefficient and exponents of the general equations of the plasma torch thermal characteristics

Plasma forming gas	A	m	n
Water vapour	3.3×10^{-2}	0.11	-0.23
Air	6.5×10^{-3}	0.16	-0.54
Air/water vapour	2.3×10^{-5}	0.43	-1.36
Ar/water vapour	1.3×10^{-2}	0.12	-1.44

Obtained results (Table 3.2) shows that the generalised thermal characteristics of the plasma torch depend on the Reynolds number $\left(\frac{G}{d_2}\right)^n$ and the energy criterion $\left(\frac{I^2}{Gd_2}\right)^m$ in all cases. It must be noted that Reynolds number (Re) describes the nature of the fluid flow (laminar, transitional, or turbulent) which determines the type of the dominant heat losses (convective, radiant, and conductive) in the discharge chamber of the plasma torch. Laminar fluid flow is observed when the Reynolds number varies from 0.2 to 0.5. The fluid flow passes from laminar to turbulent when Re number reaches 0.8. Furthermore, the energy criterion determines the intensity of the energy exchange between the column of the electric arc and the heated gas. Also, it shows the extent by which the power of heat generation of the arc is higher than the thermal power of the jet, i.e. characterises the efficiency of the plasma torch as a thermal system (Zhukov et al., 2007).

Additionally, the thermal characteristics can also be described by the thermal efficiency (η), which depends on the heat exchange between the electric arc, heated

gas and walls of the discharge chamber. Figure 3.4 shows that the thermal efficiency decreased with the increase of the arc current due to the increased heat losses to the cooled walls of the discharge chamber of the plasma torch. The increased current caused the formation of an electric arc with a bigger diameter (Tamošiūnas et al., 2011). Thus, the space between electric arc and walls of the discharge chamber, through which plasma forming gas circulates, reduced. It means that the thickness of the boundary layer formed by the plasma forming gas decreased and this influenced the increase of the heat losses to the walls of the discharge chamber.

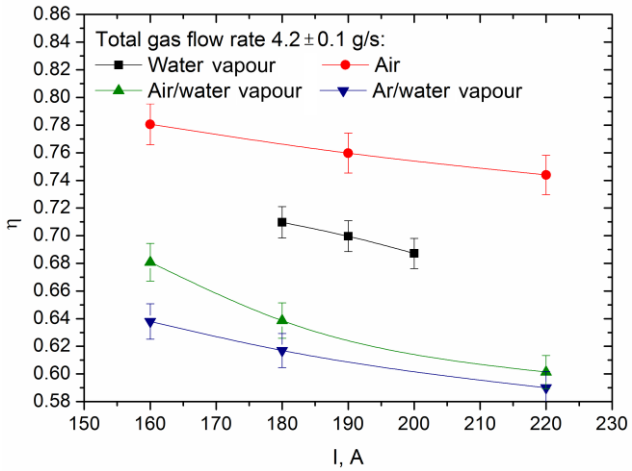

Fig. 3.4 Changes in plasma torch thermal efficiency, when the total gas flow rate is 4.2±0.1 g/s

Moreover, the obtained results revealed that the highest thermal efficiency of the plasma torch slightly differs in the cases of Ar/ water vapour ($\eta = 0.64 \pm 0.02$), air/water vapour ($\eta = 0.68 \pm 0.03$) and water vapour ($\eta = 0.71 \pm 0.01$) at the total gas flow rate of working gas of 4.2±0.1 g/s. However, in comparison with air/water vapour and Ar/water vapour, the water vapour required a higher current (I=180A instead of I=160A). This phenomenon was observed due to the fact that in the case of water vapour, the plasma torch did not work at the lower current (I=160A) because of the geometrical parameters of the plasma torch.

Additionally, comparing the thermal efficiency of air and water vapour, the higher thermal efficiency of the plasma torch was achieved using air plasma ($\eta = 0.78 \pm 0.02$). Such a tendency was observed due to the features of used gases. Firstly, the air has a lower enthalpy in comparison with water vapour. It means that energy consumption needed to generate air plasma is lower than in the case of the water vapour plasma. Secondly, air mainly contains nitrogen, oxygen, and argon in its composition, while water vapour consists of hydrogen and oxygen. Atomic hydrogen has higher thermal conductivity than atomic nitrogen or oxygen (Rutberg et al., 2013a, 2013b). It signifies that the heat exchange between electric arc, boundary gas layer, and walls of the discharge chamber is more intense in the case of water vapour. Thus,

this results in lower thermal efficiency ($\eta = 0.71 \pm 0.01$) compared to air plasma ($\eta = 0.78 \pm 0.02$).

Summarily, the evaluation of the plasma torch electrical and thermal characteristics in the case of using four different types of plasma forming gas (water vapour, air, air/water vapour, and Ar/water vapour) led to determine that air and mixture of air/water vapour ensure the most stable work of the plasma torch. Also, the highest thermal efficiency of the plasma torch was obtained in the cases of air/water vapour plasma ($\eta = 0.68 \pm 0.03$) and air plasma ($\eta = 0.78 \pm 0.02$). Consequently, air/water vapour plasma and air plasma is chosen for further experimental research – waste conversion (crude glycerol and diesel fuel contaminated soil) utilising thermal plasma. For simplicity, the term air/water vapour plasma in the following sections will be specified as water vapour plasma.

3.3. Gasification of crude glycerol into synthesis gas by thermal air plasma and thermal water vapour plasma

The experimental studies on waste conversion began with the gasification of liquid waste (crude glycerol) using thermal plasma. The effects of the gasifying agent (air plasma and water vapour plasma) flow rate and the plasma torch power on the conversion of crude glycerol to synthesis gas are discussed below. Also, quantification of the gasification system in terms of the producer gas composition, the lower heating value (LHV), the carbon conversion efficiency (CCE), energy conversion efficiency (ECE), and specific energy requirement (SER) are given below.

The concentrations of produced gases obtained after the gasification of crude glycerol by thermal air plasma and thermal water vapour plasma are presented in Fig. 3.5.

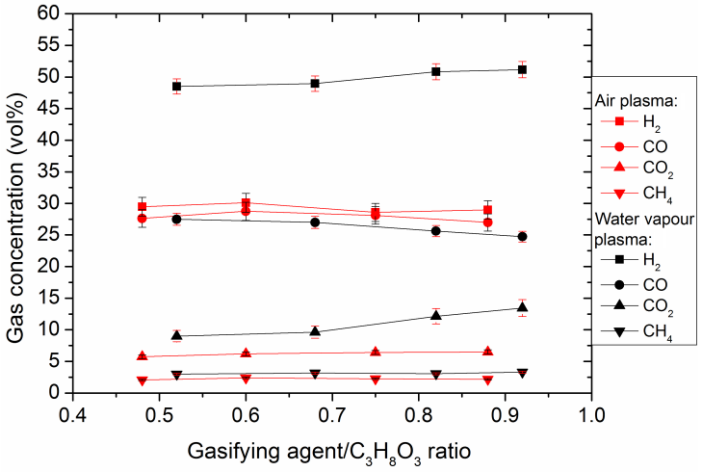

Fig. 3.5 Effect of the gasifying agent/$C_3H_8O_3$ ratio on the produced gas composition

As the Air/$C_3H_8O_3$ ratio increased from 0.48 to 0.88, the concentrations of produced gases remained basically stable. Synthesis gas accounted for 56.00 ± 0.30

vol% (29.00±0.30 vol% of H_2 and 27.00±0.30 vol% of CO) in the obtained producer gas. The concentrations of CO_2 and CH_4 were equal to 6.00±0.30 vol% and 2.00±0.20 vol%, respectively. The remaining gas was nitrogen (33.00±0.60 vol%).

As the water vapour/$C_3H_8O_3$ ratio increased from 0.52 to 0.92, the concentrations of H_2 and CO gases remained, in essence, stable, synthesis gas accounted to 76.00 ±1.36 vol% (51.16±1.26 vol% of H_2 and 24.74±1.46 vol% of CO) in the obtained producer gas. The concentration of the CO_2 increased from 9.00±2.10 vol% to 13.50±2.40 vol%, when the water vapour/$C_3H_8O_3$ ratio increased from 0.52 to 0.92. Such a tendency was observed due to the predominant steam reforming reaction (Eq. 1.15). Also, the water-gas shift (Eq. 1.16) and hydrogenolysis (Eq. 1.17) reactions influenced the increase of CO_2 concentration. The concentration of CH_4 remained basically stable (3.30± 0.20 vol%).

Moreover, the effect of the gasifying agent/$C_3H_8O_3$ ratio on the H_2/CO ratio was assessed (Fig. 3.6). As the Air/$C_3H_8O_3$ ratio increased from 0.48 to 0.88, the H_2/CO ratio slightly changed from 1.02 to 1.07. The change in the Air/$C_3H_8O_3$ ratio caused a negligible change in the H_2/CO ratio. This was mostly attributed to stable concentrations of produced gases of H_2 and CO.

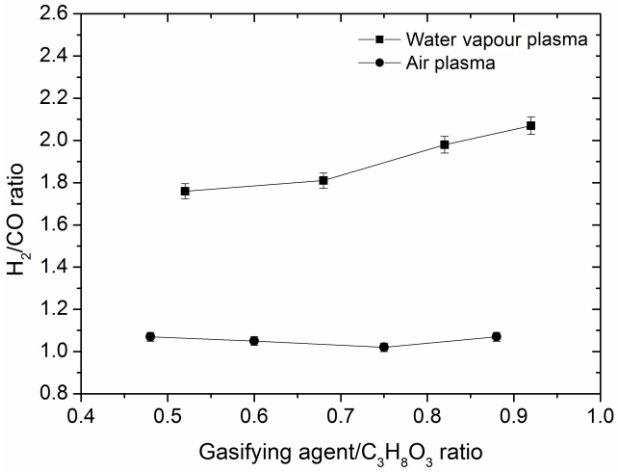

Fig. 3.6 Effect of the gasifying agent/$C_3H_8O_3$ ratio on the change of H_2/CO ratio

Also, the effect of the water vapour/$C_3H_8O_3$ ratio on the H_2/CO ratio was evaluated. As the water vapor/$C_3H_8O_3$ ratio increased from 0.52 to 0.92, the H_2/CO ratio changed from 1.76 to 2.07. The change in the water vapour/$C_3H_8O_3$ ratio caused a slight change in the H_2/CO ratio. This was mostly attributed to the generation of the slightly higher content of H_2 and slightly lower content of CO. Such tendency was observed due to the predominance of the steam reforming reaction (Eq. 1.15) and crude glycerol cracking (Eq. 1.9) reactions. Also, the obtained higher H_2/CO ratio (2.07) indicates that generated synthesis gas is appropriate for the direct biodiesel production via Fisher-Tropsch synthesis since the required H_2/CO ratio have to be 2:1 (Lin, 2013).

The composition of producer gas and H_2/CO ratio after crude glycerol gasification process with air plasma (at the Air/$C_3H_8O_3$ ratio 0.88) and water vapour plasma (at the H_2O/$C_3H_8O_3$ ratio 0.92) is present in Fig 3.7.

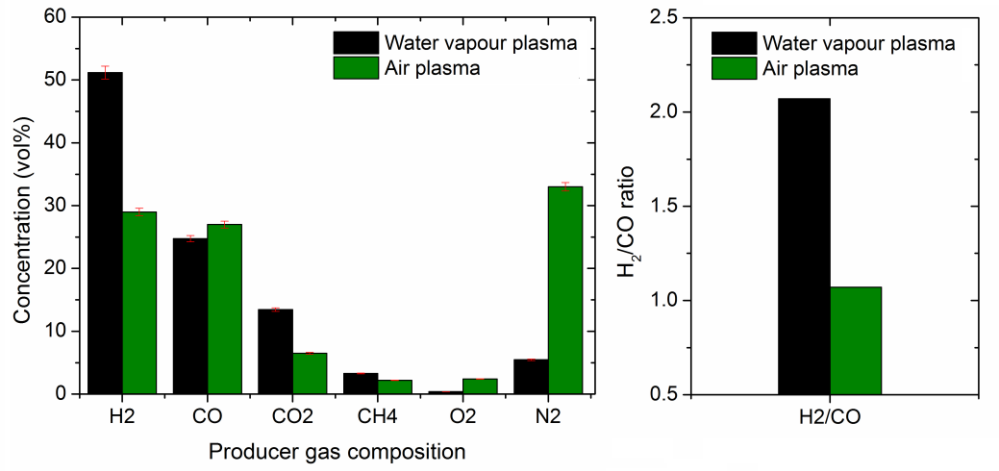

Fig. 3.7 Producer gas composition and the H_2/CO ratio after crude glycerol gasification (Air/$C_3H_8O_3$ ratio 0.88, Water vapour/$C_3H_8O_3$ ratio 0.92)

The generated producer gas mainly consisted of H_2 and CO (56.00±0.30 vol% and 76.00±1.36 vol% in the cases of air plasma and water vapour plasma, respectively). Also, a small content of CO_2 and CH_4 was obtained. Moreover, a higher amount of N_2 (33.00±0.60 vol%) was recorded, when the gasification of crude glycerol was carried out using air plasma. Nitrogen is a main compound in the air composition. Therefore, nitrogen composed a significant proportion of the produced synthesis gas. Also, a smaller amount of nitrogen (5.50±0.90 vol%) was recorded in the case of crude glycerol gasification with water vapour plasma. This was attributed to the usage of air (10–17 %) as a shielding gas protecting cathode of the plasma torch from the erosion.

Furthermore, the higher amount and higher quality synthesis gas were recorded performing crude glycerol gasification with water vapour plasma. Also, the higher H_2/CO ratio was obtained in the case of water vapour plasma. Once again, such a tendency was observed due to the dominance of the steam reforming (Eq. 1.15) and crude glycerol cracking (Eq. 1.9) reactions. Moreover, a higher amount of CO_2 was recorded using water vapor plasma. Such results were obtained due to the prevailing water-gas shift (Eq. 1.16), steam reforming (Eq. 1.15) and hydrogenolysis (Eq.1.17) reactions. Additionally, a lower formation of CO_2 during the gasification of crude glycerol in the environment of air plasma suggests insight into the predominance of partial oxidation reactions (Eq. 1.10–1.11) instead of complete oxidation reaction (Eq. 1.12) via the gasification process.

Moreover, the effect of the gasifying agent/$C_3H_8O_3$ ratio on the lower heating value of the produced synthesis gas was evaluated (Fig. 3.8). As the Air/$C_3H_8O_3$ ratio

increased from 0.48 to 0.88, the LHV of the synthesis gas slightly increased from 7.32 MJ/nm^3 to 7.74 MJ/nm^3. Thus, the variation of the Air/$C_3H_8O_3$ ratio caused slight changes in the LHV of the syngas due to the same effect as described for the H_2/CO ratio. Moreover, the dominance of crude glycerol cracking (Eq. 1.9) and partial oxidation reaction (Eq. 1.10) let to the formation of the stable concentrations of H_2 and CO. Methanation (Eq. 1.13) and oxidation reactions (Eq. 1.11–1.12) led to a slight increase of CH_4 and CO_2 concentrations as the Air/$C_3H_8O_3$ ratio increased. Thus, these reactions also had an effect on the slight increase in the lower heating value of produced syngas. Usually, synthesis gas generated using air as a gasifying agent is referred as a low calorific value gas. Its LHV ranges from 4.00 to 7.00 MJ/nm^3 (Basu, 2010; McKendry, 2002). Hereby, the synthesis gas with a lower calorific value of 7.74 MJ/nm^3 was generated during the gasification of crude glycerol by thermal air plasma.

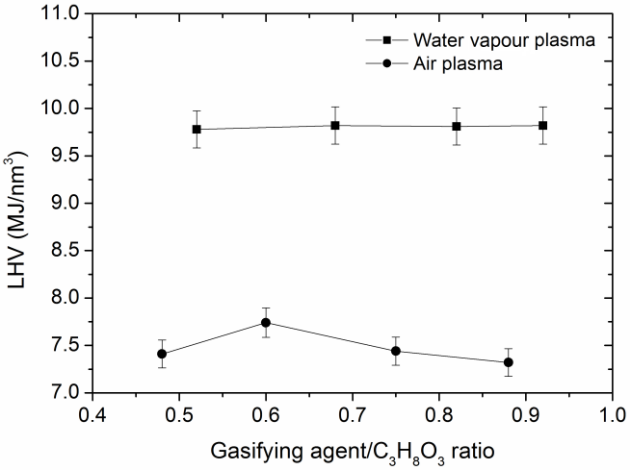

Fig. 3.8 Effect of the gasifying agent/$C_3H_8O_3$ ratio on the lower heating value

Also, the effect of the water vapour/$C_3H_8O_3$ ratio on the lower heating value of the generated synthesis gas was evaluated. As the water vapour/$C_3H_8O_3$ ratio increased from 0.52 to 0.92, the LHV of the synthesis gas remained about 9.82 MJ/Nm^3. Thus the negligible change in the LHV of synthesis gas was caused due to the steady concentrations of H_2 and CO gases generated via predominance crude glycerol cracking (Eq. 1.9) and steam reforming (Eq. 1.15) reactions. Furthermore, methanation (Eq. 1.13-1.14), water-gas shift (Eq. 1.16), hydrogenolysis (Eq. 1.17) as well as steam reforming (Eq. 1.15) reactions let to a formation of CH_4 and CO_2. Hence, these reactions also affected the lower heating value of the generated synthesis gas. Additionally, the lower heating value of produced synthesis gas obtained after the crude glycerol gasification with air plasma was lower (7.74 MJ/Nm^3) compared to the water vapour plasma. Such a trend was obtained because air consists of a high amount of nitrogen, which is also present in the generated producer gas.

The effect of the gasifying agent/$C_3H_8O_3$ ratio on the carbon conversion efficiency is shown in Fig. 3.9. As the Air/$C_3H_8O_3$ ratio increased from 0.48 to 0.88,

the carbon conversion efficiency increased from 51.30 % to 75.19 %. The obtained trend demonstrates that the increased airflow rate, at the glycerol flow rate being stable at 5.64±0.2 g/s, caused an increase in the flow rate of produced syngas. As a result, this directly affected the increase of carbon conversion efficiency. Furthermore, the increase in the airflow rate, at the other parameters, such as the arc current, being constant at 160 A, led to the higher power of the plasma torch, which increased from 45.60 kW to 56.00 kW. This was mostly attributed to a significant increase in voltage from 285 V to 350 V, which was directly affected by the increased airflow rate.

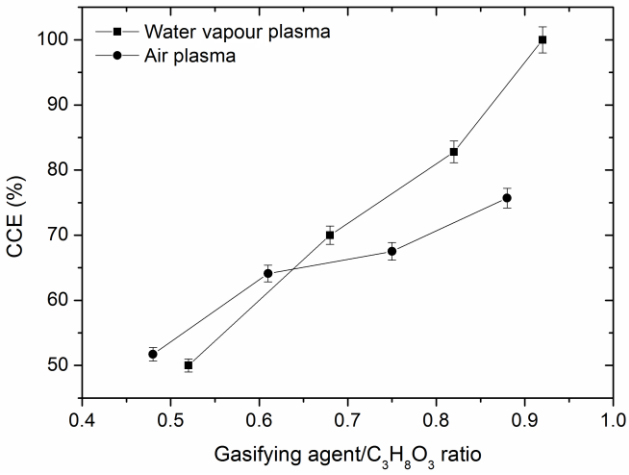

Fig. 3.9 Effect of the gasifying agent/$C_3H_8O_3$ ratio on the carbon conversion efficiency

The obtained results are in a good agreement with Yoon et al. (Yoon et al., 2010, 2013) and Zhang et al. (Zhang et al., 2017b) experimental investigations. Yoon et al. (Yoon et al., 2010) indicated that increased air ratio enlarged oxidation reaction and gasification process. Thus, carbon conversion efficiency increased from approximately 56 % to 78 %. Zhang et al. (Zhang et al., 2017b) found that the carbon conversion increased from around 35 % to 95 % with an increase in input power from 7 kW to 15 kW. The conversion of almost 100 % was gained at the input power of 17.1 kW. Yoon et al. (Yoon et al., 2013) determined that growing microwave power from 1 kW to 1.8 kW raised the H_2 and CO content in the synthesis gas from approximately 25 % and 31% to 38 % and 35 %, respectively. Also, increased power caused an increase in the carbon conversion efficiency from around 78 % to almost 100 %.

Additionally, the increase of the water vapour/$C_3H_8O_3$ ratio from 0.52 to 0.92 caused the rise in the carbon conversion efficiency from 50 % to 100 %. The obtained tendency shows that the increased water vapour rate, the arc current being constant (160A), induced the increase of the arc voltage from 350 V to 390 V. Consequently, the power of the plasma torch was raised from 56.00 kW to 62.40 kW. Moreover, the higher power of the plasma torch ensures the higher temperature and energy density, which is useful for complete crude glycerol valorisation. Furthermore, the carbon

conversion efficiency obtained in the case of crude glycerol gasification with air plasma was equal to 75.19 %, while the water vapour plasma can provide complete carbon conversion during the crude glycerol gasification process.

The effect of the gasifying agent/$C_3H_8O_3$ ratio on the crude glycerol conversion process performance in terms of the energy conversion efficiency is given in Fig. 3.10. As the Air/$C_3H_8O_3$ ratio increased from 0.48 to 0.88, the energy conversion efficiency increased from 13.12 % to 17.35 %. The optimum crude glycerol gasification to synthesis gas process effectiveness was obtained at the ECE of 17.35 % when the flow rate of air and the plasma torch power were the highest at 4.90 g/s and 56.00 kW, respectively. Since the change in the airflow rate directly affects the increase/decrease of the voltage of the arc, the arc current intensity being constant, this however directly influences the energy conversion efficiency. Therefore, the increased power of the plasma torch from 45.60 kW to 56.00 kW should decrease the efficiency of the gasification process according to Eq. 1.11. However, in this particular case, the ECE increased as the power of the plasma torch also increased due to the fact that more syngas was produced.

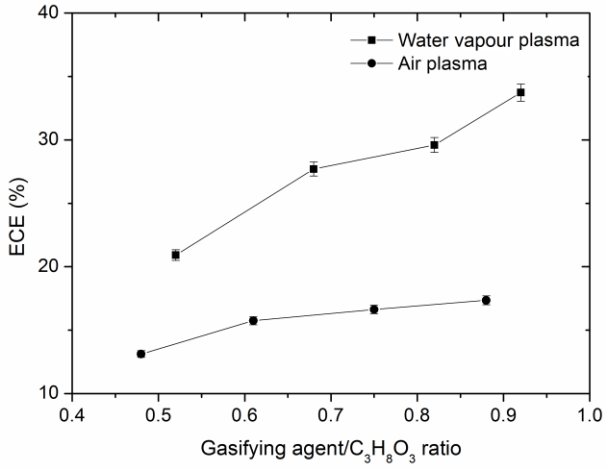

Fig. 3.10 Effect of the gasifying agent/$C_3H_8O_3$ ratio on the energy conversion efficiency

Additionally, as the water vapour/$C_3H_8O_3$ ratio increased from 0.52 to 0.92, the energy conversion efficiency increased from 20.91 % to 33.73 %. The highest crude glycerol gasification to synthesis gas process effectiveness was received at the ECE of 33.73 %, when the flow rate of water vapour and the power of the plasma torch were at the highest values of 5.15 g/s and 62.40 kW, respectively. As in the case with air plasma, the change in the water vapour flow rate affects the change of the power of the plasma torch. Hence, the power of the plasma torch increased from 56.00 kW to 62.40 kW and this caused the raise of the energy conversion efficiency. The gained experimental results demonstrated that crude glycerol gasification with water vapour plasma is more efficient compared to air plasma gasification, where the highest ECE

was equal to 17.35 %. Water vapour, as a gasifying agent, led to generate a higher amount of synthesis gas, and this ensured better energy conversion efficiency.

The effect of the gasifying agent/$C_3H_8O_3$ ratio on the crude glycerol conversion process performance in terms of the specific energy requirements is given in Fig. 3.11. As the Air/$C_3H_8O_3$ ratio increased from 0.48 to 0.88, the SER decreased from 310.50 kJ/mol to 266.50 kJ/mol (or from 2.88 kWh/kg to 2.47 kWh/kg). The best crude glycerol gasification to synthesis gas process efficiency was achieved at the SER of 266.50 kJ/mol when the flow rate of air and the plasma torch power were at 4.90 g/s and 56.00 kW, respectively. Regardless of the highest power of the plasma torch at the Air/$C_3H_8O_3$ ratio of 0.88, the SER was the lowest. This can be explained due to a higher amount of syngas produced according to Eq. 1.11.

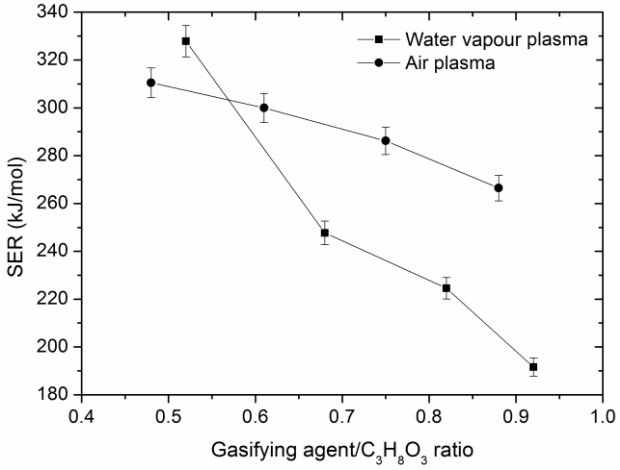

Fig. 3.11 Effect of the gasifying agent/$C_3H_8O_3$ ratio on the specific energy requirements

Further, as the water vapour/$C_3H_8O_3$ ratio increased from 0.52 to 0.92, the SER decreased from 327.88 kJ/mol to 191.60 kJ/mol (or from 3.04 kWh/kg to 1.78 kWh/kg). The greatest crude glycerol gasification to synthesis gas process was obtained at the SER of 191.60 kJ/mol, when the flow rate of water vapour and the power of the plasma torch was equal to 5.15 g/s and 62.40 kW, respectively. Despite the highest power of the plasma torch at the water vapour/$C_3H_8O_3$ ratio of 0.92, the SER was the lowest. Such a trend was observed due to the predominance of the steam reforming (Eq. 1.15), glycerol decomposition (Eq. 1.9) and water gas shift (Eq. 1.16) reactions which induced the generation of the higher amount of synthesis gas. Moreover, at the highest air/$C_3H_8O_3$ ratio (0.88), the SER was equal to 266.50 kJ/mol (or 2.47 kWh/kg). Thus, the specific energy requirement was lower in the case when the water vapour was used as a plasma forming gas and a gasifying agent. Accordingly, the usage of water vapour plasma for crude glycerol gasification ensures the generation of the higher amount of synthesis gas with the lower energy requirement compared to oxidation process which appears during the usage of the air plasma.

The summary of the experimental results gained during the gasification of crude glycerol with the thermal plasma is given in Table 3.3. Obtained results revealed that crude glycerol conversion efficiency using thermal water vapour plasma is higher via all evaluated parameters in comparison with the case of air plasma.

Table 3.3 Summary of the data obtained during the crude glycerol conversion using thermal plasma (Air/$C_3H_8O_3$ ratio 0.88, Water vapour/$C_3H_8O_3$ ratio 0.92)

Parameter	Air plasma	Water vapour plasma
H_2, vol.%	29.00	51.16
CO, vol.%	27.00	24.74
H_2/CO	1.07	2.07
LHV, MJ/Nm^3	7.74	9.82
CCE, %	75.19	100.00
ECE, %	17.35	33.73
SER, kJ/mol	266.50	191.60
SER, kWh/kg	2.47	1.78

Such a tendency was obtained due to the predominance of the steam reforming reaction (Eq. 1.15) in the case of the water vapour plasma. The latter reaction led to generate a higher amount of H_2 comparing to the amount gained via the partial oxidation (Eq. 1.10–1.11) or complete oxidation (Eq. 1.12) reactions, which is predominant in the case of the air plasma. Also, the higher amount of N_2 was recorded in the producer gas, when the air was used as a plasma forming gas and the gasifying agent. Consequently, N_2 also contributed to the lower crude glycerol conversion process efficiency.

3.4. Evaluation of energy efficiency of crude glycerol gasification using thermal air plasma

The evaluation of the energy efficiency of the crude glycerol gasification system was performed by determining mass and energy balance in separate nodes (Eq. 2.19 – 2.34) of the thermal air plasma technological system (Fig. 3.12). Firstly, the 17.60 kg/h of air and 56.00 kWh of electrical energy was supplied to the plasma torch to generate the thermal air plasma which was utilised for gasification of crude glycerol. The electrical energy was transformed into thermal energy during the formation of the air plasma. The plasma torch was water-cooled. Thus, part of the thermal energy was transferred to the water which cools cathode (5.60 kWh) and anode (8.90 kWh) in the plasma torch. Consequently, the cathode cooling water and anode cooling water were heated up to 37.7 °C and 40.3 °C, respectively, from the initial 20 °C temperature of the cooling water. Hence, the energy supplied to the plasma-chemical reactor was equal to 41.50 kWh. Also, the 20.30 kg/h of crude glycerol was provided to a plasma-chemical reactor for the gasification process.

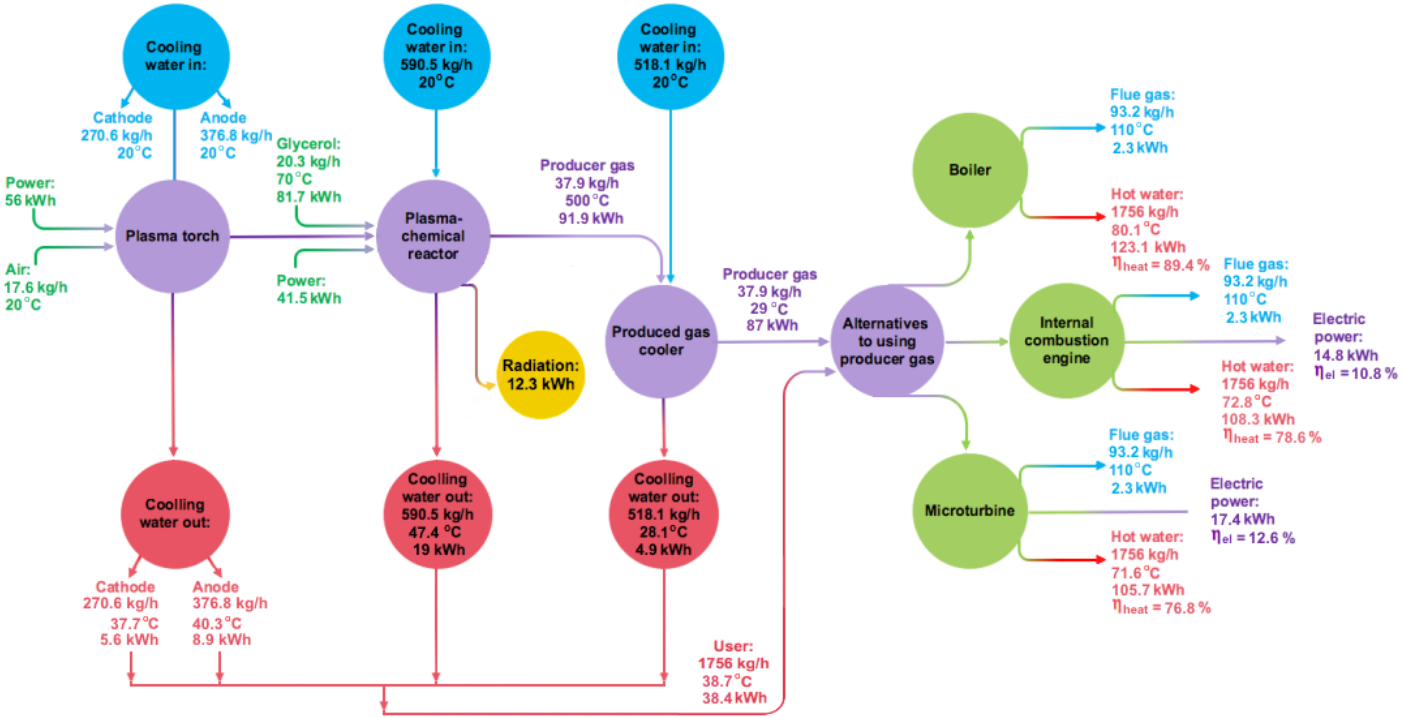

Fig. 3.12 Energy balance of the thermal air plasma technology used for the crude glycerol gasification

The amount of energy stored in the feedstock was equal to 81.70 kWh. Thus, the total supplied energy to the plasma-chemical reactor was equal to 123.20 kWh. However, the part of the energy was lost in the cooling water (19.00 kWh) which heated up to 40.9 °C from the primary 20 °C of the cooling water. Another part of the energy was lost via the radiation of the plasma-chemical reactor (12.30 kWh). Hence, the remaining content of the energy (91.90 kWh) took part in the crude glycerol gasification and synthesis gas formation process.

Further, 37.90 kg/h of producer gas was generated during the gasification process. The energy content of the producer gas was equal to 91.90 kWh. The generated producer gas was diverted downstream to the gas cooler. The 4.9 kWh of the energy was lost into the cooling water here, and producer gas temperature decreased from 500 °C to 29 °C. Thus, the remained total producer gas energy was equal to 87 kWh. Summarily, a significant amount of the energy was lost into the cooling water of the plasma technological system. Therefore, the cooling system must be optimised to reduce energy losses.

Moreover, the generated producer gas can be used for the generation of thermal energy in the boiler, or electrical and thermal energy in the internal combustion engine or microturbine. The efficiency of these possible utilisation ways was determined by Equations 2.32 and 2.33, respectively. The conversion efficiency of the producer gas into electricity in an internal combustion engine could be 10.8%, while in the microturbine it can be equal to 12.60% (Chaves et al., 2016; Messerle et al., 2018; Striūgas et al., 2017).

Accordingly, the total efficiency of the process may be equal to 89.40% (or 123.10 kWh), if the producer gas would be used in the boiler. In the case, when producer gas would be utilised in the internal combustion engine, the thermal energy of the process may be equal to 78.60 % (or 108.30 kWh) and the electrical energy of the process could be equivalent to 10.80 % (or 14.80 kWh). If the producer gas would be used in the microturbine, 76.80 % (or 105.70 kWh) of the thermal energy and 12.60 % (or 17.40 kWh) of the electrical energy may be obtained. Also, the calculation of the electrical efficiency showed that 26.40 % and 31.10 % of the energy required for the formation of plasma can be recovered after producer gas usage in the internal combustion engine and the microturbine, respectively. Thus, the performed calculation revealed that a higher part of the energy is recovered in the form of the thermal energy, while a small part of the energy could be received in the form of electrical energy. Moreover, the estimation of possible ways to use producer gas was performed assuming that the hot water produced during the cooling of the crude glycerol gasification system could be used as the feed water provided for example to the boiler.

3.5. Evaluation of energy efficiency of crude glycerol gasification using thermal water vapour plasma

The determination of the energy efficiency of the crude glycerol gasification system was performed by evaluating mass and energy balance in separate nodes (Eq. 2.19–2.34) of the thermal water vapour plasma technological system (Fig. 3.13).

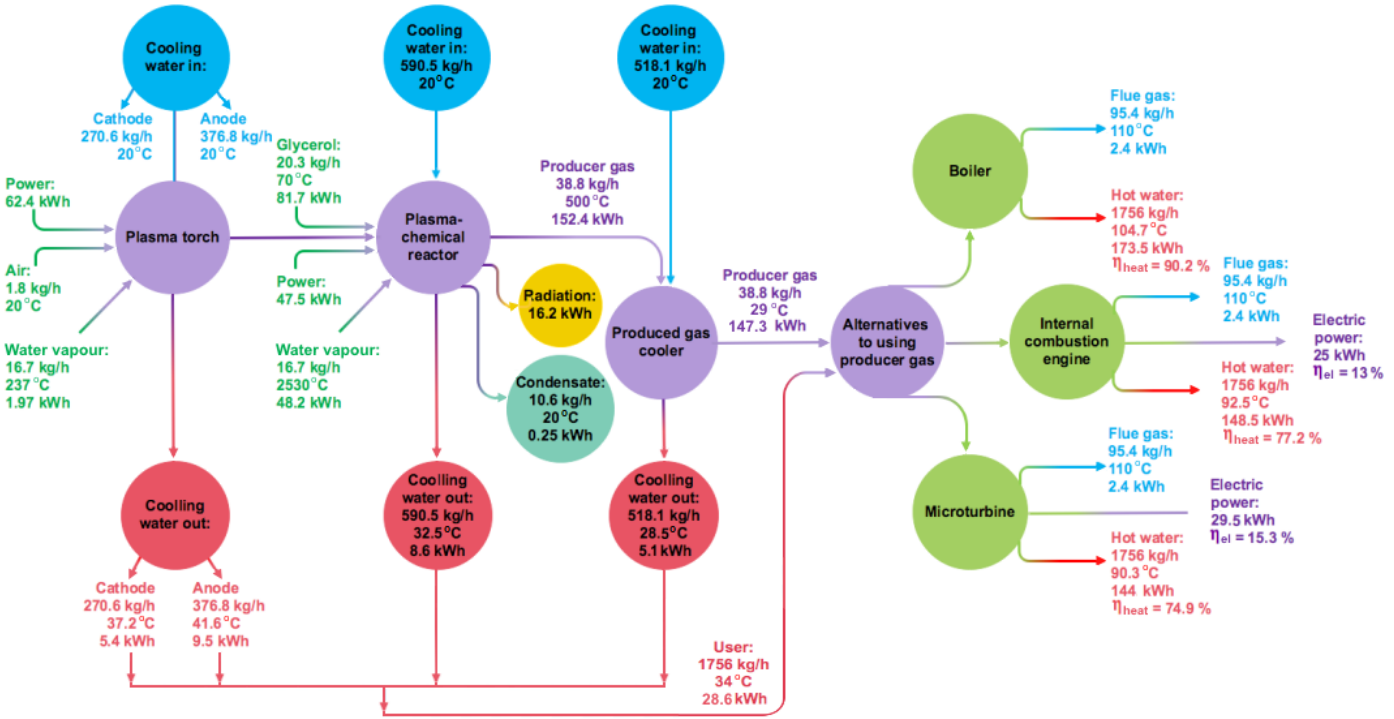

Fig. 3.13 Energy balance of the thermal water vapor plasma technology used for the crude glycerol gasification

Firstly, the 1.80 kg/h of air, 16.70 kg/h (or 1.97 kWh) of water vapour and 62.40 kWh of electrical energy was provided to the plasma torch for the generation of the thermal water vapour plasma. The part of the supplied total energy was transferred to the cooling water of the cathode (5.40 kWh) and anode (9.50 kWh) in the plasma torch. Therefore, the cathode cooling water and anode cooling water were heated up to 37.2 °C and 41.6 °C compared to the room temperature. Thus, the energy provided to the plasma-chemical reactor was equal to 47.50 kWh. Moreover, the 20.30 kg/h (or 81.70 kWh) of crude glycerol was supplied to a plasma-chemical reactor. Also, the water vapour was used as a plasma forming gas. Thus, after passing the plasma torch, the energy provided by the water vapour increased to 48.20 kWh, since the plasma was formed. The total supplied energy to the plasma-chemical reactor was equal to 177.40 kWh.

Nevertheless, the part of the energy was lost in the cooling water (8.60 kWh) which heated up to 32.5 °C from the initial 20 °C temperature of the cooling water. Another part of the energy was lost via the radiation of the plasma-chemical reactor (16.20 kWh) and the condensation of the water vapour (0.25 kWh). Accordingly, the remaining content of the energy (152.40 kWh) was used in the crude glycerol gasification and synthesis gas generation process. Consequently, 38.80 kg/h of producer gas was generated via the gasification process. The energy content of the producer gas was equal to 152.40 kWh. The formed producer gas was channelled to the gas cooler there 5.10 kWh of producer gas energy was transferred to the cooling water. Hence, the remained total producer gas energy was equal to 147.30 kWh.

As in the case when air plasma was used as a gasifying agent, a noticeable amount of the energy was lost into the cooling water of the gasification system.

Also, the estimation of the producer gas possible use in the boiler, internal combustion engine and microturbine was performed. If the producer gas would be used in the boiler, 90.20 % (or 173.50 kWh) of the thermal energy may be obtained. In the case, when producer gas would be used in the internal combustion engine, the thermal energy of the process may be equivalent to 77.20 % (or 148.50 kWh) and the electrical energy of the process could be equal to 13.00 % (or 25.00 kWh). The thermal efficiency of the process may be equal to 74.90 % (or 144.00 kWh), and the electrical energy of the process could be equal to 15.30 % (or 29.50 kWh) if the producer gas would be used in the microturbine. Moreover, the calculation of the electrical efficiency revealed that 40.10 % and 47.10 % of the energy needed for the formation of plasma can be recovered after the usage of the producer gas in the internal combustion engine and the microturbine, respectively. The rest of the energy is recovered in the heat form (for the most part in hot water).

The obtained results led to indicate that the slightly higher amount of electrical energy can be received when the producer gas is utilised in the microturbine. This trend was also seen in the case of air plasma. Moreover, the producer gas with higher energy (152.40 kWh) was generated in the case of the water vapour plasma, compared to the air plasma (91.90 kWh). Such results were influenced by the predominant steam reforming (Eq. 1.15), pyrolysis (Eq. 1.9), water-gas shift (Eq. 1.16) reactions.

The evaluation of producer gas utilisation options showed that a higher amount of energy could be obtained when the gasification of the crude glycerol is performed using the water vapour plasma instead of the air plasma (Table 3.4).

Table 3.4 The energy obtained from the producer gas

	The gasification of 20.3 kg/h of crude glycerol		The gasification of 1 kg/h of crude glycerol	
	Air plasma	Water vapour plasma	Air plasma	Water vapour plasma
Producer gas, kWh	91.90	152.40	4.53	7.51
Boiler, thermal energy, kWh	123.10	173.50	6.06	8.55
ICE, thermal energy, kWh	108.30	148.50	5.34	7.32
ICE, electrical energy, kWh	14.80	25.00	0.73	1.23
Microturbine, thermal energy, kWh	105.70	144.00	5.21	7.09
Microturbine, electrical energy, kWh	17.40	29.50	0.86	1.45
The energy required for plasma formation, recovered from the producer gas using ICE, %	26.40	40.10	1.30	1.98
The energy required for plasma formation, recovered from producer gas using Microturbine, %	31.10	47.10	1.53	2.32

The calculated system electrical efficiency showed that almost one-third (26.40–31.10 %) of the energy needed for the formation of the plasma could be recovered during the crude glycerol conversion with the air plasma. Moreover, more than one-third (40.10–47.10 %) of the energy required for the plasma generation could be recovered during the crude glycerol conversion with the water vapour plasma.

3.6. Diesel fuel contaminated soil remediation using the thermal plasma

The experimental studies on waste conversion were continued with the diesel fuel contaminated soil remediation with the thermal plasma. The analysis of the soil surface morphology, soil elemental composition and produced gas composition, as well as thermogravimetric analysis, are provided below. Also, the mechanism of diesel fuel polluted soil remediation with the thermal plasma and the comparison of proposed technology with other plasma technologies applied for the petroleum products contaminated soil remediation are given below.

3.6.1. Loamy-sandy soil surface morphology analysis

Investigation of surface morphology of the clean soil, contaminated soil (with 80±3 g/kg, 120±3 g/kg and 160±3 g/kg of diesel fuel) and plasma-treated soil was carried out by means of the SEM (Fig 3.14). Clean soil (Fig 3.14 a) had a granular structure and consisted of small grains. SEM images of the contaminated soil (Fig 3.14 b, c, d) revealed surface modification. Contaminated soil consisted of larger clumps which merged into bigger agglomerates when diesel fuel concentration

increased from 80±3 g/kg to 160±3 g/kg. The soil humidity increased following the increase in the concentration of diesel fuel (Table 2.2) which induced the growing adhesion of soil grains into the larger agglomerates. Furthermore, after the treatment of contaminated soil in the ambient of water vapour plasma (Fig 3.14 e, f, g) or the ambient of air plasma (Fig 3.14 h, i, j), soil grains became akin in size and structure to the clean soil grains.

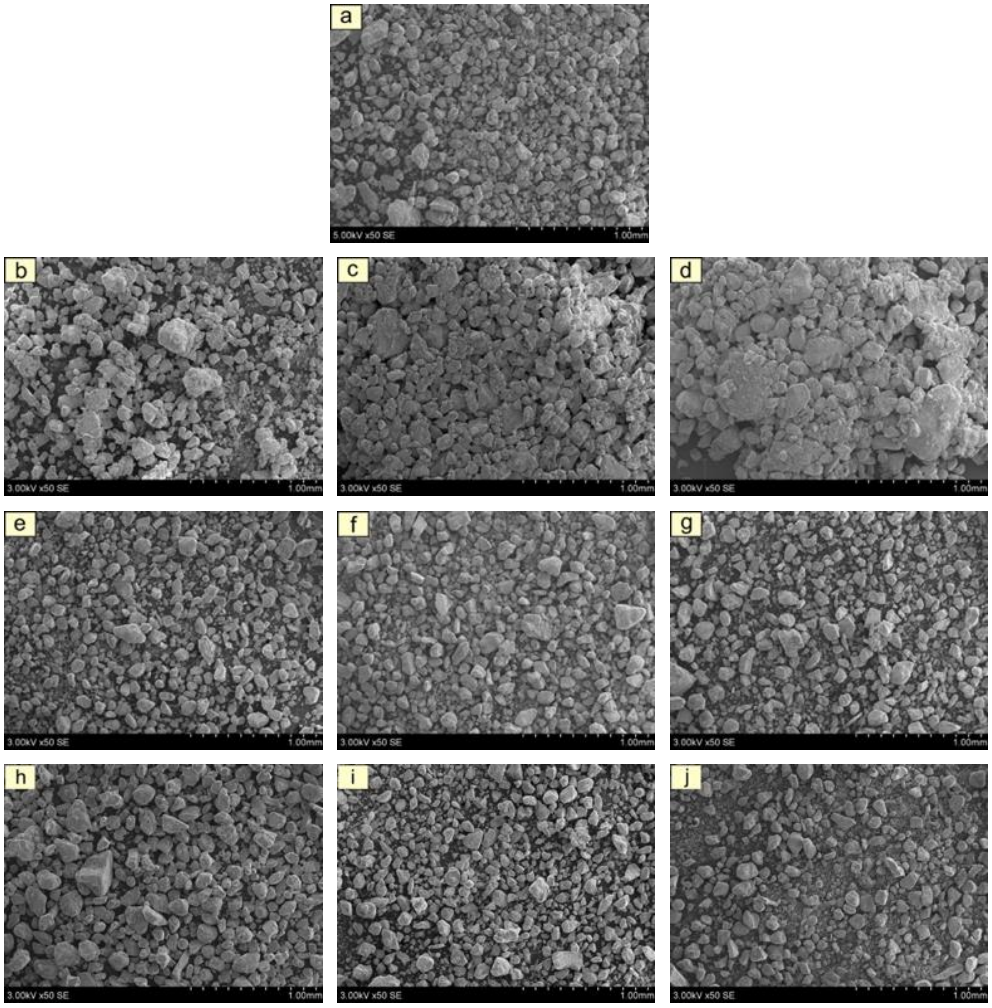

Fig. 3.14 SEM images of soil surface: a – clean soil; b, c, d – soil contaminated with diesel fuel 80±3 g/kg, 120±3 g/kg, and 160±3 g/kg, respectively; e, f, g – contaminated soil (80±3 g/kg, 120±3 g/kg, and 160±3 g/kg, respectively) after the remediation in the water vapour plasma; h, i, j – contaminated soil (80±3 g/kg, 120±3 g/kg, and 160±3 g/kg, respectively) after the remediation in the air plasma

Similar changes in the soil surface morphology were observed by Taheri et al. (Taheri et al., 2018). SEM images of clean soil (sand-bentonite mixture), as well as soil contaminated with 4 %, 8 % and 12 % of diesel by weight of dry soil, indicated that the grains in the contaminated soil were noticeably larger than those in the clean soil. Researches summed up that this tendency was obtained due to the coverage of clay grains with oil (diesel), which caused soil flocculation (formation of larger clumps). Moreover, Kermani and Ebadi (Kermani et al., 2012) performed a consolidation test of soil contaminated by oil and determined that compressibility distinctively increased as the pollutant concentration increased. Authors stated that such a trend could be assigned to the lubrication effect of the oil. Thus, it caused easier soil compression into denser configurations.

3.6.2. Elemental composition analysis of loamy-sandy soil

The elemental composition of clean soil, soil contaminated with diesel fuel and soil remediated in the water vapour plasma, or air plasma determined by EDX are shown in Table 3.5. Comparison of the soil elemental composition revealed that as the concentration of diesel fuel increased from 80±3 g/kg to 160±3 g/kg, the carbon concentration increased to 10.39±0.10 %, 15.56±0.16 % and 20.29±0.20 %, respectively, from the initial 5.06±0.05 % concentration of the clean soil. The obtained results are in line with the CHNS's data presented in Table 2.2 in terms of the increased amount of the carbon concentration in the soil. However, the values are not equal or similar due to the measurement difference of the methods. Furthermore, after the interaction between the contaminated soil and water vapour plasma, the carbon concentration decreased to 4.03±0.04 %, 2.23±0.02 % and 3.45±0.04 %, respectively. Also, the noticeable change in the carbon concentration was observed after interaction between the polluted soil and air plasma. Thus, the carbon concentration in the soil reduced to 1.84±0.02 %, 1.72±0.02 %, and 1.88±0.02 %, respectively. According to the obtained results it could be said that the remediation process caused the desorption of carbon, which come from diesel fuel in the form of hydrocarbon to the soil. Moreover, during soil remediation with air plasma, a slight decomposition of organic matter (natural carbon) present in the soil was also observed, when the temperature of the gasification environment was equal to 4100±113 K. Hence some organic carbon was evaporated from the soil during the gasification process since carbon sublimation starts to happen at the temperature of 3925–4073 K. The concentrations of soil minerals (K, Ca, Mg, Al, Fe, Na, Ti) changed inconsiderably. Latter results are consistent with Snellings et al. (Snellings et al., 2012) remarks. Authors stated that most of the minerals that are presented in the burned sediments not volatilise. Hence, some of the minerals stayed unaltered, and some become amorphous or recrystallised to form secondary minerals. Additionally, after the remediation process, soil samples were tested according to the normative document LAND-89-2010. The concentration of diesel fuel in the soil was not detected or was below the laboratory detection limit (< 89 mg/kg).

Table 3.5 Elemental composition of clean, contaminated and plasma treated loamy-sandy soil

Element	Clean soil, at[c] %	Soil contaminated with diesel fuel, at %		
		80 g/kg[d]	120 g/kg	160 g/kg
Carbon	5.06±0.05	10.39±0.10	15.56±0.16	20.29±0.20
Oxygen	63.95±0.64	61.05±0.61	61.68±0.62	58.68±0.59
Silicon	21.71±0.22	18.62±0.19	15.33±0.15	12.49±0.12
Potassium	1.38±0.01	1.15±0.01	0.80±0.01	0.77±0.01
Calcium	1.23±0.01	1.26±0.01	1.09±0.01	1.30±0.01
Magnesium	0.60±0.01	0.92±0.01	0.59±0.01	0.82±0.01
Aluminium	4.32±0.04	4.69±0.05	3.13±0.03	3.86±0.04
Iron	1.20±0.01	1.52±0.01	1.43±0.01	1.38±0.01
Sodium	0.36±0.01	0.22±0.01	0.21±0.01	0.21±0.01
Titanium	0.19±0.01	0.18±0.01	0.18±0.01	0.20±0.01

Element	Contaminated soil treated in the water vapour plasma, at %			Contaminated soil treated in the air plasma, at %		
	80 g/kg	120 g/kg	160 g/kg	80 g/kg	120 g/kg	160 g/kg
Carbon	4.03±0.04	2.23±0.02	3.45±0.04	1.84±0.02	1.72±0.02	1.88±0.02
Oxygen	61.57±0.62	63.84±0.64	62.30±0.62	64.35±0.64	62.92±0.63	64.36±0.64
Silicon	23.8±0.24	23.88±0.24	25.87±0.26	23.45±0.23	23.74±0.24	24.54±0.25
Potassium	1.73±0.02	1.29±0.01	0.94±0.01	1.43±0.01	2.37±0.02	0.84±0.01
Calcium	1.29±0.01	1.77±0.02	1.06±0.01	1.38±0.01	2.18±0.02	1.67±0.02
Magnesium	0.71±0.01	0.72±0.01	0.68±0.01	1.00±0.01	0.93±0.01	0.69±0.01
Aluminium	4.74±0.05	4.22±0.04	3.92±0.04	3.83±0.04	3.98±0.04	3.71±0.04
Iron	1.70±0.02	1.58±0.02	1.41±0.01	1.46±0.02	1.50±0.02	1.97±0.02
Sodium	0.16±0.01	0.22±0.01	0.19±0.01	0.98±0.01	0.38±0.01	0.13±0.01
Titanium	0.27±0.01	0.24±0.01	0.18±0.01	0.28±0.01	0.28±0.01	0.23±0.01

[c] Atomic concentration of element, %

[d] Diesel concentration in the soil, g/kg

3.6.3. Loamy-sandy soil thermal analysis

The TGA (TG), DTG, and DSC measurements were performed through the combustion process (Fig. 3.15 a–d) to identify diesel fuel behaviour in the soil during the remediation process. Firstly, the research was carried out with clean soil (Fig. 3.15 a). The combustion process of clean soil can be divided into three mass loss stages. In the first stage, the TGA curve represents the slight decrease of the moisture content in the soil (0.45±0.02 %). The second mass loss stage (between 11 and 23 min) represents the decrease of organic matter and volatiles in the soil (3.12±0.13 %). According to TGA and DTG data, the third mass loss of the sample (1.73±0.07 %) lasts up to 28 min of the measurement. The maximum DTG negative peak (at 746.90 °C) represents the maximum decrease of char in the soil during the combustion process. Also, the formation of ash (94.62±3.78 %) was recorded. DSC curve shows the endothermic process.

Further studies were carried out with contaminated soil (Fig. 3.15 b–d). Regardless of the diesel concentration (80±3 g/kg, 120±3 g/kg, or 160±3 g/kg) in the soil, four stages of mass loss were observed (Fig. 3.15 b–d). On the base of TGA data, the first mass loss stage corresponds to the reduction of the moisture content in the soil (1.75±0.07 %), while the first DTG negative peak (the second stage of mass loss) recorded between 10 and 15 min of the measurement (at 180–205 °C) represents vaporisation of volatile organic compounds (VOCs) followed by combustion of VOCs. It could be related to diesel's boiling point, which varies from 180 °C to 370 °C (O'Brien et al., 2018; Vempatapu et al., 2017). The third and fourth mass loss stages represent the decrease of volatiles and char in the soil similarly as in the case of the clean soil. Moreover, the formation of ash (81.05±3.24–86.87±3.47 %) was observed.

Furthermore, the comparison of DTG curves in Fig. 3.15 b, c, and d shows a difference between the negative peaks that correspond to VOCs (diesel fuel). As the concentration of diesel fuel increased from 80±3 g/kg to 160±3 g/kg, the negative peak also increased. Such tendency emphasises that soil was contaminated with different diesel fuel concentrations. Additionally, DSC curves show the endothermic process. The obtained results are in a good correlation with the results obtained by Raslavičius et al. (Raslavičius et al., 2018), the one who performed a thermogravimetric (TGA/DTG and DSC) analysis. Authors indicated that diesel fuel was thermally unstable and evaporated at low temperature (253.5 °C).

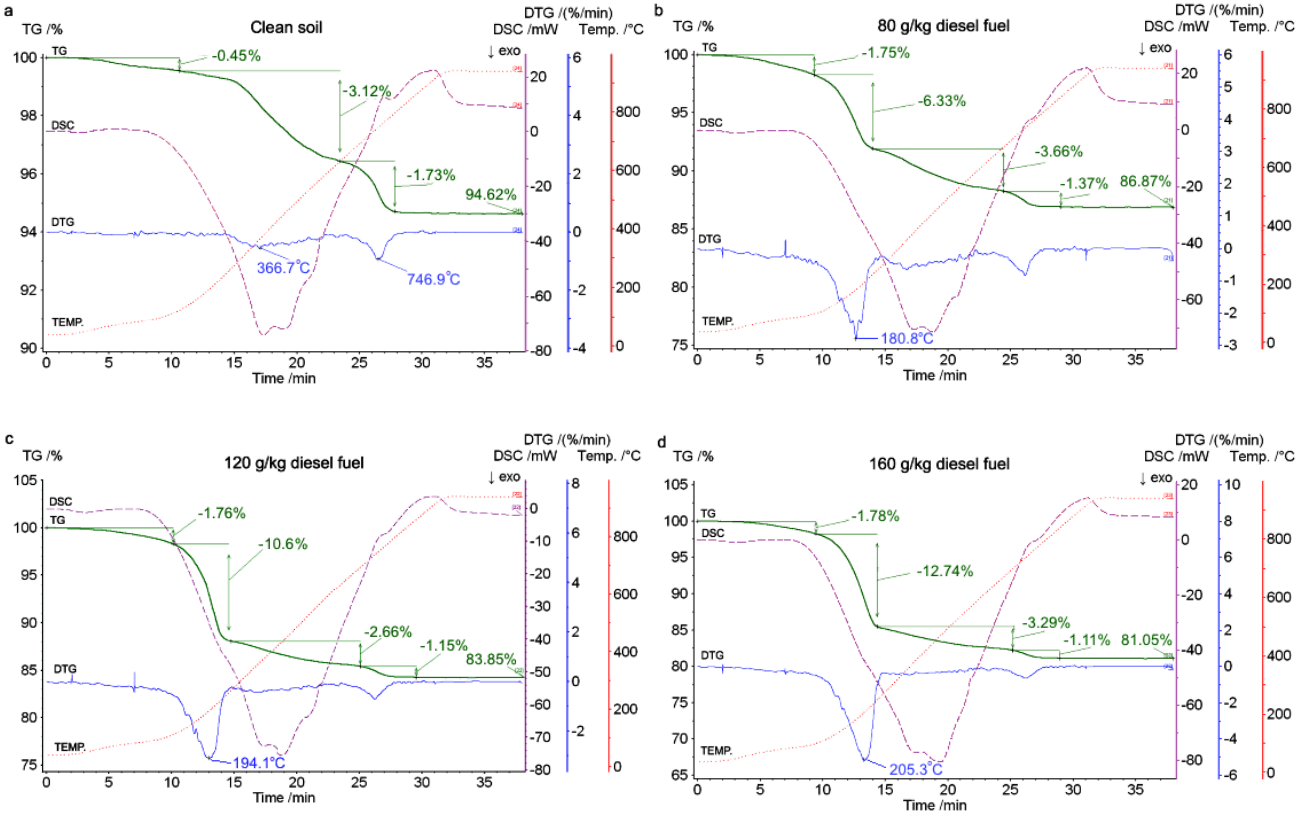

Fig. 3.15 Dynamics of mass loss during combustion process: a – Clean soil; b – Soil contaminated with 80 g/kg diesel; c – Soil contaminated with 120 g/kg diesel; d – Soil contaminated with 160 g/kg diesel

3.6.4. Producer gas analysis after soil remediation with thermal plasma

The highest values and average values of producer gas concentrations obtained during the soil remediation with water vapour plasma are given in Table 3.6. The concentration of the synthesis gas (H_2 + CO) increased with the increase of the diesel fuel concentration in the soil from 80±3 g/kg to 120±3 g/kg. In contrast, the concentration of synthesis gas decreased when the soil was contaminated with 160±3 g/kg of diesel fuel. The concentrations of NO_x, SO_2, and C_3H_8 changed negligibly in all three experimental cases.

Table 3.6 Producer gas concentrations obtained during the soil remediation process

	Gas concentrations extracted during the soil remediation with the water vapour plasma:					
Diesel fuel concentration:	80±3 g/kg		120±3 g/kg		160±3 g/kg	
	Highest value, vol%	Average value, vol%	Highest value, vol%	Average value, vol%	Highest value, vol%	Average value, vol%
H_2	30.94±0.62	20.76±0.42	37.53±0.75	23.07±0.46	23.7±0.47	17.58±0.35
CO	5.78±0.12	4.22±0.09	6.96±0.14	4.64±0.09	3.84±0.08	2.98±0.06
CO_2	24.6±0.49	17.17±0.34	15.9±0.32	10.19±0.20	15.3±0.31	10.29±0.21
NO	0.55±0.01	0.33±0.01	0.55±0.01	0.30±0.01	0.55±0.01	0.35±0.01
NO_2	0.07±0.001	0.03±0.001	0.07±0.001	0.04±0.001	0.07±0.001	0.05±0.001
SO_2	0.04±0.001	0.04±0.001	0.04±0.001	0.03±0.001	0.04±0.001	0.03±0.001
C_3H_8	0.21±0.004	0.15±0.003	0.13±0.003	0.10±0.002	0.13±0.003	0.09±0.002

The changes in the producer gas concentrations during the contaminated soil remediation process are shown in Figure 3.16 a–f. Despite the diesel fuel concentration (80±3 g/kg, 120±3 g/kg or 160±3 g/kg) in the soil, a decrease of oxygen from 21.00±0.42 vol% to 2.88±0.06 vol%, 1.03±0.02 vol%, and 1.29±0.03 vol%, as well as the formation of synthesis gas (H_2 + CO) were recorded in all three experimental cases (Fig 3.16 a, c, e). In this context, up to 30.94±0.62 vol% of hydrogen and 5.78±0.12 vol% of CO were observed when the soil was contaminated with 80 g/kg of diesel fuel (Fig 3.16 a). While up to 37.53±0.75 vol%, 23.7±0.47 vol% of hydrogen and 6.96±0.14 vol%, 3.84±0.08 vol% of CO were measured when the soil was contaminated with 120±3 g/kg and 160±3 g/kg of diesel fuel, respectively (Fig 3.16 c, e). The synthesis gas formation was observed due to the prevailing steam reforming reaction (Eq. 1.23) and decomposition reaction (Eq. 1.27). The highest amount of synthesis gas was recorded during the remediation of soil contaminated by 120±3 g/kg diesel fuel. These results were obtained due to the higher pollutant concentration (comparing to 80±3 g/kg) and a fast steam reforming reaction (Eq. 1.23). However, the reaction (Eq.1.23) slowed down and the interaction time between the pollutant and active species increased, when diesel fuel concentration was raised to 160±3 g/kg. The higher diesel fuel concentration meant that a higher amount of contaminant molecules existed. Firstly, these molecules competed with each other for the reactive species in the plasma environment. Secondly, the higher diesel fuel

concentrations created a thicker top layer above the grain of the soil by covering it. Thus, plasma reactive species needed more energy and time to remove diesel fuel molecules located above the soil (top layer) and in the inner soil layers. Because of these reasons, the remediation process slowed down and a lower amount of synthesis gas was observed.

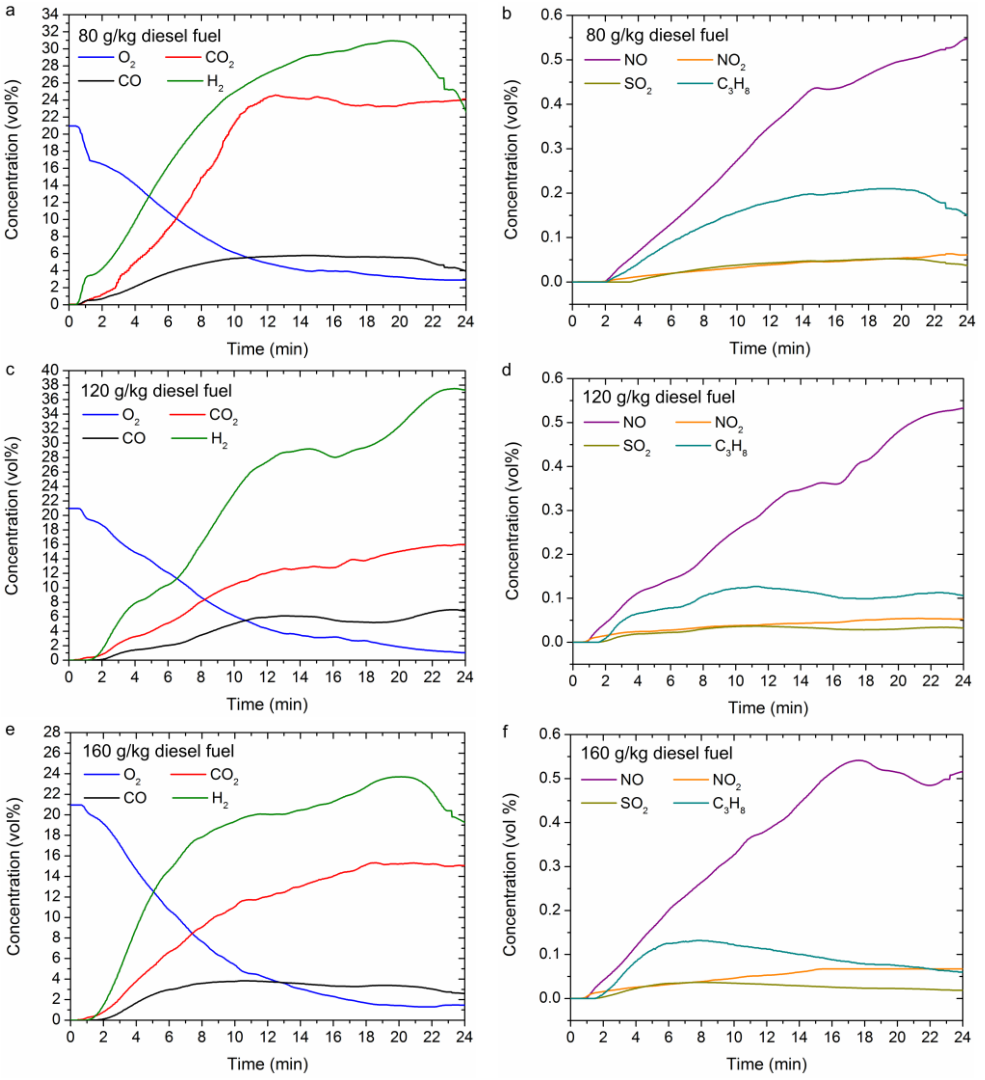

Fig. 3.16 Gas concentrations extracted during the remediation process: a, b – Soil contaminated with 80±3 g/kg diesel; c, d – Soil contaminated with 120±3 g/kg diesel; e, f – Soil contaminated with 160±3 g/kg diesel

Moreover, the water-gas shift reaction (Eq. 1.24) and the Boudouard reaction (Eq. 1.25) let to the formation of CO_2. In this respect, up to 24.6±0.49 vol%,

15.9±0.32 vol%, 15.3±0.31 vol% of CO_2 were obtained when the soil was contaminated with 80 g/kg, 120 g/kg, and 160 g/kg of diesel fuel, respectively. Additionally, the side reactions (Eq. 1.25–1.27) caused the formation of coke.

Furthermore, insignificant contents of NO (0.55±0.01 vol%), NO_2 (0.07±0.001 vol%), SO_2 (0.04±0.001 vol%), and C_3H_8 (0.13±0.003–0.21±0.004 vol%) were measured in all three cases (Fig 3.16 b, d, f). This was mainly attributed to the air used as a shielding gas (up to 13 %) in order to protect the cathode of the plasma torch from erosion. Also, diesel fuel contains small amounts of nitrogen, oxygen, and sulphur. Thus, NO_x and SO_2 formation could possibly occur due to the diesel fuel interaction with plasma active species (e.g. ·O radical).

In addition, Aggelopoulos et al. (Aggelopoulos et al., 2016b) performed the remediation of 100 g/kg non-aqueous phase liquid polluted soils. In the research, it was found that at the end of the plasma treatment, the carbon-based materials were completely released in the exhaust gases as VOCs, CO_2, and CO. When the applied voltage was 28 kV and the air flow rate was 0.082 g/s, the concentrations of VOCs, CO_2, and CO were equal to 74.5 %, 8 % and 17.5 %, respectively. The concentrations changed with the change of the airflow rate (0.0031 g/s). Accordingly, VOC generation decreased, while CO_2 and CO increased to 40 % and 59 %, respectively. The results obtained by the researchers indicated complete pollutant conversion and soil remediation.

The highest values and average values of producer gas concentrations obtained during the soil remediation with air plasma are given in Table 3.7. The concentration of the CO_2 increased with the increase of the diesel fuel concentration in the soil from 80±3 g/kg to 160±3 g/kg. The concentrations of NO_x, SO_2, and C_3H_8 changed insignificantly in all three experimental cases.

Table 3.7 Producer gas concentrations obtained during the soil remediation process

	Gas concentrations extracted during the soil remediation with air plasma:					
Diesel fuel concentration:	80±3 g/kg		120±3 g/kg		160±3 g/kg	
	Highest value, vol%	Average value, vol%	Highest value, vol%	Average value, vol%	Highest value, vol%	Average value, vol%
H_2	0	0	0	0	1.42±0.03	0.44±0.01
CO	0	0	0	0	2.91±0.06	0.71±0.01
CO_2	6.67±0.13	3.46±0.07	7.86±0.16	4.57±0.09	9.14±0.18	5.05±0.10
NO	0.13±0.003	0.08±0.002	0.16±0.003	0.08±0.002	0.19±0.004	0.09±0.002
NO_2	0.05±0.001	0.03±0.001	0.05±0.001	0.03±0.001	0.04±0.001	0.03±0.001
SO_2	0.001±0.00002		0.001±0.00002		0.014±0.0003	0.01±0.0002
C_3H_8	0.001±0.00002		0.001±0.00002		0.044±0.001	0.02±0.0003

The changes in the producer gas concentrations during the interaction between the diesel fuel contaminated soil and air plasma are given in Figure 3.17 a–f. Formation of the carbon dioxide was observed during the remediation of the soil

contaminated with 80±3 g/kg and 120±3 g/kg of diesel fuel, respectively. In this context, up to 6.67±0.13 vol% and 7.86±0.16 vol% of CO_2 were measured when the concentrations of diesel fuel in the soil were equal to 80±3 g/kg and 120±3 g/kg, respectively (Fig 3.17 a, c).

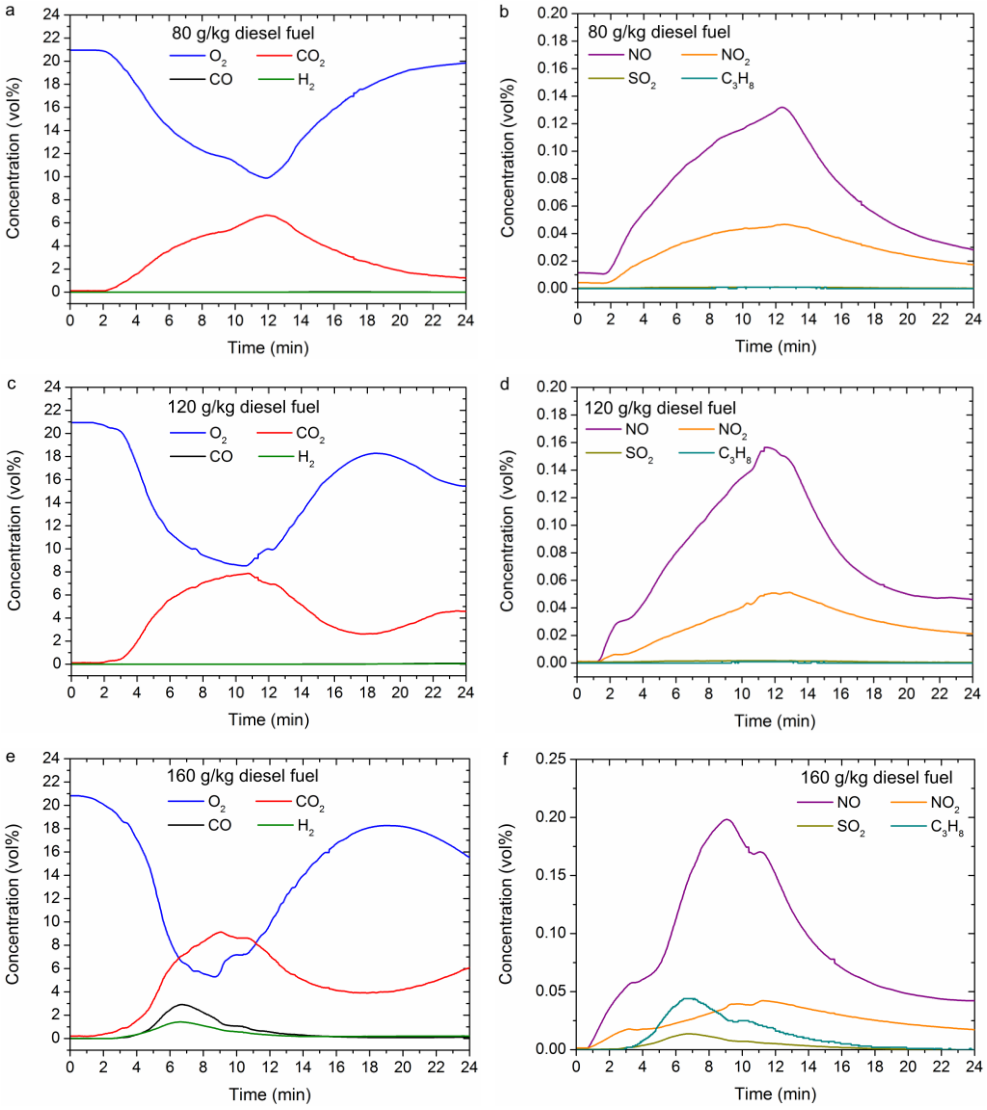

Fig. 3.17 Gas concentrations extracted during the remediation process: a, b – Soil contaminated with 80±3 g/kg diesel; c, d – Soil contaminated with 120±3 g/kg diesel; e, f – Soil contaminated with 160±3 g/kg diesel

Within the soil remediation process, the oxidation of the diesel fuel takes place. Consequently, a decrease in oxygen from 21±0.42 vol% to 9.88±0.19, and 8.52±0.17

vol%, as well as the formation of CO_2, were recorded due to the predominant complete oxidation reaction (Eq. 1.22). The higher concentration of CO_2 was observed during the treatment of soil polluted with 120±3 g/kg diesel fuel. These results were obtained due to the higher contaminant concentration compared to 80±3 g/kg.

Additionally, when diesel fuel concentration in the soil was increased to 160±3 g/kg, the formation of CO_2 (9.14±0.18 vol%) and synthesis gas (4.33±0.09 vol%) was observed (Fig. 3.20 e). Firstly, during the interaction between air plasma and contaminant, the typical complete oxidation reaction (Eq. 1.22) caused the generation of carbon dioxide. However, after some time, the lack of oxygen caused a slowdown of the complete oxidation reaction (Eq. 1.22) and predominance of partial oxidation reactions (Eq. 1.19-1.21). Consequently, the generation of synthesis gas was observed. Furthermore, the highest decrease in oxygen concentration from 21±0.42 vol% to 5.29±0.11 vol% was recorded during this soil remediation process.

Moreover, small contents of NO (0.13±0.002–0.2±0.004 vol%), NO_2 (0.04±0.001–0.05±0.001 vol%), SO_2 (0.001±0.00002–0.014±0.0003 vol%), and C_3H_8 (0.001±0.00002–0.044±0.0009 vol%) were recorded in all three experimental cases (Fig 3.17 b, d, f). Similarly, as in the case of using the water vapour plasma, the formation of NO, NO_2, SO_2, and C_3H_8 were mostly attributed to the composition of diesel fuel and the usage of the air as a plasma forming gas.

The obtained experimental results are in good agreement with Lee et al., (2010), who investigated the effect of excess oxygen in plasma reforming of diesel fuel. Researchers indicated that the addition of O_2 in the reforming process increased the oxidative cracking of heavy hydrocarbons mostly into the CO_2. Moreover, the authors specified that the surplus of oxygen preferably affects the oxidation process of carbonaceous species instead of the hydrogen generation process. Also, Dinh et al., (2017) used the non-thermal, rotating arc plasma for partial oxidation of diesel fuel. In this research, the authors suggested that the diesel fuel reforming reaction possibly may appear in two stages. Firstly, the reaction between the oxidiser and diesel fuel prevails and induces synthesis gas (H_2+CO) generation. This diesel fuel cracking reaction is the primary reaction in the first stage. In the second stage, the diesel fuel is already decomposed and the generation of hydrogen and carbon monoxide is not recorded. Instead, synthesis gas reacts with a remaining oxidiser. Thus, the formation of CO_2 and H_2O is observed.

3.6.5. The mechanism of the diesel fuel contaminated soil remediation with the thermal plasma

Diesel fuel conversion to gaseous compounds includes complex chemical reactions (Eq. 1.19–1.27). Firstly, the formation of thermal plasma occurred. The energetic electrons emitted from cathode interacted with preheated water vapour and formed reactive radicals including ·O, ·H, and ·OH (Eq. 1.1–1.4), in the case of the water vapour plasma. The air plasma was formed by the interaction between energetic electrons and air, which led to the formation of reactive species, such as ·O, ·N. The

produced charged and reactive species initiated and accelerated the diesel fuel decomposition reactions in the plasma-chemical reactor (Fig. 3.18).

During the soil contamination process, the diesel fuel created a top layer above the grain of the soil by covering it. Also, diesel fuel adsorbed into the soil pores during the penetration into the inner layers. The increasing contaminant concentration caused increasing soil compressibility, the formation of larger soil agglomerates (Fig. 3.14 b-d) and reduction of soil porosity. Moreover, the higher diesel fuel concentration created a thicker top layer above the grain of the soil by covering it.

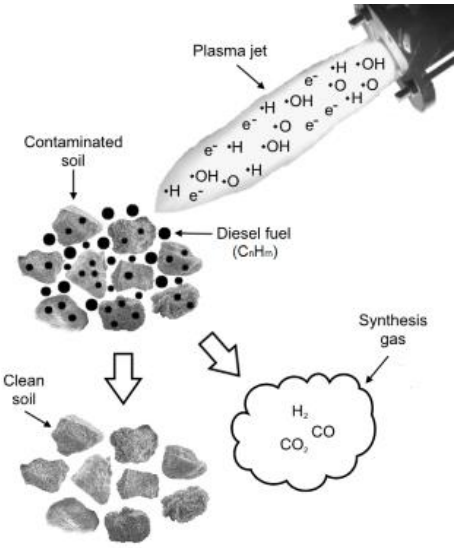

Fig. 3.18 The mechanism of the contaminated soil remediation with a thermal plasma

At the beginning of the polluted soil remediation process with thermal plasma, high-temperature reactive species interacted with diesel fuel molecules located above the soil (top layer). Due to the high temperature (2880±60 K and 4100±113 K at the environment of the water vapour plasma and air plasma, respectively), part of these molecules evaporated and interacted with reactive species in the gas phase. When the top layer of contaminants was decomposed, active species started to penetrate into the soil pores and interacted with diesel molecules located into the deeper soil layers. Contaminants were treated layer-by-layer in the vertical direction. The contaminant conversion process with the thermal plasma ensured soil purification and diesel fuel decomposition to gaseous compounds, mainly H_2, CO, and CO_2.

Summarily, the purpose of the performed experiments was to clean the soil from the diesel fuel. Thus, the thermal plasma potential to remediate soil contaminated with diesel fuel is given in Table 3.8. Obtained results revealed that both types of plasma (air and water vapour) are suitable to remediate pollutant from the soil. Also, the thermal plasma environment ensures high contaminant removal efficiency.

Table 3.8 Thermal plasma potential to remediate soil contaminated with diesel fuel (80±3 g/kg, 120±3 g/kg and 160±3 g/kg)

Parameter	Air plasma	Water vapour plasma
Diesel fuel content in the soil after remediation	< 0.089 g/kg	< 0.089 g/kg
Contaminant removal efficiency, %	99.90	99.90

Also, the comparison of petroleum products contaminated soil remediation by various plasma methods is given in Table 3.9. Accordingly, the thermal plasma method presented in this dissertation was suitable for the efficient removal (99.90 %) of relatively high concentrations of diesel fuel (80±3–160±3 g/kg) from the soil in a short time (24 min). Meanwhile, the contaminant removal efficiency from the soil using non-thermal plasma varied between 23.00–97.00 %.

Table 3.9 Comparison of petroleum products contaminated soil remediation by various plasma methods

Reference	Discharge type, power kW	Gasifying agent	Soil pollutant	Pollutant content, g/kg	Treatment time, min	Removal efficiency, %
This work	DC, 56.00	Water vapour	Diesel fuel	80–160	24	99.90
This work	DC, 52.80	Air	Diesel fuel	80–160	24	99.90
(Zhan et al., 2019)	PCD, 0.02-0.06	Air	Gasoline	2–4	60	86.00
(Zhan et al., 2019)	PCD, 0.02-0.06	Oxygen	Gasoline	2–4	60	84.00
(Zhan et al., 2019)	PCD, 0.02-0.06	Argon	Gasoline	2–4	60	39.00
(Zhan et al., 2019)	PCD, 0.02-0.06	Nitrogen	Gasoline	2–4	60	23.00
(Li et al., 2017)	PCD, 30 kV	Un-named	Gasoline	2.5–10	60	57.00–81.00
(Aggelopoulos, 2016)	DBD, 0.025	Air	n-dodecane	0.5–50	22	84.00–94.00
(Aggelopoulos, 2016)	DBD, 0.025	Air	n-dodecane	0.5–50	34	91.00–97.00
(Redolfi et al., 2009)	DBD, 0.002	Air	Kerosene	0.074	8	90.00

Additionally, the other researchers have remediated soil contaminated with much lower concentrations of petroleum products (0.5–50 g/kg). In some cases, the purification of petroleum products (2–4 g/kg) from soil took a longer time (60 min) compared to the method presented in this work (24 min). Consequently, the thermal plasma has a higher ability to remove higher concentrations of petroleum products from the soil, in a short time, compared to the non-thermal plasma.

CONCLUSIONS

Plasma-based conversion of liquid (crude glycerol) and solid (diesel contaminated soil) wastes was implemented in this dissertation. After researching the electrical and thermal characteristics of the plasma torch, the operating conditions ensuring the most stable work of the plasma torch and the most suitable environment for waste conversion were determined. The plasma-based conversion process of crude glycerol was experimentally investigated when the gasifying agent/$C_3H_8O_3$ ratio varied between 0.48–0.88 and 0.52–0.92 in the cases of air plasma and water vapour plasma, respectively. Experimental research studies on the remediation of diesel fuel contaminated soil were also performed to evaluate the dependence of the treatment process on the type of plasma forming gas (air, water vapour) and the pollutant concentration (80–160 g/kg) in the soil. The obtained researches results can be summarised as follows:

1. The highest thermal efficiency of η=78 % and η=68 % was received at the current of 160 A when air and a mixture of air/water vapour were used as a plasma forming gas. These plasma torch working parameters ensure the most suitable conditions for the waste conversion process.
2. The increase of the gasifying agent content in the total gasifying agent/$C_3H_8O_3$ ratio induces a slight rise of H_2/CO ratio and lower heating value as well as the increase of carbon conversion and energy conversion efficiency and decrease of specific energy requirements.
3. The comparison of different types of the gasifying agent at maximum gasifying agent/$C_3H_8O_3$ ratios showed that the use of the water vapour plasma led to the generation of 35.50 % higher values of synthesis gas, two times higher H_2/CO ratio (2.07), 2.10 MJ/Nm^3 higher lower heating value, 33 % higher carbon conversion efficiency, 94.40 % higher energy conversion efficiency, 74.9 kJ/mol lower specific energy requirement, compared to the air plasma.
4. The energy content of the producer gas was 91.90 kWh and 152.40 kWh when the glycerol conversion process was performed using the air plasma and water vapour plasma, respectively. Potentially, 14.80–29.50 kWh of electrical energy, as well as 105.60–173.50 kWh of thermal energy can be generated from producer gas in the cases of the air plasma and water vapour plasma, respectively. Also, up to 31 % and 47 % of the electricity required for the formation of air plasma and water vapour plasma can be recovered by using producer gas in an internal combustion engine or microturbine.
5. The efficiency of the soil remediation process does not depend on the investigated diesel fuel concentrations (80 g/kg, 120 g/kg, and 160 g/kg) in the soil and the type of plasma forming gases (air, water vapour). In all cases, the thermal plasma treatment efficiency of the diesel fuel contaminated soil is 99.90 % by remediating 5.4 kg/h of soil.

REFERENCES

1. AGGELOPOULOS, C. A. Atmospheric pressure dielectric barrier discharge for the remediation of soil contaminated by organic pollutants. *International Journal of Environmental Science and Technology*. 2016, 13(7), 1731–1740. ISSN 17352630.

2. AGGELOPOULOS, C. A., GKELIOS, A., KLAPA, M. I., KALTSONOUDIS, C., SVARNAS, P., TSAKIROGLOU, C. D. Parametric analysis of the operation of a non-thermal plasma reactor for the remediation of NAPL-polluted soils. *Chemical Engineering Journal*. 2016, 301, 353–361. ISSN 13858947.

3. AGON, N., HRABOVSKY, M., CHUMAK, O., HLINA, M., KOPECKY, V., MASLANI, A., BOSMANS, A., HELSEN, L., SKOBLJA, S., VAN OOST, G., VIERENDEELS, J. Plasma gasification of refuse derived fuel in a single-stage system using different gasifying agents. *Waste Management*. 2016, 47, 246–255. ISSN 18792456.

4. ALEME, H. G., CORGOZINHO, C. N. C., BARBEIRA, P. J. S. Diesel oil discrimination by origin and type using physicochemical properties and multivariate analysis. *Fuel*. 2010, 89(11), 3151–3156. ISSN 00162361.

5. ALGOUFI, Y. T., KABIR, G., HAMEED, B. H. Synthesis of glycerol carbonate from biodiesel by-product glycerol over calcined dolomite. *Journal of the Taiwan Institute of Chemical Engineers*. 2017, 70, 179–187. ISSN 18761070.

6. ALQATTAN, N., ACHEAMPONG, M., JAWARD, F. M., ERTEM, F. C. Reviewing the potential of Waste-to-Energy (WTE) technologies for Sustainable Development Goal (SDG) numbers seven and eleven. *Renewable Energy Focus*. 2018, 27, 97–110. ISSN 17550084.

7. ANITHA, M., KAMARUDIN, S. K., KOFLI, N. T. The potential of glycerol as a value-added commodity. *Chemical Engineering Journal*. 2016, 295, 119–130. ISSN 13858947.

8. ARENA, U. Process and technological aspects of municipal solid waste gasification. A review. *Waste Management*. 2012, 32(4), 625–639. ISSN 0956053X.

9. BAGHERI, S., JULKAPLI, N. M., YEHYE, W. A. Catalytic conversion of biodiesel derived raw glycerol to value added products. *Renewable and Sustainable Energy Reviews*. 2015, 41, 113–127. ISSN 18790690.

10. BASU, P. Biomass gasification and pyrolysis : practical design and theory. Elsevier Inc. Academic Press, 2010.

11. BEPARI, S., PRADHAN, N. C., DALAI, A. K. Selective production of hydrogen by steam reforming of glycerol over Ni/Fly ash catalyst. *Catalysis Today*. 2017, 291, 36–46. ISSN 09205861.

12. BEYENE, H. D., WERKNEH, A. A., AMBAYE, T. G. Current updates on waste to energy (WtE) technologies: a review. *Renewable Energy Focus*. 2018, 24, 1–11. ISSN 17550084.

13. BOCOS, E., FERNANDEZ-COSTAS, C., PAZOS, M., SANROMAN, M. A. Removal of PAHs and pesticides from polluted soils by enhanced electrokinetic-Fenton treatment. *Chemosphere*. 2015, 125, 168–174. ISSN 18791298.

14. BOGAERTS, A., NEYTS, E. C. Plasma Technology: An Emerging Technology for Energy Storage. *ACS Energy Letters*. 2018, 3, 1013−1027.

15. BOULAKRADECHE, M. O., AKRETCHE, D. E., CAMESELLE, C., HAMIDI, N. Enhanced Electrokinetic Remediation of Hydrophobic Organics ontaminated Soils by the Combinations of Non-Ionic and Ionic Surfactants. *Electrochimica Acta*. 2015, 174, 1057–

1066. ISSN 00134686.

16. BOULOS, M. I., FAUCHAIS, P., PFENDER, E. Thermal plasmas : fundamentals and applications. US: Springer, 1994.

17. BP (2019). *BP Energy Outlook 2019 edition*. BP

18. BUBLIEVSKY, A. F., GORBUNOV, A. V., MARQUESI, A. R., CHARAKHOVSKY, L. I., BICUDO, R. O., HALINOUSKI, A. A., FILHO, G. P., MACIEL, H. S., OTANI, C. Generalization of the Total Current-Voltage Characteristics for Transferred Arc Plasma Torch with Steam and Air Plasmas Based on the Analytical Anisotropic Model. *IEEE Transactions on Plasma Science*. 2015, 43(10), 3707–3715. ISSN 00933813.

19. CACHADA, A., ROCHA-SANTOS, T., DUARTE, A. C. Soil and Pollution: An Introduction to the Main Issues. Elsevier Inc. Academic Press, 2018.

20. CAHYANTI, M. N., DODDAPANENI, T. R. K. C., KIKAS, T. Biomass torrefaction: An overview on process parameters, economic and environmental aspects and recent advancements. *Bioresource Technology*. 2020, 301, 122737. ISSN 18732976.

21. CAO, L., ZHANG, C., CHEN, H., TSANG, D. C. W., LUO, G., ZHANG, S., CHEN, J. Hydrothermal liquefaction of agricultural and forestry wastes: state-of-the-art review and future prospects. *Bioresource Technology*. 2017, 245, 1184–1193. ISSN 18732976.

22. CHAU, S. W., LU, S. Y., WANG, P. J. Modeling of axis-symmetric steam plasma flow in a non-transferred torch. *Computer Physics Communications*. 2011, 182(1), 152–154. ISSN 00104655.

23. CHAVES, L. I., DA SILVA, M. J., DE SOUZA, S. N. M., SECCO, D., ROSA, H. A., NOGUEIRA, C. E. C., FRIGO, E. P. Small-scale power generation analysis: Downdraft gasifier coupled to engine generator set. *Renewable and Sustainable Energy Reviews*. 2016, 58, 491–498. ISSN 1364-0321.

24. CHEN, T., DELGADO, A. G., YAVUZ, B. M., MALDONADO, J., ZUO, Y., KAMATH, R., WESTERHOFF, P., KRAJMALNIK-BROWN, R., RITTMANN, B. E. Interpreting Interactions between Ozone and Residual Petroleum Hydrocarbons in Soil. *Environmental Science & Technology*. 2017, 51, 506–513.

25. CHEN, W. H. et al. A comprehensive analysis of food waste derived liquefaction bio-oil properties for industrial application. *Applied Energy*. 2019, 237(November 2018), 283–291. ISSN 03062619.

26. CHENG, M., ZENG, G., HUANG, D., LAI, C., XU, P., ZHANG, C., LIU, Y. Hydroxyl radicals based advanced oxidation processes (AOPs) for remediation of soils contaminated with organic compounds: A review. *Chemical Engineering Journal*. 2016, 284, 582–598. ISSN 13858947.

27. CUBAS, A. L. V., DE MEDEIROS MACHADO, M., DOS SANTOS, J. R., ZANCO, J. J., RIBEIRO, D. H. B., ANDRE, A. S., DEBACHER, N. A., MOECKE, E. H. S. Effect of chemical species generated by different geometries of air and argon non-thermal plasma reactors on bacteria inactivation in water. *Separation and Purification Technology*. 2019, 222, 68–74. ISSN 18733794.

28. CUCCHIELLA, F., D'ADAMO, I., GASTALDI, M. Strategic municipal solid waste management: A quantitative model for Italian regions. *Energy Conversion and Management*. 2014, 77, 709–720. ISSN 01968904.

29. CUCCHIELLA, F., D'ADAMO, I., GASTALDI, M. Sustainable waste management:

Waste to energy plant as an alternative to landfill. *Energy Conversion and Management*. 2017, 131, 18–31. ISSN 01968904.

30. CZAJCZYŃSKA, D., NANNOU, T., ANGUILANO, L., KRZYZYNSKA, R., GHAZAL, H., SPENCER, N., JOUHARA, H. Potentials of pyrolysis processes in the waste management sector. *Energy Procedia*. 2017, 123, 387–394.

31. DA SILVA, G. P., MACK, M., CONTIERO, J. Glycerol: A promising and abundant carbon source for industrial microbiology. *Biotechnology Advances*. 2009, 27(1), 30–39. ISSN 07349750.

32. DAVAZDAH EMAMI, S., MD. KASMANI, R., HAMID, M. D., HASSAN, C. R. C., MOKHTAR, K. M. Kinetic and dynamic analysis of hydrogen-enrichment mixtures in combustor systems - A review paper. *Renewable and Sustainable Energy Reviews*. 2016, 62, 1072–1082. ISSN 18790690.

33. DEBNATH, D., WHISTANCE, J., WESTHOFF, P., BINFIELD, J. W. T. International Biofuel Baseline Briefing Book. US: FAPRI-MU, 2018.

34. DEMIRBAS, A., BAMUFLEH, H. S. Optimization of crude oil refining products to valuable fuel blends*Petroleum Science and Technology*, 2017. ISSN 15322459.

35. DINH, D. K., KANG, H. S., JO, S., LEE, D. H., SONG, Y-H. Partial oxidation of diesel fuel by plasma – Kinetic aspects of the reaction. *International Journal of Hydrogen Energy*. 2017, 42(36), 22756–22764. ISSN 03603199.

36. DU, C. M., SUN, Y. W., ZHUANG, X. F. The effects of gas composition on active species and byproducts formation in gas-water gliding arc discharge. *Plasma Chemistry and Plasma Processing*. 2008, 28(4), 523–533. ISSN 02724324.

37. EEA. Progress in management of contaminated sites. [Accessed 2019-12-10] Internet access: https://www.eea.europa.eu/data-and-maps/indicators/progress-in-management-of-contaminated-sites-3/assessment

38. EIA. International Energy Outlook 2019 with projections to 2050. [Accessed 2019-12-18] Internet access: https://www.eia.gov/outlooks/ieo/pdf/ieo2019.pdf

39. EUROBSERV'ER (2010). *Biofuels Barometer 2010.* EurObserv'ER.

40. EUROBSERV'ER (2011). *Biofuels Barometer 2011.* EurObserv'ER.

41. EUROBSERV'ER (2012). *Biofuels Barometer 2012.* EurObserv'ER.

42. EUROBSERV'ER (2013). *Biofuels Barometer 2013.* EurObserv'ER.

43. EUROBSERV'ER (2014). *Biofuels Barometer 2014.* EurObserv'ER.

44. EUROBSERV'ER (2015). *Biofuels Barometer 2015.* EurObserv'ER.

45. EUROBSERV'ER (2016). *Biofuels Barometer 2016.* EurObserv'ER.

46. EUROBSERV'ER (2017). *Biofuels Barometer 2017.* EurObserv'ER.

47. EUROBSERV'ER (2018). *Biofuels Barometer 2018.* EurObserv'ER.

48. EUROBSERV'ER (2019). *Biofuels Barometer 2019.* EurObserv'ER.

49. EUROPEAN COMMISSION. Closing the loop - An EU action plan for the Circular Economy. Communication from the Commission to the European Parliament, the Council, the European Economic and Social Committee and the Committee of the Regions. [Accessed 2019-12-16] Internet access: https://ec.europa.eu/transparency/regdoc/rep/1/2015/EN/1-2015-614-EN-F1-1.PDF

50. EUROPEAN PARLIAMENT AND COUNCIL. Directive 2008/98/EC of the European Parliament and of the Council of 19 November 2008 on waste and repealing certain directives (Waste Framework). [Accessed 2019-12-16] Internet access: http://ec.europa.eu/environment/waste/framework

51. EXXONMOBIL. Outlook for energy: a perspective to 2040. [Accessed 2019-12-10] Internet access: https://corporate.exxonmobil.com/-/media/Global/Files/outlook-for-energy/2019-Outlook-for-Energy_v4.pdf

52. FAO AND ITPS (2015) Status of the World's Soil Resources. FAO and ITPS.

53. FERNÁNDEZ-GONZÁLEZ, J. M., GRINDLAY, A. L., SERRANO-BERNARDO, F., RODRIGUEZ-ROJAS, M. I., ZAMORANO, M. Economic and environmental review of Waste-to-Energy systems for municipal solid waste management in medium and small municipalities. *Waste Management*. 2017, 67, 360–374. ISSN 18792456.

54. FERRONATO, N., RADA, E. C., PORTILLO, M. A. G., CIOCA, L. I., RAGAZZI, M., TORRETTA, V. Introduction of the circular economy within developing regions: A comparative analysis of advantages and opportunities for waste valorization. *Journal of Environmental Management*. 2019, 230, 366–378. ISSN 10958630.

55. FREITAS, A. C. D., GUIRARDELLO, R. Comparison of several glycerol reforming methods for hydrogen and syngas production using Gibbs energy minimization. *International Journal of Hydrogen Energy*. 2014, 39(31), 17969–17984. ISSN 03603199.

56. GALLO, A., PIROVANO, C., FERRINI, P. MARELLI, M., PSARO, R., SANTANGELO, S., FAGGIO, G., DAL SANTO, V. Influence of reaction parameters on the activity of ruthenium based catalysts for glycerol steam reforming. *Applied Catalysis B: Environmental*. 2012, 121–122, 40–49. ISSN 09263373.

57. GLUSHKOV, D. O., PAUSHKINA, K. K., SHABARDIN, D. P. Co-combustion of coal processing waste, oil refining waste and municipal solid waste: Mechanism, characteristics, emissions. *Chemosphere*. 2020, 240, 124892. ISSN 18791298.

58. GOLLAKOTA, A. R. K., KISHORE, N., GU, S. A review on hydrothermal liquefaction of biomass. *Renewable and Sustainable Energy Reviews*. 2018, 81, 1378–1392. ISSN 18790690.

59. GOMEZ, E., RANI, D. A., CHEESEMAN, C. R., DEEGAN, D., WISE, M., BOCCACCINI, A. R. Thermal plasma technology for the treatment of wastes: A critical review. *Journal of Hazardous Materials*. 2009, 161(2–3), 614–626. ISSN 03043894.

60. GRAY, L. Plasma Gasification as a Viable Waste-to-Energy Treatment of Municipal Solid Waste. *Technical Report. Solid and Hazardous Waste Prevention and Control Engineering.* 2014, 1–15.

61. GRIGAITIENĖ, V., SNAPKAUSKIENĖ, V., VALATKEVIČIUS, P., TAMOŠIŪNAS, A., VALINČIUS, V. Water vapor plasma technology for biomass conversion to synthetic gas. *Catalysis Today*. 2011, 167(1), 135–140. ISSN 09205861.

62. HÁJEK, M., SKOPAL, F. Treatment of glycerol phase formed by biodiesel production. *Bioresource Technology*. 2010, 101(9), 3242–3245. ISSN 09608524.

63. HE, Q. (SOPHIA), MCNUTT, J., YANG, J. Utilization of the residual glycerol from biodiesel production for renewable energy generation. *Renewable and Sustainable Energy Reviews*. 2017, 71(January), 63–76. ISSN 18790690.

64. HOWATSON, A. M. (1976) *An Introduction to gas discharges* (2nd ed.) Oxford: Pergamon

Press.

65. HRABOVSKY, M., HLINA, M., KOPECKY, V., MASLANI, A., ZIVNY, O., KRENEK, P., SEROV, A., HURBA, O. Steam Plasma Treatment of Organic Substances for Hydrogen and Syngas Production. *Plasma Chemistry and Plasma Processing*. 2017, 37(3), 739–762. ISSN 02724324.

66. HRABOVSKY, M., HLINA, M., KOPECKY, V., MASLINI, A., KRENEK, P., SEROV, A., HURBA, O. Steam Plasma Methane Reforming for Hydrogen Production. *Plasma Chemistry and Plasma Processing*. 2018, 38(4), 743–758. ISSN 02724324.

67. HUANG, H., TANG, L. Treatment of organic waste using thermal plasma pyrolysis technology. *Energy Conversion and Management*. 2007, 48(4), 1331–1337. ISSN 01968904.

68. HUGHES, I., HASE, T. Measurements and their Uncertainties: A practical guide to modern error analysis. 1 edition ed. New York: Oxford University Press, 2010.

69. IBRAHIMOGLU, B., YILMAZOGLU, M. Z. Numerical modeling of a downdraft plasma coal gasifier with plasma reactions. *International Journal of Hydrogen Energy*. 2020, 45(5), 3532–3548. ISSN 03603199.

70. IROBA, K. L., BAIK, O. D., TABIL, L. G. Torrefaction of biomass from municipal solid waste fractions I: Temperature profiles, moisture content, energy consumption, mass yield, and thermochemical properties. *Biomass and Bioenergy*. 2017, 105, 320–330. ISSN 18732909.

71. IWASZKO, J., ZAJEMSKA, M., ZAWADA, A., SZWAJA, S., POSKART, A. Vitrification of environmentally harmful by-products from biomass torrefaction process. *Journal of Cleaner Production*. 2020, 249. ISSN 09596526.

72. JANAJREH, I., RAZA, S. S., VALMUNDSSON, A. S. Plasma gasification process: Modeling, simulation and comparison with conventional air gasification. *Energy Conversion and Management*. 2013, 65, 801–809. ISSN 01968904.

73. JIA, S., NING, S., YING, H., SUN, Y., XU, W., YIN, H. High quality syngas production from catalytic gasification of woodchip char. *Energy Conversion and Management*. 2017, 151, 457–464. ISSN 01968904.

74. JRC (2018). *Status of local soil contamination in Europe.* Luxembourg: Publications Office of the European Union.

75. KAPUSTA, K. Effect of ultrasound pretreatment of municipal sewage sludge on characteristics of bio-oil from hydrothermal liquefaction process. *Waste Management*. 2018, 78, 183–190. ISSN 18792456.

76. KAZA, S., YAO, L., BHADA-TATA, P., VAN WOERDEN, F. (2018) What a Waste 2.0: A Global Snapshot of Solid Waste Management to 2050. Washington: The World Bank.

77. KERMANI, M., EBADI, T. The Effect of Oil Contamination on the Geotechnical Properties of Fine-Grained Soils*Soil and Sediment Contamination*, 2012. ISSN 15320383.

78. KHUDUR, L. S., SHAHSAVARI, E., MIRANDA, A. F., MORRISON, P. D., NUGEGODA, D., BALL, A. S. Evaluating the efficacy of bioremediating a diesel-contaminated soil using ecotoxicological and bacterial community indices. *Environmental Science and Pollution Research*. 2015, 22(19), 14809–14819. ISSN 16147499.

79. KIM, K. S., KIM, T. H. Nanofabrication by thermal plasma jets: From nanoparticles to low-dimensional nanomaterials. *Journal of Applied Physics*. 2019, 125 (070901), 1–26.

80. KONG, P. S., AROUA, M. K., DAUD, W. M. A. W. Conversion of crude and pure glycerol into derivatives: A feasibility evaluation. *Renewable and Sustainable Energy Reviews*. 2016, 63, 533–555. ISSN 18790690.

81. KUMAR, A., SAMADDER, S. R. A review on technological options of waste to energy for effective management of municipal solid waste. *Waste Management*. 2017, 69, 407–422. ISSN 18792456.

82. KWON, E. E., KIM, S., LEE, J. Pyrolysis of waste feedstocks in CO_2 for effective energy recovery and waste treatment. *Journal of CO_2 Utilization*. 2019, 31(February), 173–180. ISSN 22129820.

83. LAHEL, A., FANTA, A. B., SERGIENKO, N., SHAKYA, M., LOPEZ, M. E., BEHERA, S. K., RENE, E. R., PARK, H-S. Effect of process parameters on the bioremediation of diesel contaminated soil by mixed microbial consortia. *International Biodeterioration and Biodegradation*. 2016, 113, 375–385. ISSN 09648305.

84. LEE, D. H., KIM, K-T., CHA, M. S., SONG, Y-H. Effect of excess oxygen in plasma reforming of diesel fuel. *International Journal of Hydrogen Energy*. 2010, 35(10), 4668–4675. ISSN 03603199.

85. LEE, H. J., PLAKSIN, V. Y., RIABY, V. A. The volt-ampere characteristics of a DC arc plasmatron with a distributed anode spot. *Thin Solid Films*. 2007, 515(12), 5197–5201. ISSN 00406090.

86. LI, G., PAN, W., MENG, X., WU, C. Application of similarity theory to the characterization of non-transferred laminar plasma jet generation. *Plasma Sources Science and Technology*. 2005, 14(2), 219–225. ISSN 09630252.

87. LI, J., LIU, K., YAN, S., LI, Y., HAN, D. Application of thermal plasma technology for the treatment of solid wastes in China: An overview. *Waste Management*. 2016a, 58, 260–269. ISSN 18792456.

88. LI, R., LIU, Y., CHENG, W., ZHANG, W., XUE, G., OGNIER, S. Study on remediation of phenanthrene contaminated soil by pulsed dielectric barrier discharge plasma: The role of active species. *Chemical Engineering Journal*. 2016b, 296, 132–140. ISSN 13858947.

89. LI, R., LIU, Y., MU, R., CHENG, W., OGNIER, S. Evaluation of pulsed corona discharge plasma for the treatment of petroleum-contaminated soil. *Environmental Science and Pollution Research*. 2017, 24(2), 1450–1458. ISSN 16147499.

90. LI, T., CHOI, S., WATANABE, T. Discharge characteristics of DC arc water plasma for environmental applications. *Plasma Science and Technology*. 2012, 14(12), 1097–1101. ISSN 10090630.

91. LIM, M. W., LAU, E. VON, POH, P. E. A comprehensive guide of remediation technologies for oil contaminated soil — Present works and future directions. *Marine Pollution Bulletin*. 2016, 109(1), 14–45. ISSN 0025326X.

92. LIN, Y.C. Catalytic valorization of glycerol to hydrogen and syngas. *International Journal of Hydrogen Energy*. 2013, 38(6), 2678–2700. ISSN 0360-3199.

93. LIU, F., YU, D., LV, C., DUAN, Y., ZHONG, Y., YAO, J. Experimental study on the jet characteristics of a steam plasma torch. *Plasma Science and Technology*. 2018, 20(12), 1–9. ISSN 20586272.

94. LIU, X., JENSEN, P. R., WORKMAN, M. Bioconversion of crude glycerol feedstocks into ethanol by Pachysolen tannophilus. *Bioresource Technology*. 2012, 104, 579–586. ISSN

09608524.

95. LOMINCHAR, M. A., SANTOS, A., DE MIGUEL, E., ROMERO, A. Remediation of aged diesel contaminated soil by alkaline activated persulfate. *Science of the Total Environment*. 2018, 622–623, 41–48. ISSN 18791026.

96. LU, N., WANG, C., LOU, C. Remediation of PAH-contaminated soil by pulsed corona discharge plasma. *Journal of Soils and Sediments*. 2017, 17(1), 97–105. ISSN 16147480.

97. LUTZ, A. E., BRADSHAW, R. W., KELLER, J.O., WITMER, D. E. Thermodynamic analysis of hydrogen production by partial oxidation reforming. *International Journal of Hydrogen Energy*. 2004, 29(8), 809–816. ISSN 03603199.

98. MA, F., ZHANG, Q., WU, B., PENG, C., LI, N., LI, F., GU, Q. Treatment of PAH-contaminated soil using cement-activated persulfate. *Environmental Science and Pollution Research*. 2018, 25(1), 887–895. ISSN 16147499.

99. MA, J. WEN, G-D., SU, B-G., YANG, Y-W., REN, Q-L. Current-voltage characteristics of hydrogen DC plasma torches with different sizes in an external axial magnetic field. *Chinese Physics B*. 2015, 24(6). ISSN 20583834.

100. MAGHBOULI, A., YANG, W., AN, H., SHAFEE, S., LI, J., MOHAMMADI, S. Modeling knocking combustion in hydrogen assisted compression ignition diesel engines. *Energy*. 2014, 76, 768–779. ISSN 03605442.

101. MALINAUSKAITE, J., JOUHARA, H., CZAJCZYNSKA, D., STANCHEV, P., KATSOU, E., ROSTKOWSKI, P., THRONE, R. J., COLON, J., PONSA, S., AL-MANSOUR, F., ANGUILANO, L., KRZYZYNSKA, R., LOPEZ, I. C., VLASOPOULOS, A., SPENCER, N. Municipal solid waste management and waste-to-energy in the context of a circular economy and energy recycling in Europe. *Energy*. 2017, 141, 2013–2044. ISSN 03605442.

102. MARGALLO, M., ZIEGLER-RODRIGUE, K., VAZQUEZ-ROWE, I., ALDACO, R., IRABIEN, A., KAHHAT, R. Enhancing waste management strategies in Latin America under a holistic environmental assessment perspective: A review for policy support. *Science of the Total Environment*. 2019, 689, 1255–1275. ISSN 18791026.

103. MARTIN, S., KRAAIJ, G., ASCHER, T., BALTZOPOULOU, P., KARAGIANNAKIS, G., WAILS, D., WORNER, A. Direct steam reforming of diesel and diesel-biodiesel blends for distributed hydrogen generation. *International Journal of Hydrogen Energy*. 2015, 40(1), 75–84. ISSN 03603199.

104. MATERAZZI, M., LETTIERI, P., MAZZEI, L., TAYLOR, R., CHAPMAN, C. Thermodynamic modelling and evaluation of a two-stage thermal process for waste gasification. *Fuel*. 2013, 108, 356–369. ISSN 00162361.

105. MAXIMINI, M., ENGELHARDT, P., GROTE, M., BRENNER, M. Further development of a microchannel steam reformer for diesel fuel. *International Journal of Hydrogen Energy*. 2012, 37(13), 10125–10134. ISSN 03603199.

106. MAZZONI, L., JANAJREH, I. Plasma gasification of municipal solid waste with variable content of plastic solid waste for enhanced energy recovery. *International Journal of Hydrogen Energy*. 2017, 42(30), 19446–19457. ISSN 03603199.

107. MCKENDRY, P. Energy production from biomass (part 3): gasification technologies. *Bioresource Technology*. 2002, 83(1), 55–63. ISSN 09608524.

108. MENEZES, J. P. DA S. Q., MANFRO, R. L., SOUZA, M. M. V. M. Hydrogen production

from glycerol steam reforming over nickel catalysts supported on alumina and niobia: Deactivation process, effect of reaction conditions and kinetic modeling. *International Journal of Hydrogen Energy*. 2018, 43(32), 15064–15082. ISSN 03603199.

109. MESSERLE, V. E., MOSSE, A. L., USTIMENKO, A. B. Processing of biomedical waste in plasma gasifier. *Waste Management*. 2018, 79, 791–799. ISSN 18792456.

110. MOHSENIAN, S., ESMAILI, M. S., SHOKRI, B., GHORBANALILU, M. Physical characteristics of twin DC thermal plasma torch applied to polymer waste treatment. *Journal of Electrostatics*. 2015, 76, 231–237. ISSN 03043886.

111. MUNIR, M. T., MARDON, I., AL-ZUHAIR, S., SHAWABKEH, A., SAQIB, N. U. Plasma gasification of municipal solid waste for waste-to-value processing. *Renewable and Sustainable Energy Reviews*. 2019, 116, 109461. ISSN 18790690.

112. MURPHY, A. B., UHRLANDT, D. Foundations of High-Pressure Thermal Plasmas. *Plasma Sources Science and Technology*. 2018, 27(063001), 1–20.

113. NANDA, M. R., ZHANG, Y., YUAN, Z., QIN, W., GHAZIASKAR, H. S., XU, C. C. Catalytic conversion of glycerol for sustainable production of solketal as a fuel additive: A review. *Renewable and Sustainable Energy Reviews*. 2016, 56(1), 1022–1031. ISSN 18790690.

114. NASA. Measurement Uncertainty Analysis Principles and Methods. Washington: NASA, 2010.

115. NAYLOR, R. L., HIGGINS, M. M. The political economy of biodiesel in an era of low oil prices. *Renewable and Sustainable Energy Reviews*. 2017, 77(April 2016), 695–705. ISSN 18790690.

116. NAYLOR, R. L., HIGGINS, M. M. The rise in global biodiesel production: Implications for food security. *Global Food Security*. 2018, 16(July 2017), 75–84. ISSN 22119124.

117. NEHRA, V., KUMAR, A., DWIVEDI, H. K. Atmospheric Non-Thermal Plasma Sources. *International Journal of Engineering*. 2008, 2(1), 53–68.

118. NEWELL, R. G., RAIMI, D., ALDANA, G. (2019). *Global Energy Outlook 2019: The Next Generation of Energy.* [Accessed 2019-11-29] Internet access: http://www.econ2.jhu.edu/courses/101/GlobalEnergyOutlook2019.pdf

119. NIU, Y., LV, Y., LEI, Y., LIU, S., LIANG, Y., WANG, D., HUI, S. Biomass torrefaction: properties, applications, challenges, and economy. *Renewable and Sustainable Energy Reviews*. 2019, 115, 109395. ISSN 18790690.

120. O'BRIEN, P. L., DESUTTER, T. M., CASEY, F. X. M., KHAN, E., WICK, A. F. Thermal remediation alters soil properties – a review. *Journal of Environmental Management*. 2018, 206, 826–835. ISSN 10958630.

121. OECD-FAO (2017). *OECD-FAO Agricultural Outlook 2017-2026.* Paris: OECD-FAO.

122. OECD-FAO (2019). *OECD-FAO Agricultural Outlook 2019-2028.* Paris: OECD-FAO.

123. OKOLIE, J. A., NANDA, S., DALAI, A. K., BERRUTI, F., KOZINSKI, J. A. A review on subcritical and supercritical water gasification of biogenic, polymeric and petroleum wastes to hydrogen-rich synthesis gas. *Renewable and Sustainable Energy Reviews*. 2020, 119, 109546. ISSN 18790690.

124. OUDA, O. K. M., RAZA, S. A., NIZAMI, A. S., REHAN, M., AL-WAKED, R., KORRES, N. E. Waste to energy potential: A case study of Saudi Arabia. *Renewable and*

Sustainable Energy Reviews. 2016, 61, 328–340. ISSN 18790690.

125. PAN, W. X., MENG, X., HUANG, H. J., WU, C. K. Effects of anode temperature on the arc volt-ampere characteristics and ejected plume property of a low-power supersonic plasma. *Plasma Sources Science and Technology*. 2011, 20(6). ISSN 09630252.

126. PENGRA, D. B., DILLMAN, L. T. Notes on Data Analysis and Experimental Uncertainty. [Accessed 2020-01-15] Internet access: https://courses.washington.edu/phys431/uncertainty_notes.pdf

127. PERNA, A., MINUTILLO, M., LAVADERA, A. L., JANNELLI, E. Combining plasma gasification and solid oxide cell technologies in advanced power plants for waste to energy and electric energy storage applications. *Waste Management*. 2018, 73, 424–438. ISSN 18792456.

128. PETITPAS, G., ROLLIER, J. D., DARMON, A., GONZALEZ-AGUILAR, J., METKEMEIJER, R., FULCHERI, L., A comparative study of non-thermal plasma assisted reforming technologies. *International Journal of Hydrogen Energy*. 2007, 32(14), 2848–2867. ISSN 03603199.

129. PIRES, A., MARTINHO, G. Waste hierarchy index for circular economy in waste management. *Waste Management*. 2019, 95, 298–305. ISSN 18792456.

130. RAHMAN, M. S., XU, C. C., QIN, W. Biotransformation of biodiesel-derived crude glycerol using newly isolated bacteria from environmental consortia. *Process Biochemistry*. 2017, 63, 177–184. ISSN 13595113.

131. RAHMAN, Z., RAHMAN, H., RAHMAN, A. Classification and Generation of Atmospheric Pressure Plasma and Its Principle Applications. *International Journal of Mathematics and Physical Sciences Research*. 2015, 2(2), 127–146.

132. RAMOS, A., MONTEIRO, E., SILVA, V., ROUBOA, A. Co-gasification and recent developments on waste-to-energy conversion: A review. *Renewable and Sustainable Energy Reviews*. 2018, 81, 380–398. ISSN 18790690.

133. RAMOS, A., MONTEIRO, E., ROUBOA, A. Numerical approaches and comprehensive models for gasification process: A review. *Renewable and Sustainable Energy Reviews*. 2019, 110, 188–206. ISSN 18790690.

134. RASLAVIČIUS, L., STRIŪGAS, N., FELNERIS, M., SKVORČINSKIENĖ, R., MIKNIUS, L. Thermal characterization of P. moriformis oil and biodiesel. *Fuel*. 2018, 220, 140–150. ISSN 00162361.

135. REDOLFI, M., MAKHLOUFI, C., OGNIER, S., CAVADIAS, S., TZOVOLOU, D., TSAKIROGLOU, CH. Kerosene contaminated soil removal by non-thermal atmospheric plasma discharge. *High Temperature Material Processes (An International Quarterly of High-Technology Plasma Processes)*. 2009, 13(3–4), 427–437. ISSN 1093-3611.

136. REDOLFI, M., MAKHLOUFI, C., OGNIER, S., CAVADIAS, S. Oxidation of kerosene components in a soil matrix by a dielectric barrier discharge reactor. *Process Safety and Environmental Protection*. 2010, 88(3), 207–212. ISSN 09575820.

137. REN21 (2017). *Renewable Global Futures Report. Great debates towards 100 % renewable energy.* Paris: REN21.

138. REN21 (2018). *Renewables 2018 Global Status Report.* Paris: REN21.

139. REŞITOĞLU, I. A., ALTINIŞIK, K., KESKIN, A. The pollutant emissions from diesel-engine vehicles and exhaust aftertreatment systems. *Clean Technologies and Environmental*

Policy. 2015, 17(1), 15–27. ISSN 16189558.

140. RODRÍGUEZ-EUGENIO, N., MCLAUGHLIN, M., PENNOCK, D. Soil Pollution A Hidden Reality. Rome: FAO, 2018. ISSN 01406736.

141. ROSER, M. (2019). *Future Population Growth Global population growth Two centuries of rapid global population growth will.* [Accessed 2019-12-04] Internet access: https://ourworldindata.org/future-population-growth#global-population-growth

142. ROY, A. S., BARUAH, R., BORAH, M., SINGH, A. K., BORUAH, H. P. D., SAIKIA, N., DEKA, M., DUTTA, N., BORA, T. C. Bioremediation potential of native hydrocarbon degrading bacterial strains in crude oil contaminated soil under microcosm study. *International Biodeterioration and Biodegradation*. 2014, 94, 79–89. ISSN 09648305.

143. RUJ, B., GHOSH, S. Technological aspects for thermal plasma treatment of municipal solid waste - A review. *Fuel Processing Technology*. 2014, 126, 298–308. ISSN 03783820.

144. RUTBERG, P. G., KUZNETSOV, V. A., SERBA, E. O., NAKONECHNYI, G. V., NIKONOV, A. V., POPOV, S. D., SUROV, A. V. Study of electric arcs in an air-steam mixture in AC plasma torches. *High Temperature*. 2013a, 51(5), 608–614. ISSN 0018-151X.

145. RUTBERG, P. G., KUZNETSOV, V. A., SERBA, E. O., POPOV, S. D., SUROV, A. V., NAKONECHNY, G. V., NIKONOV, A. V. Novel three-phase steam-air plasma torch for gasification of high-caloric waste. *Applied Energy*. 2013b, 108, 505–514. ISSN 03062619.

146. SAFA, S., SOUCY, G. Liquid and solution treatment by thermal plasma: A review. *International Journal of Environmental Science and Technology*. 2014, 11(4), 1165–1188. ISSN 17352630.

147. SAMAL, S. Thermal plasma technology: The prospective future in material processing. *Journal of Cleaner Production*. 2017, 142, 3131–3150. ISSN 09596526.

148. SANCHEZ, E. A., COMELLI, R. A. Hydrogen by glycerol steam reforming on a nickel-alumina catalyst: Deactivation processes and regeneration. *International Journal of Hydrogen Energy*. 2012, 37(19), 14740–14746. ISSN 03603199.

149. SANDU, C., POPESCU, M., ROSALES, E., PAZOS, M., LAZAR, G., SANROMAN, M. A. Electrokinetic oxidant soil flushing: A solution for in situ remediation of hydrocarbons polluted soils. *Journal of Electroanalytical Chemistry*. 2017, 799, 1–8. ISSN 15726657.

150. SANLISOY, A., CARPINLIOGLU, M. O. A review on plasma gasification for solid waste disposal. *International Journal of Hydrogen Energy*. 2017, 42(2), 1361–1365. ISSN 03603199.

151. SARANGAPANI, C., MISRA, N. N., MILOSAVLJEVIC, V., BOURKE, P., O'REGAN, F., CULLEN, P. J. Pesticide degradation in water using atmospheric air cold plasma. *Journal of Water Process Engineering*. 2016, 9, 225–232. ISSN 22147144.

152. SAUCHYN, V., KHVEDCHYN, I., AL-MAYMAN, S., AL-ABBADI, N., AL-JUHANI, M., AL-ENAZI, K. Plasma Technology for Vitrification of Ash From Power Plants. *High Temperature Material Processes (An International Quarterly of High-Technology Plasma Processes)*. 2012, 16(1), 1–13. ISSN 1093-3611.

153. SCAFUTTO, R. D. P. M., DE SOUZA FILHO, C. R., DE OLIVEIRA, W. J. Hyperspectral remote sensing detection of petroleum hydrocarbons in mixtures with mineral substrates: Implications for onshore exploration and monitoring. *ISPRS Journal of Photogrammetry and Remote Sensing*. 2017, 128, 146–157. ISSN 09242716.

154. SCHWENGBER, C. A., ALVES, H. J., SCHAFFNER, R. A., SILVA, F. A., SEQUINEL,

R., BACH, V. R., FERRACIN, R. J. Overview of glycerol reforming for hydrogen production. *Renewable and Sustainable Energy Reviews*. 2016a, 58, 259–266. ISSN 18790690.

155. SHEN, J., ZHANG, H., XU, Z., ZHANG, Z., CHENG, C., NI, G., LAN, Y., MENG, Y., XIA, W., CHU, P. K. Preferential production of reactive species and bactericidal efficacy of gas-liquid plasma discharge. *Chemical Engineering Journal*. 2019, 362, 402–412. ISSN 13858947.

156. SIERADZKA, M., RAJCA, P., ZAJEMSKA, M., MILONKA-MEDRALA, A., MAGDZIARZ, A. Prediction of gaseous products from refuse derived fuel pyrolysis using chemical modelling software - Ansys Chemkin-Pro. *Journal of Cleaner Production*. 2020, 248. ISSN 09596526.

157. SNELLINGS, R., MERTENS, G., ELSEN, J. Supplementary Cementitious Materials. *Reviews in Mineralogy and Geochemistry*. 2012, 74(1), 211–278. ISSN 1529-6466.

158. STRIŪGAS, N., VALINČIUS, V., PEDIŠIUS, N., POŠKAS, R., ZAKARAUSKAS, K., Investigation of sewage sludge treatment using air plasma assisted gasification. *Waste Management*. 2017, 64, 149–160. ISSN 18792456.

159. SZYMKOWICZ, P. G., BENAJES, J. Development of a Diesel Surrogate Fuel Library. *Fuel*. 2018, 222, 21–34. ISSN 00162361.

160. TAHERI, S., EBADI, T., MAKNOON, R., AMIRI, M. Predicting variations in the permeability and strength parameters of a sand-bentonite mixture (SBM) contaminated simultaneously with lead (II) and diesel. *Applied Clay Science*. 2018, 157, 102–110. ISSN 01691317.

161. TAMOŠIŪNAS, A., GRIGAITIENĖ, V., VALATKEVIČIUS, P., VALINČIUS, V. Syngas production from hydrocarbon-containing gas in ambient of water vapor plasma. *Catalysis Today*. 2012, 196(1), 81–85. ISSN 09205861.

162. TAMOŠIŪNAS, A., VALATKEVIČIUS, P., VALINČIUS, V., GRIGAITIENĖ, V. Production of synthesis gas from propane using thermal water vapor plasma. *International Journal of Hydrogen Energy*. 2014, 39(5), 2078–2086. ISSN 03603199.

163. TAMOŠIŪNAS, A., VALATKEVIČIUS, P., GRIGAITIENĖ, V., VALINČIUS, V., STRIŪGAS, N. A cleaner production of synthesis gas from glycerol using thermal water steam plasma. *Journal of Cleaner Production*. 2016, 130, 187–194. ISSN 09596526.

164. TAMOŠIŪNAS, A. Termohidrodinaminių procesų tyrimas vandens garo plazmoje ir jos taikymas organinių medžiagų konversijai. Lithuanian Energy Institute, 2014.

165. TAMOŠIŪNAS, A., GRIGAITIENĖ, V., VALATKEVIČIUS, P. Creation of linear DC plasma generator for pyrolysis/gasification of organic materials. *Nukleonika*. 2011, 56(2), 131–135. ISSN 00295922.

166. TANG, L., HUANG, H., HAO, H., ZHAO, K. Development of plasma pyrolysis/gasification systems for energy efficient and environmentally sound waste disposal. *Journal of Electrostatics*. 2013, 71(5), 839–847. ISSN 03043886.

167. TATAROVA, E., BUNDALESKA, N., SARRETTE, J. PH., FERREIRA, C. M. Plasmas for environmental issues: From hydrogen production to 2D materials assembly. *Plasma Sources Science and Technology*. 2014, 23(6). ISSN 13616595.

168. TENDERO, C., TIXIER, C., TRISTANT, P., DESMAISON, J., LEPRINCE, P. Atmospheric pressure plasmas: A review. *Spectrochimica Acta - Part B Atomic Spectroscopy*. 2006, 61(1), 2–30. ISSN 05848547.

169. TONG, S., XIAO, L., LI, X., ZHU, X., LIU, H., LUO, G., WORASUWANNARAK, N., KERDSUWAN, S., FUNGTAMMASAN, B., YAO, H. A gas-pressurized torrefaction method for biomass wastes. *Energy Conversion and Management*. 2018, 173, 29–36. ISSN 01968904.

170. TOOR, S. S., ROSENDAHL, L., RUDOLF, A. Hydrothermal liquefaction of biomass: A review of subcritical water technologies. *Energy*. 2011, 36(5), 2328–2342. ISSN 03605442.

171. TORRY, J., ATTACHÉ, A. USDA STAFF AND NOT NECESSARILY STATEMENTS OF OFFICIAL U . S . GOVERNMENT Sugar Annual Sugar Annual Report Approved By : *Forecast*. 2011, 1–9. ISSN 2356-6140.

172. UFOP (2018). *UFOP Report on Global Market Supply 2017/2018*. Berlin: UFOP.

173. UNITED NATIONS (2016). *Transforming Our World: The 2030 Agenda For Sustainable Development.* New York: UNITED NATIONS.

174. UNITED NATIONS (2019). *World Population Prospects 2019.* New York: UNITED NATIONS.

175. UNITED NATIONS (2019). *Waste-to-energy: Considerations for informed decision-making.* New York: UNITED NATIONS.

176. VARRONE, C., LIBERATORE, R., CRESCENZI, T., IZZO, G., WANG, A. The valorization of glycerol: Economic assessment of an innovative process for the bioconversion of crude glycerol into ethanol and hydrogen. *Applied Energy*. 2013, 105, 349–357. ISSN 03062619.

177. VEMPATAPU, B. P., KANAUJIA, P. K. Monitoring petroleum fuel adulteration: A review of analytical methods. *Trends in Analytical Chemistry*. 2017, 92, 1–11. ISSN 18793142.

178. WANG, T., QU, G., SUN, Q., LIANG, D., HU, S. Formation and roles of hydrogen peroxide during soil remediation by direct multi-channel pulsed corona discharge in soil. *Separation and Purification Technology*. 2015, 147, 17–23. ISSN 18733794.

179. WANG, T. C., LU, N., LI, J., WU, Y. Degradation of pentachlorophenol in soil by pulsed corona discharge plasma. *Journal of Hazardous Materials*. 2010, 180(1–3), 436–441. ISSN 03043894.

180. WANG, T. C., QU, G., LI, J., LIANG, D. Evaluation and optimization of multi-channel pulsed discharge plasma system for soil remediation. *Vacuum*. 2014a, 103, 72–77. ISSN 0042207X.

181. WANG, T. C., QU, G., LI, J., LIANG, D. Evaluation of the potential of soil remediation by direct multi-channel pulsed corona discharge in soil. *Journal of Hazardous Materials*. 2014b, 264, 169–175. ISSN 18733336.

182. WANG, W. Thermodynamic analysis of glycerol partial oxidation for hydrogen production. *Fuel Processing Technology*. 2010, 91(11), 1401–1408. ISSN 03783820.

183. WATANABE, T., NARENGERILE. Decomposition of glycerine by water plasmas at atmospheric pressure. *Plasma Science and Technology*. 2013, 15(4), 357–361. ISSN 10090630.

184. WATSON, J., ZHANG, Y., SI, B., CHEN, W-T., DE SOUZA, R. Gasification of biowaste: A critical review and outlooks. *Renewable and Sustainable Energy Reviews*. 2018, 83, 1–17. ISSN 18790690.

185. WATSON, J., WANG, T., SI, B., CHEN, W-T., AIERZHATI, A., ZHANG, Y.

Valorization of hydrothermal liquefaction aqueous phase: pathways towards commercial viability. *Progress in Energy and Combustion Science*. 2020, 77, 100819. ISSN 03601285.

186. YANG, F. X., HANNA, M. A., SUN, R. C. Value-added uses for crude glycerol—A byproduct of biodiesel production. *Biotechnol. Biofuels*. 2012, (5), 1–10.

187. YOON, S. J., CHOI, Y-C., SON, Y-I., LEE, S-H., LEE, J-G. Gasification of biodiesel by-product with air or oxygen to make syngas. *Bioresource Technology*. 2010, 101(4), 1227–1232. ISSN 09608524.

188. YOON, S. J., YUN, Y. M., SEO, M. W., KIM, Y. K., RA, H. W., LEE, J-G. Hydrogen and syngas production from glycerol through microwave plasma gasification. *International Journal of Hydrogen Energy*. 2013, 38(34), 14559–14567. ISSN 03603199.

189. YUS, M., SOLER, J., HERGUIDO, J., MENENDEZ, M. Glycerol steam reforming with low steam/glycerol ratio in a two-zone fluidized bed reactor. *Catalysis Today*. 2018, 299, 317–327. ISSN 09205861.

190. ZHAN, J., ZHANG, A., HEROUX, P., LI, X., LI, Z., ZHAO, J., GUO, Y., LIU, Y. Gasoline degradation and nitrogen fixation in soil by pulsed corona discharge plasma. *Science of the Total Environment*. 2019, 661, 266–275. ISSN 18791026.

191. ZHANG, H., MA, D., QIU, R., TANG, Y., DU, C. Non-thermal plasma technology for organic contaminated soil remediation: A review. *Chemical Engineering Journal*. 2017a, 313, 157–170. ISSN 13858947.

192. ZHANG, M., XUE, W., SU, B., BAO, Z., WEN, G., XING, H., REN, Q. Conversion of glycerol into syngas by rotating DC arc plasma. *Energy*. 2017b, 123, 1–8. ISSN 03605442.

193. ZHANG, Q., DOR, L., FENIGSHTEIN, D., YANG, W., BLASIAK, W. Gasification of municipal solid waste in the Plasma Gasification Melting process. *Applied Energy*. 2012, 90(1), 106–112. ISSN 03062619.

194. ZHANG, Y., CUI, Y., LIU, S., FAN, L., ZHOU, N., PENG, P., WANG, Y., GUO, F., MIN, M., CHENG, Y., LIU, Y., LEI, H., CHEN, P., LI, B., RUAN, R. Fast microwave-assisted pyrolysis of wastes for biofuels production – A review. *Bioresource Technology*. 2020, 297, 122480. ISSN 18732976.

195. ZHENG, J., YANG, R., XIE, L. QU, J., LIU, Y., LI, X. Plasma-assisted approaches in inorganic nanostructure fabrication. *Advanced Materials*. 2010, 22(13), 1451–1473. ISSN 09359648.

196. ZHUKOV, M. F., ZASYPKIN, I. M., TIMOSHEWSKII, A. N., MIKHAILOV, B. I, DESYATKOV, G. A. (1999). *Thermal Plasma Torches* Novosibirsk: Nauka.

197. ZHUKOV, M. F., ZASYPKIN, I. M. (2007) *Thermal plasma torches* UK: Cambridge International Science Publishing Ltd.

PUBLICATIONS RELATED TO THE DISSERTATION

Articles in journals from "Clarivate Analytics Web of Science" list

1. Tamošiūnas A., Valatkevičius P., **Gimžauskaitė D**., Valinčius V., Jeguirim M. Glycerol steam reforming for hydrogen and synthesis gas production (doi.org/10.1016/j.ijhydene.2016.12.071) // Hydrogen Energy. ISSN 0360-3199. Vol. 42. 2017. p. 12896-12904
2. Tamošiūnas A., Valatkevičius P., **Gimžauskaitė D.**, Jeguirim M., Mėčius V., Aikas M. Energy recovery from waste glycerol by utilizing thermal water vapor plasma (doi: 10.1007/s11356-016-8097-8) // Environmental Science and Pollution Research. ISSN 0944-1344. Vol. 24. Iss. 11. 2017. p. 10030-10040
3. Tamošiūnas A., **Gimžauskaitė D.**, Uscila R., Aikas M. Thermal arc plasma gasification of waste glycerol to syngas (doi.org/10.1016/j.apenergy.2019.113306) // Applied Energy. ISSN 0306-2619. Vol. 251. 2019. Article ID 113306. p. 1-8
4. **Gimžauskaitė D.,** Tamošiūnas A., Tučkutė S., Snapkauskienė V., Aikas M., Uscila R. Treatment of diesel-contaminated soil using thermal water vapor arc plasma (doi.org/10.1007/s11356-019-06697-4) // Environmental Science and Pollution Research. ISSN 0944-1344. eISSN 1614-7499. Vol. 27. 2020. p. 43–54

Publications in the international conferences

1. **Gimžauskaitė D.**, Tamošiūnas A., Valatkevičius P., Valinčius V. The influence of gas type on the plasma torch electrical and thermal characteristics // 13th Annual international conference of young scientists on energy issues (CYSENI 2016), Kaunas, Lithuania, May 26–27, 2016. Kaunas: LEI, 2016. ISSN 1822-7554. p. 251-259
2. Tamošiūnas A., Jeguirim M., Valatkevičius P., **Gimžauskaitė D.**, Valinčius V. Hydrogen and synthesis gas production from glycerol by utilizing thermal water vapor plasma // 7th International Renewable Energy Congress „IREC 2016“. ISBN 978-1-4673-9768-1. Hammamet-Tunisia March 22nd-24th 2016. p. 1-6
3. **Gimžauskaitė D.**, Tamošiūnas A., Snapkauskienė V., Valatkevičius P., Valinčius V. Remediation of petroleum hydrocarbons contaminated soil using water vapor plasma // The 14th International Conference of Young Scientists on energy Issues (CYSENI 2017), Kaunas, Lithuania, May 25-26, 2017. Kaunas: LEI, 2017, ISSN 1822-7554. p. 233-238
4. Tamošiūnas A., **Gimžauskaitė D.** Gasification of glycerol into syngas (H_2+CO) by thermal air plasma // 16th International Conference on Clean Energy (ICCE-2018) 9-11 May 2018, Famagusta, N. Cyprus. p. 1-7
5. **Gimžauskaitė D.**, Tamošiūnas A., Aikas M., Uscila R., Samosionokas J. The use of thermal plasma for the treatment of soil contaminated by petroleum hydrocarbons // The 15th International Conference of Young Scientists on

Energy Issues (CYSENI 2018) Kaunas, Lithuania, May 23-25, 2018. Kaunas:LEI, 2018, ISSN 1822-7554. p. 286-292

6. Tamošiūnas A., **Gimžauskaitė D.**, Uscila R., Aikas M. A comparative study on syngas production from crude glycerol by utilizing DC arc plasma (http://www.naxos2018.uest.gr) // 6th International Conference on Sustainable Solid Waste Management 13-16 June 2018, Greece. p. 1-10
7. **Gimžauskaitė D.**, Tamošiūnas A., Tučkutė S., Snapkauskienė V., Aikas M., Uscila R. The use of thermal water vapor arc plasma as an oily soil remediation technique // Presented at 2nd International Research Conference on Sustainable Energy, Engineering, Materials and Environment, Mieres, Spain, 25-27 July 2018. ISBN 978-84-17238-93-3. p. 1-4

Presentations in the international conferences

1. **Gimžauskaitė D.,** Tamošiūnas A., Valatkevičius P., Valinčius V. The influence of gas type on the plasma torch electrical and thermal characteristics // 13th Annual international conference of young scientists on energy issues (CYSENI 2016), Kaunas, Lithuania, May 26–27, 2016. Kaunas: LEI, 2016. ISSN 1822-7554. p. 251-259
2. **Gimžauskaitė D.,** Tamošiūnas A., Snapkauskienė V., Valatkevičius P., Valinčius V. Remediation of petroleum hydrocarbons contaminated soil using water vapor plasma // The 14th International Conference of Young Scientists on energy Issues (CYSENI 2017), Kaunas, Lithuania, May 25-26, 2017. Kaunas: LEI, 2017, ISSN 1822-7554. p. 233-238
3. Tamošiūnas A., **Gimžauskaitė D.** Gasification of glycerol into syngas (H_2+CO) by thermal air plasma // 16th International Conference on Clean Energy (ICCE-2018) 9-11 May 2018, Famagusta, N. Cyprus. p. 1-7
4. **Gimžauskaitė D.,** Tamošiūnas A., Aikas M., Uscila R., Samosionokas J. The use of thermal plasma for the treatment of soil contaminated by petroleum hydrocarbons // The 15th International Conference of Young Scientists on Energy Issues (CYSENI 2018) Kaunas, Lithuania, May 23-25, 2018. Kaunas:LEI, 2018, ISSN 1822-7554. p. 286-292
5. **Gimžauskaitė D.,** Tamošiūnas A., Tučkutė S., Snapkauskienė V., Aikas M., Uscila R. The use of thermal water vapor arc plasma as an oily soil remediation technique // Presented at 2nd International Research Conference on Sustainable Energy, Engineering, Materials and Environment, Mieres, Spain, 25-27 July 2018. ISBN 978-84-17238-93-3. p. 1-4

ACKNOWLEDGEMENTS

I want to express sincere gratitude to my supervisor Dr V. Valinčius, for giving me the opportunity to become the part of the Plasma Processing Laboratory team, and the granting freedom in accomplishing my scientific research interests.

I want to thank Prof Dr L. Marcinauskas and Dr R. Pabarčius for giving their time in reviewing this dissertation. Their shared valuable experience and knowledge has enriched this thesis a lot.

I want to especially thank Dr A. Tamošiūnas for his guidance, patience, valuable advice and insightful comments in various aspects of my work. His engagement to help and support was a solid pillar in my PhD scientific journey.

I express my sincere appreciation to Dr D. Milčius, who has given me the motivation and support throughout this process.

I owe my deepest gratitude to my former supervisor Prof Dr L. Pranevičius for introducing and giving me the opportunity to work in the plasma research field.

I want to thank Dr E. Urbonavičius for his beneficial consultations and inspiration throughout the PhD studies.

Many thanks belong to my research group, who was helping me with the experiments.

I want to thank my colleagues from the Centre for Hydrogen Energy Technologies, Laboratory of Combustion Processes and Laboratory of Heat Equipment Research and Testing who have directly or indirectly contributed to the research results presented in this dissertation.

I want to kindly thank Studies Administrator J. Kazakevičienė for help and consultations during the period of PhD studies.

I also want to thank J. Samosionokas for the cooperation during the research of capabilities to remediate petroleum products contaminated soil with thermal plasma technology.

I wish to express profound thanks to my family and friends for their understanding, support and encouragement during the whole period of my doctoral studies.

Finally, I want to thank those who were interfering my life by causing various obstacles. All this experience allowed me to become stronger as a person and start my path as a researcher.

SL344. 2020-07-16, 13,75 leidyb. apsk. l. Tiražas 12 egz.
Išleido Kauno technologijos universitetas, K. Donelaičio g. 73, 44249 Kaunas
Spausdino leidyklos „Technologija“ spaustuvė, Studentų g. 54, 51424 Kaunas